Titre: Title:	Random vibration of a curved structure subjected to a turbulent flow
Auteur: Author:	Mitra Esmailzadeh Kandjani
Date:	2009
Type:	Mémoire ou thèse / Dissertation or Thesis
Référence: Citation:	Esmailzadeh Kandjani, M. (2009). Random vibration of a curved structure subjected to a turbulent flow [Ph.D. thesis, École Polytechnique de Montréal]. PolyPublie. https://publications.polymtl.ca/8467/

URL de PolyPublie: PolyPublie URL:	https://publications.polymtl.ca/8467/
Directeurs de recherche: Advisors:	
Programme: Program:	Unspecified

UNIVERSITÉ DE MONTRÉAL

RANDOM VIBRATION OF A CURVED STRUCTURE SUBJECTED TO A TURBULENT FLOW

MITRA ESMAILZADEH KANDJANI
DÉPARTEMENT DE GÉNIE MÉCANIQUE
ÉCOLE POLYTECHNIQUE DE MONTRÉAL

THÈSE PRÉSENTÉE EN VUE DE L'OBTENTION
DU DIPLÔME DE PHILOSOPHIAE DOCTOR
(GÉNIE MÉCANIQUE)
JUIN 2009

Your file Votre référence
ISBN: 978-0-494-53796-1
Our file Notre référence
ISBN: 978-0-494-53796-1

UNIVERSITÉ DE MONTRÉAL

ÉCOLE POLYTECHNIQUE DE MONTRÉAL

Cette thèse intitulée:

RANDOM VIBRATION OF A CURVED STRUCTURE SUBJECTED TO A TURBULENT FLOW

Présentée par: ESMAILZADEH KANDJANI Mitra
en vue de l'obtention du diplôme de: Philosophiae Doctor
a été dûment acceptée par le jury d'examen constitué de:

M. KAHAWITA René, Ph.D., président
M. LAKIS Aouni A., Ph.D., membre et directeur de recherche
M. SHIRAZI-ADL Aboulfazl, Ph.D., membre
M. ENSAN NEJAD Manouchehr, Ph.D., membre externe

Dedicated to

my parents

my husband Kiarash

and my son Ryan

ACKNOWLEDGEMENTS

First and foremost, I wish to express my deepest gratitude to Professor Aouni Lakis for his constant support and encouragement during my study.

The financial support provided from his research grants by the Natural Sciences and Engineering Research Council of Canada and Hydro-Québec is also acknowledged.

I am grateful to Parvin Zahedi for her support during the writing of this thesis.

Finally, I would like to thank my husband Kiarash Aminollahi for his encouragement, understanding and dedication throughout my studies that allowed me to meet the challenges.

RÉSUMÉ

Les coques minces soumises au fluide au repos ou en écoulement turbulent sont trouvées partout dans l'application pratique de technologie. La présence du fluide au repos au voisinage d'une coque a une influence importante sur le comportement dynamique de la structure et cause une chute significative de fréquence naturelle et peut affecter la stabilité dynamique du système. Beaucoup d'efforts de recherches ont été effectués pour étudier les structures axisymétriques, mais peu d'études ont traité les structures tridimensionnelles telles que le réservoir rectangulaire élastique et l'aube d'une turbine hydraulique en contact avec le fluide stationnaire.

La pression aléatoire induite par la couche limite turbulente est une source fréquente d'excitation et peut causer la vibration de basse amplitude et finalement peut causer des défaillances de fatigue des structures impliquées. Par conséquent, la détermination de la réponse des structures soumises à pression turbulente induite par la couche limite est importante. Tandis qu'un grand volume de travaux dans la littérature a été effectué pour étudier des fluctuations de pression sous une couche limite turbulente ainsi que la densité spectrale de la réponse d'une plaque due à l'écoulement turbulent, moins de tentative a été consacrée à calculer la valeur quadratique moyenne du déplacement de plaque et coque mince.

Dans la première phase de cette thèse, un modèle a été développé afin de prédire le comportement dynamique des structures courbées minces tridimensionnelles à vide et en contact avec un fluide stationnaire non visqueux incompressible. L'élément

fini utilisé dans ce travail a été obtenu par la combinaison de la théorie de plaque mince et de l'analyse des éléments finis dans laquelle les éléments finis sont la coque plate rectangulaire ayant quatre nœuds avec cinq degrés de liberté par nœud. Les équations d'équilibre ont été obtenues à partir de la théorie de Sanders. On assume que les déplacements de membrane sont des polynômes bilinéaires et le déplacement transversal est approximé par une fonction exponentielle ayant la forme générale de la solution des équations d'équilibre. Les matrices élémentaires de masse et de rigidité sont déterminées par intégration exacte en utilisant l'analyse des éléments finis. Les fréquences naturelles d'un réservoir rectangulaire et d'une aube à vide prédites par notre méthode ont été bien rivalisées avec celles obtenues en utilisant ANSYS.

Cette méthode peut facilement être adaptée pour tenir compte des effets hydrodynamiques. D'ailleurs, elle peut calculer les hautes et les basses fréquences avec une grande précision qui est d'une importance considérable pour déterminer la réponse des structures soumises aux champs de pression aléatoire tels que ceux produits par écoulement turbulent.

La pression du fluide stationnaire exercée sur chaque élément fini est calculée en utilisant le potentiel de vitesse, l'équation de Bernoulli et la condition d'imperméabilité. La pression du fluide est exprimée en fonction de l'accélération du déplacement transversal de la structure, de la densité du fluide et des conditions aux limites du fluide. Une intégration analytique du produit de la pression de fluide et du champ de déplacement sur la surface de l'élément produit la force d'inertie du fluide et est interprétée comme une masse ajoutée virtuelle de fluide. Les fréquences naturelles

d'un réservoir rectangulaire rempli de fluide ont été analysées par notre méthode et ont été comparées à celles obtenues en utilisant ANSYS. Cette méthode a été appliquée avec succès pour prédire le comportement dynamique d'un réservoir rectangulaire partiellement rempli avec le fluide ainsi qu'une aube submergée. Un code de calcul a été développé afin de calculer des fréquences naturelles et des modes des structures minces tridimensionnelles à vide et en contact avec le fluide au repos.

Dans la phase finale de cette thèse, une méthode capable de prédire la réponse d'une structure mince soumise à un champ aléatoire arbitraire de pression aussi bien qu'une pression aléatoire induite par la couche limite turbulente en écoulement subsonique est présentée. On propose une approche numérique basée sur la méthode mentionnée ci-dessus pour obtenir la valeur quadratique moyenne du déplacement des structures minces. Pour une pression aléatoire homogène ergodique, la valeur quadratique moyenne du déplacement est exprimée en termes de densité spectrale croisée de champ de pression. La description du champ turbulent de pression est basée sur la formulation de Corcos pour la densité spectrale croisée de la fluctuation de pression. Dans le modèle de Corcos la densité spectrale croisée de la pression est formulée par le produit de la densité spectrale de puissance et de la fonction de corrélation croisée de pression aux parois. L'ajustement de courbe proposé par Lakis basé sur les mesures de Bakewell est adopté pour exprimer la densité spectrale de puissance de pression aux parois. Les intégrations exactes sur la surface et la fréquence sont effectuées analytiquement et une expression pour la valeur quadratique moyenne du déplacement est obtenue en termes de fréquences naturelles du système en

interaction avec le fluide, mode à vide, masse généralisée du système et d'autres caractéristiques de la structure et de l'écoulement. Ces expressions sophistiquées sont mises en application dans le code de calcul afin de prédire les valeurs quadratiques moyennes totales des déplacements des structures minces.

L'effet de la vitesse de l'écoulement et le taux d'amortissement sur la valeur quadratique moyenne totale des déplacements d'une plaque mince sous différentes conditions aux rives excitée par la couche limite turbulente ont été étudiés. On a constaté que la valeur quadratique moyenne totale des déplacements était inversement proportionnelle au taux d'amortissement et proportionnelle à la vitesse de l'écoulement. La valeur quadratique moyenne totale du déplacement radial d'une coque cylindrique mince a été obtenue et a été comparée favorablement à celle dans la littérature.

Les structures partiellement submergées dans le fluide peuvent être modélisées en utilisant cette méthode due au fait que la pression du fluide est individuellement calculée pour chaque élément fini. Cette méthode est plus précise que les méthodes des éléments finis conventionnelles parce que la combinaison de la théorie de coque mince et la méthode des éléments finis ont été utilisées. En outre, cette méthode n'est pas limitée à une géométrie spécifique, mais elle est capable de modéliser les structures tridimensionnelles. Elle peut également être utilisée pour modéliser des structures ayant des discontinuités dans le matériau et dans l'épaisseur. L'avantage principal de la méthode développée dans cette thèse réside dans le fait que la valeur quadratique moyenne totale du déplacement des structures minces peut être prédite ainsi que la densité spectrale de puissance de la réponse.

ABSTRACT

Thin shell structures subjected to stationary fluid or turbulent flow are found everywhere in practical engineering applications. The presence of quiescent fluid in the vicinity of a shell has an important influence on the dynamic behavior of the structure, causing a significant decrease in natural frequencies and affecting dynamic stability of the system. Much research effort has been carried out to study axisymmetric structures however few studies have dealt with three-dimensional structures such as elastic rectangular reservoirs and turbine blades in contact with stationary fluid.

Turbulent boundary-layer-induced random pressure is a frequent source of excitation and can cause low-amplitude vibration leading to fatigue failures of the structures involved. Therefore, determination of the response of structures subjected to turbulent boundary layer pressure fields is important. While a great volume of works in the literature have been dedicated to the investigation of pressure fluctuations beneath a turbulent boundary layer as well as auto spectral density of the response of a plate due to turbulent flow, less research has been devoted to calculating the total root mean square displacement response of thin plate and shell structures.

In the first phase of this thesis a model was developed in order to predict dynamic behavior of three-dimensional thin curved structures in a vacuum and in contact with inviscid incompressible stationary fluid. The finite element approach used in this study was obtained by combining classic thin plate theory and finite element

analysis, in which the finite elements are rectangular four-noded flat shells with five degrees of freedom per node. The equilibrium equations were derived from Sanders' thin shell theory. The in-plane displacements are assumed to be bilinear polynomials. The out-of-plane displacement is approximated by an exponential function which is a general solution of equilibrium equations. The structural mass and stiffness matrices are determined by exact integration using finite element analysis. The predicted natural frequencies of a rectangular reservoir and a blade in a vacuum compared well with those obtained using ANSYS.

This method may easily be adapted to take hydrodynamic effects into account. Moreover, it is able to compute both high and low frequencies with high accuracy which is of considerable importance for determining the response of structures subjected to random pressure fields such as those generated by turbulent flow.

The stationary fluid pressure exerting on each finite element is calculated using the potential flow theory, Bernoulli's equation and an impermeability condition. This fluid pressure is expressed as a function of the acceleration of the normal displacement of the structure, the fluid density and the boundary conditions of the fluid. An analytical integration of the product of the fluid pressure and shape function over the element surface produces the inertial force of the fluid and is interpreted as the virtual added-mass of fluid. The natural frequencies of a fluid-filled rectangular reservoir were analyzed using our method and compared well with those obtained using ANSYS. This method was successfully applied to predict dynamic behavior of a rectangular tank partially filled with fluid as well as a submerged blade. An in-house program was

developed in order to calculate natural frequencies and mode shapes of three dimensional thin structures in a vacuum and in contact with quiescent fluid

In the final phase of this thesis, a method capable of predicting the response of a thin structure subjected to an arbitrary random pressure field as well as a turbulent boundary-layer-induced random pressure in subsonic flow is presented. A numerical approach based on the aforementioned method is proposed to obtain total root mean square displacements of thin structures. For an ergodic homogenous random pressure fluctuation, mean square displacement response is expressed in terms of cross spectral density of the pressure field. Description of the turbulent pressure field is based on the Corcos formulation for the cross spectral density of pressure fluctuation. In the Corcos model the cross spectral density of the pressure is formulated as the product of the power spectral density of the pressure and the wall-pressure cross correlation function. Lakis' curve fit based on Bakewell's measurements in pipe airflow is adopted to express wall-pressure power spectral density. Exact integrations over surface and frequency are carried out analytically and an expression for the mean square displacement response is obtained in terms of the wetted natural frequencies, undamped mode shapes in a vacuum, generalized mass of the system and other characteristics of the structure and flow. These sophisticated expressions are incorporated into the in-house program to predict the total root mean square displacement response of thin structures.

The effect of free stream velocity and damping ratio on total root mean square displacements of a thin plate under different boundary conditions excited by a turbulent

boundary layer were investigated. It was observed that the total root mean square displacement response was inversely proportional to damping ratio and directly proportional to free stream velocity. The total root mean square radial displacement of a thin cylindrical shell was obtained and it compared favorably with that in the literature.

Structures partially submerged in fluid can be modeled using this method due to the fact that fluid pressure is individually calculated for each finite element. This method is more accurate than conventional finite element methods because a combination of classic thin shell theory and the finite element method were employed. Furthermore, the method is not limited to a specific geometry but is extended to analyze three dimensional structures. It can also be used to model structures with discontinuities in material properties and thickness. The key advantage of the method developed in this thesis is that the total root mean square displacement response of thin structures can be predicted along with the power spectral density of the response.

CONDENSÉ EN FRANÇAIS

Introduction

Les coques minces soumises au fluide au repos ou en écoulement turbulent ont un champ d'application large dans pratiquement plusieurs domaines de l'industrie moderne. La présence du fluide au voisinage d'une structure a une influence importante sur son comportement dynamique et cause une chute significative de fréquence naturelle et peut endommager la structure. L'instabilité hydroélastique due au fluide stationnaire peut causer la vibration de haute amplitude dans la structure et peut rapidement avoir comme conséquence l'échec catastrophique. Par contre, la pression aléatoire induite par une couche limite turbulente pleinement développée peut causer la vibration de basse amplitude et peut mener par la suite à la défaillance de fatigue structurale. En conséquence, la détermination des caractéristiques dynamiques de ces structures soumises au fluide stationnaire ou en écoulement turbulent induite par la couche limite est d'intérêt considérable.

Le premier problème qui doit d'abord être résolu afin de prédire l'amplitude de vibration des structures minces dues aux pressions aléatoires induites par couche limite turbulente est de modéliser précisément le comportement dynamique de telles structures en contact avec le fluide stationnaire. Des caractéristiques dynamiques de ces structures sont nécessaires comme entrées pour déterminer la réponse structurale due à l'écoulement turbulent.

L'examen de la littérature passée a indiqué qu'un volume considérable d'études a été consacré à analyser les coques cylindriques minces en contact avec le fluide au repos. Divers éléments tels que les éléments longitudinaux et circonférentiels ont été développés pour les coques cylindriques, coniques et sphériques fermées et ouvertes à vide ou contenant un fluide stationnaire. En outre, un grand nombre de publications existent au sujet de la plaque partiellement ou totalement submergée dans le fluide et donc plusieurs différentes approches ont été adoptées pour décrire l'interaction fluide-structure. Bien que des structures tridimensionnelles de coque soient largement rencontrées dans la technologie pratique, très peu de littérature existe pour analyser de telles structures couplées au fluide en tant que réservoir rectangulaire flexible partiellement ou complètement rempli de fluide ou de l'aube de turbine submergée dans fluide stationnaire. Par conséquent, la nécessité d'une méthode pour modéliser correctement le comportement dynamique des structures minces courbées en contact avec le fluide au repos surgit.

Au-delà du problème mentionné ci-dessus, la vibration induite par l'écoulement turbulent doit être adressée. Un grand volume d'études expérimentales et théoriques dans la littérature a été consacré à l'investigation de fluctuation de pression sous une couche limite turbulente. Les investigations théoriques se sont appliquées à comprendre comment des fluctuations de pression sur la paroi dans une couche limite turbulente relèvent des fluctuations turbulentes de vitesse, alors que les études expérimentales se sont principalement concentrées pour mesurer la fonction de corrélation croisée de pression et la densité spectrale de puissance. Les caractéristiques d'une couche limite

turbulente, telles que la densité spectrale de puissance de la pression et les fonctions de corrélation croisée ont été intensivement étudiées et bien établies. En outre, beaucoup d'efforts de recherches ont été investis pour évaluer la densité spectrale de puissance de la réponse d'une plaque due au champ turbulent de pression de couche limite, mais aucune tentative pour calculer la valeur quadratique moyenne totale du déplacement n'a été réalisée. Dans l'étude de la littérature, il s'avère que les travaux pour prévoir la valeur quadratique moyenne totale du déplacement des coques cylindriques minces aux pressions aléatoires sous la couche limite turbulente sont rares. Par exemple, une recherche a été effectuée par Lakis et Païdoussis pour déterminer la valeur quadratique moyenne totale du déplacement des coques cylindriques; cependant, leur travail s'est limité aux formes cylindriques puisque l'élément fini cylindrique a été utilisé.

À notre meilleure connaissance, aucun traitement exact de la valeur quadratique moyenne totale du déplacement d'une plaque mince excitée par une couche limite turbulente n'a été accompli jusqu'à présent. Dans les études analytiques précédentes menées sur la vibration induite par l'écoulement turbulent, les structures étaient généralement plaque ou cylindre et les forces d'excitation étaient généralement purement aléatoires. La plupart du temps, quelques hypothèses de simplification ont été adoptées afin de prévoir la réponse, telle que considérer la densité spectrale de puissance de la pression d'unité ou de négliger les effets de couplage de fluide-structure. Par conséquent, pour pouvoir traiter des géométries plus complexes de coque et des champs aléatoires plus réalistes de pression, développer une méthode pour prévoir la valeur quadratique moyenne du déplacement est souhaitable. Le premier

objectif de cette thèse est de modéliser le comportement dynamique des coques minces tridimensionnelles soumises au fluide non visqueux incompressible stationnaire. Le deuxième objectif est de prédire la valeur quadratique moyenne du déplacement d'une structure mince soumise à un champ aléatoire arbitraire de pression et subséquemment à un champ de pression résultant d'une couche limite turbulente dans l'écoulement subsonique.

Méthode

Une méthode générale afin de modéliser une structure courbée élastique mince à vide et soumise au fluide au repos est développée. Dans cette approche, l'élément fini structurel a été développé en utilisant une combinaison de la théorie de coque mince et de la méthode des éléments finis dans laquelle les éléments finis sont la coque rectangulaire plate avec cinq degrés de liberté par nœud.

Les effets de membrane et de flexion sont pris en compte simultanément dans cette méthode. Des éléments coques sont développés en superposant la rigidité de la membrane et la flexion des éléments. On assume que la solution des déplacements de membrane est un polynôme bilinéaire. Le déplacement transversal est approché par une fonction exponentielle ayant la forme générale de la solution exacte des équations d'équilibre de coque mince. Les matrices de masse et de rigidité sont déterminées par intégration analytique exacte en se basant sur la méthode des éléments finis. La transformation géométrique entre les coordonnées globales et locales s'impose afin de

produire les matrices élémentaires de la masse et de rigidité dans un repère global. La matrice de transformation pour le déplacement nodal de l'élément est établie en utilisant des cosinus directeurs (pour modéliser la structure courbée telle que l'aube de turbine) ou deux rotations successives autour des axes x et y (pour modéliser le réservoir). Cette transformation augmente le nombre de degrés de liberté. Le problème de singularité numérique surgit à cause de l'absence de la rigidité de rotation correspondant au sixième degré de liberté. La singularité numérique est résolue en insérant une rigidité et une masse fictives faibles aux termes diagonaux correspondant à ce degré de liberté dans chaque nœud de l'élément fini.

Puisque la fonction transversale de déplacement est dérivée de la théorie de coque mince, cette méthode peut être facilement adaptée pour tenir compte des effets hydrodynamiques. Le potentiel de vitesse, l'équation de Bernoulli et la condition d'imperméabilité sont utilisés pour déterminer la pression de fluide appliquée sur la structure. La pression du fluide est exprimée en fonction de l'accélération du déplacement transversal de l'élément, de la masse volumique du fluide et des conditions aux limites du fluide (mur rigide, surface libre, etc.). Une intégration analytique du produit de la pression hydrodynamique et du champ de déplacement de la structure sur l'interface de fluide-structure produit la force d'inertie du fluide et est interprétée comme une masse ajoutée virtuelle du fluide stationnaire.

Cette méthode est employée pour étudier le comportement dynamique des structures élastiques minces partiellement ou totalement remplies de ou submergées dans le fluide stationnaire. Un code de calcul est développé pour obtenir des fréquences

naturelles, des modes de la structure à vide et en contact avec le fluide stationnaire. Les caractéristiques dynamiques de la structure à vide et en interaction avec le fluide au repos sont nécessaires comme entrées pour évaluer la réponse de la structure aux fluctuations de pression dans l'écoulement turbulent. On propose une approche analytique-numérique afin de déterminer la magnitude de la réponse des structures minces due au champ de pression aléatoire induite par une couche limite turbulente. Premièrement, la structure à vide et en contact avec le fluide stationnaire a été analysée en se basant sur la méthode développée dans la première phase de cette thèse puisque les valeurs propres, les vecteurs propres et d'autres caractéristiques du système étaient nécessaires comme entrées aux calculs aléatoires. Les déplacements nodaux de la structure sont exprimés en termes de coordonnées généralisées et matrice modale en utilisant la base modale. Des équations d'équilibre sont découplées en supposant que l'amortissement structural est linéairement lié aux matrices de la masse et de la rigidité. Nous supposons que le fluide est non visqueux donc les fluctuations de pression du fluide sont normales sur la surface de la coque. Le champ de fluctuation aléatoire de pression sur la surface de l'élément de coque est translaté à une force latérale équivalente agissant à un point arbitraire par l'intégration sur la surface. Cette force latérale est alors rapprochée par un ensemble de force discrète et de moments agissant à chaque nœud de l'élément fini. Puisque la couche limite turbulente est intrinsèquement aléatoire, on doit utiliser les propriétés statistiques de l'écoulement turbulent pour obtenir l'amplitude de vibration. Nous supposons que le processus aléatoire est ergodique et que la fluctuation aléatoire de pression est homogène. Par conséquent, la

valeur quadratique moyenne du déplacement peut être exprimée en termes de la densité spectrale croisée du champ de pression. Le modèle de Corcos pour la densité spectrale croisée des fluctuations de pression est adopté pour décrire le champ turbulent de pression. Dans le modèle de Corcos, la densité spectrale croisée de la pression est formulée par le produit de la densité spectrale de puissance et la fonction de corrélation croisée de pression aux parois. L'expression proposée par Lakis, basée sur les mesures de Bakewell dans le flux d'air d'une pipe, est employée pour décrire la densité spectrale de puissance de pression. Corcos a postulé que la fonction de corrélation croisée pourrait être représentée par le produit des fonctions de corrélation latérale et longitudinale. Les corrélations longitudinale et latérale dans le modèle de Corcos sont présentées par une fonction oscillante exponentielle décroissante dans le sens de l'écoulement et par une fonction exponentielle décroissante simple dans la direction de croisement de flux respectivement. Il faut mentionner que différentes expressions empiriques pour différentes structures ont été suggérées pour des corrélations longitudinale et latérale aussi bien que la densité spectrale de puissance; cependant, ces expressions sont approximativement identiques.

Les expressions de la densité spectrale de puissance de pression, des corrélations longitudinales et latérales sont introduites dans l'expression de la valeur quadratique moyenne du déplacement. Les intégrations exactes sur la surface et la fréquence sont effectuées analytiquement et une expression pour la valeur quadratique moyenne du déplacement est obtenue en termes de fréquences naturelles du système en interaction avec le fluide, mode à vide, masse généralisée du système et d'autres

caractéristiques de la structure et de l'écoulement. Ces expressions sophistiquées sont mises en application dans le code de calcul afin de prévoir les valeurs quadratiques moyennes totales des déplacements des structures minces.

Résultats

Sur la base de l'analyse dans la première phase de cette thèse, des fréquences naturelles d'un réservoir rectangulaire élastique à vide et complètement rempli de fluide sont calculées par le code de calcul développé à cette fin. Les trois premières fréquences d'un réservoir rectangulaire simplement supporté à vide et totalement rempli de fluide sont calculées en utilisant notre méthode et favorablement comparées avec ANSYS. Des variations de fréquence en fonction de variation de niveau du fluide pour le même réservoir sous deux différentes conditions aux rives ont été étudiées. Les résultats obtenus montrent que les fréquences diminuent lorsque le niveau de remplissage augmente; cependant, on observe différents comportements des fréquences sous différentes conditions aux rives de réservoir. L'effet de la profondeur du liquide sur les trois premières fréquences d'un réservoir avec un cœur rigide et deux parois parallèles simplement supportées est étudié. On observe que l'influence du fluide en-dessous de 1/4 du remplissage partiel sur les deux premières fréquences est insignifiante mais ensuite le réservoir subit un changement substantiel des fréquences pour tous les modes entre 1/4 et 3/4 de remplissage. Les fréquences de tous les modes demeurent presque constantes en augmentation de niveau de liquide entre 3/4 et 1. Pour

un réservoir simplement supporté, la première fréquence diminue rapidement de la gamme de 0 à 1/4 et puis l'effet du fluide devient insignifiant. Pour les deuxième et troisième fréquences, une réduction substantielle est observée sur la gamme de 0 à 3/4 et après les fréquences sont presque constantes.

Pour démontrer l'applicabilité de la méthode proposée, une aube encastrée-libre à vide et submergée dans le fluide est étudiée. Des fréquences naturelles de l'aube à vide ont été obtenues et comparées favorablement avec celles obtenues par ANSYS. Le niveau du fluide au-dessus et sous l'aube aussi bien que les conditions aux limites du fluide (c.-à-d. la surface libre, le mur rigide ou l'objet élastique) affectent le comportement dynamique de l'aube jusqu'à ce qu'une certaine hauteur de fluide soit atteinte. Pour clarifier ce phénomène, des variations des trois premières fréquences en fonction des variations de la hauteur de fluide au-dessus et sous l'aube sont étudiées individuellement. La condition limite supérieure de fluide est une surface libre et la limite inférieure est un mur rigide. Nous avons constaté que pour une aube loin d'un mur rigide, lorsque la hauteur de fluide au-dessus de l'aube augmente, les fréquences diminuent; cependant, cette réduction cesse lorsque le rapport de la hauteur du fluide sur la longueur d'aube atteint 50 %. En revanche, pour une aube loin d'une surface libre, les fréquences augmentent en augmentant la hauteur de fluide sous l'aube, mais cette augmentation s'arrête quand le niveau du fluide atteint 50 % de la longueur de l'aube. Il est également important de noter que les structures avec différentes conditions aux rives se comportent différemment sous l'influence du fluide; donc le niveau du fluide auquel la fréquence cesse de changer diffère d'une structure à l'autre.

Dans la deuxième phase de cette thèse, la valeur quadratique moyenne du déplacement radial d'une plaque mince sous différentes conditions aux rives excitée par une couche limite turbulente a été étudiée. La réponse totale a été obtenue par sommation sur des modes significatifs de vibration et puis le maximum de valeur quadratique moyenne totale de déplacement radial de la plaque a été calculé. Les résultats montrent que les valeurs quadratiques moyennes de déplacements radiaux étaient faibles, comme prévu. Afin de démontrer le comportement des valeurs quadratiques moyennes de la réponse, les déplacements de membrane sont également étudiés. Comme prévu, les déplacements de membrane de la plaque sont minimaux.

On a observé que la valeur quadratique moyenne du déplacement de la plaque est directement proportionnelle à la vitesse de l'écoulement et inversement proportionnelle au taux d'amortissement de la structure. Le même comportement a été constaté pour la plaque sous différentes conditions aux rives de la plaque et de l'écoulement. Nous notons que les basses fréquences naturelles contribuent de manière significative à la réponse et comme la fréquence naturelle augmente, la réponse devient insignifiante rapidement.

Les effets de l'écoulement turbulent d'un et des deux côtés de plaque sur la valeur quadratique moyenne du déplacement radial ont été étudiés et des réponses plus élevées dans le cas de la plaque submergée dans l'écoulement étaient obtenues dues aux plus basses fréquences et à une plus grande masse ajoutée virtuelle. Aucune étude des effets d'une couche limite turbulente sur le déplacement radiale d'une plaque mince n'a été documentée, ceci empêche la validation de la plaque mince à un tel champ aléatoire

de pression. À notre meilleure connaissance, il n'y avait aucune référence dans la littérature pour la valeur quadratique moyenne totale du déplacement d'une plaque ou d'une structure courbée ouverte soumise à une telle pression aléatoire. La validation de la méthode développée a été faite en comparant les résultats obtenus pour une coque cylindrique simplement supportée avec ceux calculés par Lakis et Païdoussis. Ils ont calculé la valeur quadratique moyenne totale du déplacement radial au mi-point axial par sommation des résultats correspondants aux modes circonférentiels 2 à 6. D'abord, des fréquences naturelles ont été calculées en utilisant la méthode développée dans la première partie de cette thèse et nous avons constaté qu'il y a des fréquences correspondant au mode comportement-poutre (n=1), qui n'a pas été pris en considération dans le travail de Lakis. Il convient de noter que dans le cas d'un cylindre long, quelques fréquences correspondantes au mode n=1 sont les plus basses fréquences du système. La valeur quadratique moyenne totale du déplacement radial au mi-point axial d'une coque cylindrique simplement supportée a été calculée en utilisant notre méthode et a été comparée à celle obtenue par Lakis. On a constaté que les réponses prédites sont du même ordre mais plus hautes que celles obtenues par Lakis et Païdoussis. Cette différence est attribuée aux basses fréquences naturelles du système correspondant au mode comportement-poutre qui ont été incluses dans notre méthode. Bien que différentes expressions pour des corrélations aient été adaptées dans la méthode développée et dans le travail de Lakis, la bonne concordance a été trouvée. Puisque les résultats obtenus par Lakis ont été validés avec les mesures expérimentales de Clinch, on conclut que notre méthode est infaillible.

En outre, les densités spectrales de puissance des déplacements membranaire et radial d'une plaque simplement supportée sur deux côtés courtes soumise à l'écoulement turbulent d'un seul côté ont été calculées. La densité spectrale de puissance est calculée au nœud auquel le maximum de valeur quadratique moyenne totale de déplacement radial a été obtenu. L'étude du spectre révèle que les crêtes des densités spectrales de puissance des déplacements se produisent aux fréquences naturelles de la plaque en contact avec le fluide stationnaire. L'enveloppe des crêtes décroît rapidement avec la fréquence. La courbe de densité spectrale de puissance est brusquement aigue aux fréquences naturelles et prouve clairement que seulement les fréquences autour du voisinage des fréquences naturelles contribuent considérablement à la réponse. On a constaté que les basses fréquences naturelles contribuent de manière significative à la densité spectrale de puissance de la réponse.

Conclusions

Dans la première partie de cette thèse, la vibration libre des coques minces tridimensionnelles à vide et au voisinage de fluide stationnaire a été modélisée. La méthode a employé une combinaison de la théorie de coque mince et la méthode des éléments finis dans lesquelles les éléments finis sont les éléments plats rectangulaires avec cinq degrés de liberté par nœud. Le potentiel de vitesse, l'équation de Bernoulli et la condition d'imperméabilité ont été utilisés pour calculer la pression du liquide stationnaire exercée sur la paroi de chaque élément fini. La pression est exprimée en

fonction de l'accélération du déplacement transversal de l'élément, de la masse volumique du fluide et des conditions aux limites du fluide (mur rigide, surface libre, etc.). Une intégration analytique du produit de la pression hydrodynamique et du champ de déplacement de la structure sur l'interface de fluide-structure produit la force d'inertie du fluide et est interprétée comme une masse ajoutée virtuelle du fluide stationnaire. Puisque la pression imposée par le fluide stationnaire a été individuellement calculée pour chaque élément fini, des structures partiellement remplies avec ou submergées dans le fluide peuvent être modélisées. D'ailleurs, cette méthode n'est pas limitée à une géométrie spécifique; par contre, elle est capable de modéliser les structures tridimensionnelles sophistiquées telles que l'aube de turbine. De plus, cette méthode est capable de calculer les hautes et les basses fréquences avec une grande précision qui est d'une importance considérable pour déterminer la réponse des structures soumises aux champs aléatoires de pression comme ceux produits par écoulement turbulent. Un code de calcul a été développé afin d'obtenir des valeurs propres et des vecteurs propres des structures tridimensionnelles à vide et en contact avec le fluide. Basé sur les résultats obtenus par la méthode développée, il peut conclure que cette méthode est fiable pour analyser le comportement dynamique des structures courbées minces tridimensionnelles en contact avec le fluide stationnaire.

Dans la deuxième partie de cette thèse, une méthode analytique-numérique capable de prédire la valeur quadratique moyenne totale du déplacement d'une structure mince à un champ aléatoire arbitraire de pression a été présentée. Ensuite, la méthode a été spécialisée pour l'application où le champ de pression provenant d'une

couche limite turbulente dans un écoulement subsonique. Dans cette approche, la formulation d'élément fini de coque mince combinée avec la méthode de la base modale et la théorie aléatoire de vibration ont été utilisées pour prédire la réponse aléatoire de vibration. Premièrement, la structure à vide et en contact avec le fluide stationnaire a été analysée, comme les valeurs propres et les vecteurs propres, et d'autres caractéristiques du système étaient nécessaires comme entrées aux calculs aléatoires. La valeur quadratique moyenne du déplacement de la structure excitée par une pression aléatoire homogène ergodique a été exprimée en termes de la densité spectrale croisée de la pression de paroi. Une expression analytique a été obtenue pour la valeur quadratique moyenne du déplacement d'une structure mince excitée par des fluctuations turbulentes de pression de couche limite en termes de fréquences naturelles du système en contact avec le fluide, des modes à vide, de la masse généralisée du système et d'autres caractéristiques de la structure et de l'écoulement. La réponse totale a été obtenue par sommation sur des modes significatifs de vibration. En outre, une expression a été développée pour prévoir la densité spectrale de puissance de déplacement de la structure excitée par l'écoulement turbulent. La solution a été incorporée au code de calcul qui détermine également les caractéristiques de vibration de la coque à vide et en contact avec le fluide au repos.

La méthode aléatoire développée dans cette thèse profite du fait que les propriétés statistiques de la pression induite par une couche limite turbulente telles que la densité spectrale de puissance de la pression de paroi, les fonctions de corrélation latérale et longitudinale sont identiques pour différentes structures. Par conséquent, la

méthode proposée est applicable pour prédire la valeur quadratique moyenne du déplacement de différentes structures. Il devrait souligner que la méthode développée dans cette thèse, contrairement aux méthodes précédentes dans la littérature, n'est pas limitée pour des plaques minces mais elle est applicable aux coques cylindriques et aux géométries plus complexes. D'ailleurs, il est capable de prédire la valeur quadratique moyenne totale du déplacement qui est rare dans la littérature. La méthode développée peut être utilisée pour étudier des structures avec des discontinuités de matériaux et d'épaisseur sous différentes conditions aux limites de structure et de fluide.

Pour les structures légèrement atténuées, les termes croisés contribuent très peu à la réponse aléatoire et sont donc négligés dans cette analyse. Cependant, des structures avec le taux d'amortissement appréciable pourraient être analysées en utilisant cette méthode, si les termes croisés sont tenus compte. La méthode développée dans cette thèse peut être utilisée afin de modéliser un système de plaques parallèles ou un canal soumis à l'écoulement potentiel. Un travail pour étudier un système de plaques parallèles et de canaux soumis à une couche limite turbulente pleinement développée est en marche. Quant au futur développement, la méthode aléatoire proposée peut être aisément prolongée pour prédire la réponse des structures minces tridimensionnelles telles qu'une aube de turbine hydraulique au champ aléatoire turbulent de pression induit par une couche limite.

TABLE OF CONTENTS

LIST OF TABLES

LIST OF FIGURES

LIST OF SYMBOLS

A	plate side length in the x-direction
A_1, A_2	constants in Eq. 2.27
B	plate side length in the y-direction
C_j	unknown constants in Eqs. 2.2, 2.3 and 2.4
$\overline{C}_r$	rth element of generalized damping matrix
$\mathrm{d}A$	element surface area in Eqs. 2.14a and 2.14b
d_i	coordinate of node i in the y-direction
d_i', d_i''	limits of the area surrounding node i in the y-direction
D	membrane stiffness $Eh/(1-\nu^2)$
E	Young's modulus
f	forced frequency in Hz
f_r	natural frequency of mode r in Hz
$F(z)$	function to be specified in Eq. 2.23
$F_A(t)$	lateral force acting at an arbitrary point
F_n	lateral force acting at node c
g	gravitational acceleration
$G_{pp}(f)$	one-sided power spectral density of pressure

$G_{pp}(x_i, y_i, x_j, y_j, f)$	one-sided cross spectral density of pressure
$G_{\delta_g \delta_g}(f)$	power spectral density of nodal displacement at node g
G_{UU}	power spectral density of in-plane displacement in the x-direction
G_{VV}	power spectral density of in-plane displacement in the y-direction
G_{WW}	power spectral density of radial displacement
h	shell thickness
h_1	height of fluid over the plate in Eq. 2.32, and height of fluid over an arbitrary element of the blade in Eq. 2.36
h_2	distance between two parallel plates in Eq. 2.34, and height of fluid under an arbitrary element of the blade in Eq. 2.36
$H_r(f)$	frequency response function for the rth mode
$\lvert H_r(f) \rvert$	magnification factor for mode r
i	complex number $\mathrm{i}^2 = -1$
K	bending stiffness $Eh^3/12(1-\nu^2)$
$\bar{K}_r$	rth element of generalized stiffness matrix
l_i	coordinate of node i in the x-direction
l_i', l_i''	limits of the area surrounding node i in the x-direction

$\bar{M}_r$	rth element of generalized mass matrix
M_x	moment in the x-direction acting at node c
M_y	moment in the y-direction acting at node c
n	number of nodes
N	number of mode shapes chosen for analysis
P	hydrodynamic pressure at the wall of the shell
P_{ij}	elasticity matrix components defined by Eq. 2.12
$P(x,y,t)$	turbulent boundary layer pressure on the surface
$P(x,y,f,T)$	Fourier transform of pressure
$q_r(t)$	generalized coordinate of mode r
$Q_r(f,T)$	Fourier transform of rth generalized coordinate
Re	Reynolds number
S_c	area surrounding node c
$S(x,y,t)$	function to be specified in Eq. 2.23
S_{ξ_x}, S_{ξ_y}	Strouhal numbers define by Eqs. 3.22c and 3.22d
t	time
T	time period
U	in-plane displacement of the shell reference surface in the x-direction
U_c	convection velocity of flow

U_{cl}	centerline velocity of flow
U_x	unperturbed flow velocity along the shell in the x-direction
U_∞	free stream velocity
V	in-plane displacement of the shell reference surface in the y-direction
V_x, V_y, V_z	perturbation fluid velocities in the x-, y- and z-directions, respectively
W	out-of-plane displacement of the shell reference surface
$\partial W/\partial x$, $\partial W/\partial y$	first derivatives of transverse displacement with respect to x and y
$\partial^2 W/\partial x\partial y$	crossed derivative of transverse displacement with respect to x and y
x_e, y_e	element dimensions in the x- and y-directions, respectively
Z_f	coefficient defining fluid-structure contact model

Greek Symbols:

α_x, α_y	empirically determined constants
Γ	functions in terms of characteristics of structure and flow in Eq. 3.26
Γ_{iu}	a complicated function given in Appendix A

δ	boundary layer thickness
δ^*	boundary layer displacement thickness
Δ	Fourier transform of nodal displacement
ε_x	normal strain of reference surface in the x-direction
ε_y	normal strain of reference surface in the y-direction
$2\varepsilon_{xy}$	in-plane shear strain of reference surface
ζ_r	generalized damping ratio of mode r
θ_x	rotation about x-axis defined by Eq. 2.16
θ_y	rotation about y- axis defined by Eq. 2.16
$\theta_r(f)$	phase factor of mode r
κ_x, κ_y	changes in curvature of the reference surface
κ_{xy}	torsion of the reference surface
μ	constant defined by Eq. 2.26
ν	Poisson's ratio in Eq. 2.13, and kinematic viscosity in Reynolds number
ξ_x	streamwise distance
ξ_y	spanwise distance
ρ_f	density of fluid
ρ_s	density of shell

τ	time delay
$\phi(x,y,z,t)$	velocity potential function
$\Psi(\xi_x,\xi_y,0)$	cross correlation function
$\Psi(\xi_x,0,0)$	streamwise spatial correlation function
$\Psi(0,\xi_y,0)$	spanwise spatial correlation function
ω	radian natural frequency of shell

List of vectors and matrices:

$[\mathbf{A}]^{-1}$	matrix (20 × 20) given in Appendix 2.8
$[\mathbf{B}]$	matrix in Eq. 2.10 $[\mathbf{Q}][\mathbf{A}]^{-1}$
$[\mathbf{C}_f]$	total Coriolis force induced by potential flow
$[\mathbf{C}]$	global damping matrix of the system
$\{\mathbf{F}(x,y,t)\}$	external load vector in Eq. 3.1
$\mathbf{F}(f,T)$	Fourier transform of force vector
$\{\mathbf{F}\}_e$	fluid-induced force vector for one finite element
$[\mathbf{K}]$	global stiffness matrix of the system
$[\mathbf{K}]_e$	element stiffness matrix in local coordinate
$[\mathbf{K}_s]$	global stiffness matrix of the shell in a vacuum
$[\bar{\mathbf{K}}]$	generalized stiffness matrix $\mathbf{\Phi}^T\mathbf{K}\mathbf{\Phi}$
$[\mathbf{K}_f]$	total centrifugal force induced by potential flow

$[\mathbf{M}]$	global mass matrix of the system
$[\mathbf{M}]_e$	element mass matrix in local coordinates
$[\mathbf{M_f}]_e$	fluid virtual added mass matrix of one finite element
$[\mathbf{M_f}]$	total inertial force induced by potential flow
$[\mathbf{M_s}]$	global mass matrix of the shell in a vacuum
$[\bar{\mathbf{M}}]$	generalized mass matrix $\mathbf{\Phi}^{\mathrm{T}}\mathbf{M}\mathbf{\Phi}$
$[\mathbf{N}]$	shape function of the finite element $[\mathbf{R}][\mathbf{A}]^{-1}$
$[\mathbf{P}]$	elasticity matrix (6×6)
$\{\mathbf{q}(t)\}$	generalized coordinate
$[\mathbf{Q}]$	matrix (6 × 20) given in Appendix 2.8
$[\mathbf{R}]$	matrix (3 × 20) given in Appendix 2.8
$[\mathbf{R_f}]$	matrix (3 × 20) given in Appendix 2.8
$\{\boldsymbol{\delta}\}$	nodal displacement vector of an element given in Eq. 2.7, and global displacement vector defined by Eq. 3.3
$\{\dot{\boldsymbol{\delta}}\}$	global velocity vector in Eq. 3.1
$\{\ddot{\boldsymbol{\delta}}\}$	global acceleration vector in Eq. 3.1
$\{\boldsymbol{\delta}_g\}$	nodal displacement vector at node g
$\overline{\boldsymbol{\delta}_g^2(x_g, y_g, t)}$	mean square displacement response at node g
$\{\boldsymbol{\delta}_{\mathrm{T}}\}$	displacement vector of the whole structure in Eq. 2.41

$\{\dot{\boldsymbol{\delta}}_T\}$	velocity vector of the whole structure in Eq. 2.41
$\{\ddot{\boldsymbol{\delta}}_T\}$	acceleration vector of the whole structure in Eq. 2.41
$\{\boldsymbol{\varepsilon}\}$	strain vector
$\{\boldsymbol{\sigma}\}$	stress vector
$\{\boldsymbol{\Phi}\}$	eigenvector
$[\boldsymbol{\Phi}]$	modal matrix
$\boldsymbol{\Phi}_{gr}(x, y)$	rth mode shape at node g

Superscript:

*	complex conjugate operator
T	matrix transpose operator
∇^2	Laplace operation

LIST OF ABBREVIATIONS

2D	two-dimensional
3D	three-dimensional
CSD	cross spectral density
PSD	power spectral density
r.m.s.	root mean square
CFCF	clamped-free-clamped-free plate
CFFF	clamped-free-free-free plate
SFSF	simply supported-free-simply supported-free plate

CHAPTER I

INTRODUCTION AND LITERATURE REVIEW

1.1 Overview

Thin shells have wide applications in practically every type of modern industrial structure such as skins of a fuselage in aerospace, hulls of ships in marine applications and walls of nuclear containment vessels. These widely used structures are commonly subjected to excitation forces such as those due to wind, ocean waves and turbulence, which are inherently random. The presence of fluid in the vicinity of a shell has an important influence on the dynamic behavior of the structure and can cause damage to the structure. Fluidelastic instability has large-amplitude vibration and can result in rapid failure. Accordingly, determination of the dynamic characteristics of these structures when subjected to either stationary fluid or flowing fluid is of considerable interest.

Random pressure induced by a fully-developed turbulent boundary layer is a frequent source of excitation which can cause low-amplitude vibration and eventual fatigue failures of the structures involved. For this reason, determination of the response of structures subjected to turbulent boundary layer pressure fields is of

importance. Such small amplitudes are mainly of concern for fatigue considerations and must be below acceptable levels. The reliability of a product can be improved by predicting the dynamic response.

To predict the vibration amplitude of thin structures due to turbulent boundary-layer-induced random pressure fields, one must have a comprehensive understanding of fluid-structure interaction. Dynamic characteristics of such structures in contact with stationary fluid are needed as an input to determine the root mean square displacement of the structure.

Turbulent flow-induced vibration has received considerable research attention, mainly because of the need to optimize designs of power plants and reactors. Most of the studies in the literature are devoted to investigating pressure fluctuations beneath a turbulent boundary layer. A literature survey reveals that studies of the root mean square displacement response of thin shell structures to random pressure fields arising from a fully-developed turbulent boundary layer are scarce.

This thesis is concerned with the development of a method to predict the root mean square displacement response of thin shells subjected to a turbulent boundary-layer-induced random pressure field in subsonic flow. This research work is twofold; first, dynamic behavior of a three-dimensional thin shell structure in contact with stationary fluid is addressed. Then vibrational amplitude of a thin structure subjected to random pressure field arising from a turbulent boundary layer in subsonic flow is studied.

1.2 Literature review

An overview of three research areas relevant to this study is presented. First, linear free vibration of thin shell structures in contact with inviscid incompressible stationary fluid is reviewed. Secondly, response of structures subjected to a random force field is discussed, and finally response of thin structures to a turbulent boundary-layer-induced random pressure field is considered.

1.2.1 Thin shell structures in contact with quiescent fluid

As a structure vibrates in a fluid at rest, the fluid is set into motion. As a consequence the fluid contributes its own stiffness and mass to that of the structure. The stiffness of a quiescent fluid is negligible whereas the mass of fluid is added to the structure and reduces the natural frequency of the system. In other words, the natural frequencies of structures which are in contact with a fluid decrease substantially, compared to those of the corresponding dry modes due to the increased kinetic energy of the total system. This phenomenon has been investigated by many researchers working in aerospace, marine and reactor technologies. Early investigations in fluid-structure interaction fields can be found in the works of Lord Rayleigh [1] and Lamb [2]. The response of shell structures immersed in or conveying flowing fluid has been extensively studied and general reviews of the literature have been given by Païdoussis

[3]. Recent books by Païdoussis provide a comprehensive treatment of the subject as well as a complete bibliography of all important works in the field [4, 5]. Methods for describing fluid-structure interaction have been studied theoretically by Axisa [6]. Numerical modeling of linear vibrations of elastic structures coupled with internal fluids, such as hydroelasticity has been described by Morand [7]. Numerical [8, 9] and analytical [10-12] studies of the linear vibrations of elastic structures coupled with fluid have been carried out by researchers.

There are many ways in which the presence of fluid in the vicinity of a shell affects the dynamic behavior of the structure. In many investigations geometrical non-linearity, free surface effect (sloshing) and compressibility of the fluid have been taken into consideration. Sloshing modes for a liquid-filled cylindrical and rectangular tank have been analytically and numerically investigated by several researchers [12-17]. The effect created by compressibility of the fluid has been taken into account in many analytical and numerical research works [18-20]. However, here we concentrate on linear vibration of thin shells in contact with inviscid incompressible fluid and free surface effects are not considered. The effect of a stationary fluid on the dynamic behavior of the structure can be taken into account by considering the hydrodynamic mass, which is added to the mass of the structure.

A considerable body of literature exists on analyzing thin cylindrical shells in contact with quiescent fluid. Various elements such as longitudinal and circumferential elements have been developed for closed and open cylindrical [21-23], conical [24] and spherical [25] shells in a vacuum or containing a stationary fluid. For example, Lakis

and Païdoussis [21] studied the free vibration of a cylindrical shell partially filled with liquid using a combination of finite element method and classic shell theory by employing a circumferential element. This element is capable of analyzing cylindrical shells with axial variations in properties. Following this, Selmane and Lakis [26] developed a longitudinal element to study open cylindrical shells with discontinuities of material and thickness in the circumferential direction. Lindholm et al [27] analyzed the vibrations of thin shells partially filled with liquid for the case of unpressurized cylindrical shells. Free vibration analysis of cylindrical storage tanks with axial thickness variation and partially filled with inviscid incompressible liquid was studied by Han and Liu using Flügge's thin shell theory [28]. They solved the partial differential equations using the transfer matrix technique. Jain [29] predicted the vibration response of an orthotropic cylindrical shell filled with incompressible fluid. Amabili and Dalpiaz [30] developed an analytical approach to model horizontal cylindrical shells partially or completely filled with fluid. Mistry and Menezes [31] modeled a cylindrical shell partially filled with incompressible viscous fluid using two-node axisymmetric shell finite elements and eight-node isoparametric axisymmetric fluid elements. Dynamic behavior of a cylindrical shell partially filled or surrounded was investigated analytically by Jeong and Lee [32] using Stokes' transformation and Fourier series expansion.

Numerous studies exist for the case of plates in contact with fluid. A large number of publications exist on the subject of plates partially or totally immersed in fluid. Several different approaches have been adopted to describe the fluid actions.

Lindholm et al [33] used a strip theory approach and compared the theoretical predictions of resonance frequencies with measured data obtained for a series of cantilevered rectangular plates vibrating in still water. Fu and Price [34] adopted a combination of the finite element method and the singularity distribution panel approach to study vibration response of cantilevered plates partially or totally immersed in fluid. Soedel and Soedel [12] presented an analytical solution for a simply supported plate carrying a free surface liquid with reservoir conditions at the edges. Dynamic response of submerged plates with various boundary conditions was studied analytically and experimentally by Haddara and Cao [35]. They suggested an analytical added mass factor as a function of the height of the free surface and the depth of fluid under the plate. Recently, Ergin and Uğurlu [36] investigated linear vibration of cantilever plates partially submerged in inviscid incompressible fluid using a combination of image and boundary-integral equation methods.

Review of past literature has revealed that a considerable volume of studies have been devoted to analyzing the hydroelastic behavior of plates and cylindrical shells. Although three-dimensional shell structures are widely encountered in practical engineering, very little literature exists on analyzing such structures coupled with fluid, such as rectangular tanks partially or completely filled with fluid or a turbine blade. In most of these works some simplifications are applied to enable treatment of a 3D rectangular reservoir using 2D modeling, such as considering two parallel walls and the bottom of a tank as rigid walls [37, 38], considering an elastic bottom in a tank with rigid walls [39, 40] or assuming a tank with infinite width [41]. Kim, Koh and Kwahk

[37] presented an analytical solution to study dynamic behavior of a rectangular reservoir partially filled with fluid using the Rayleigh-Ritz method. However, in their study only one pair of walls is assumed to be flexible while the other pair and bottom remain rigid, which is similar to the case of two parallel plates. Kim and Lee [38] investigated hydroelastic analysis of a rectangular tank completely filled with liquid using NASTRAN program and compared results with analytical solutions. In their study, they considered the tank as two parallel plates because it was composed of a rigid bottom and two parallel walls. Bauer [39] studied the hydroelastic behavior of an elastic base in a rectangular reservoir with rigid walls. Cheung and Zhou [40] investigated the vibratory characteristics of an elastic rectangular plate placed at the bottom of a rigid tank using an analytical-Ritz method. Bauer and Eidel [41] conducted research on a two-dimensional rectangular container of infinite width partially covered with an elastic plate (beam) and partially filled with fluid.

1.2.2 Structures subjected to random force fields

A brief review of linear structural response due to general random pressure fields is given here, and in the subsequent section we concentrate on linear structural response to random pressure fields originating from a turbulent boundary layer.

Several methods for determining the response of beams and plates to general random pressure fields have been developed [42-44]. Early contributions in this area

dealt mainly with beams and plates. Dyer [42] studied analysis of the vibratory response of a plate exposed to a relatively simple random pressure field. The linear response problem of damped beams and plates under stochastic loading was dealt with by Eringen [43]. He evaluated cross-correlations of displacements and stresses for a white noise random load with a constant power spectral density at all frequencies. However, a review of engineering problems reveals that the actual power spectral density exhibits a peak. Wagner and Baht [45] studied the linear response of a plate to a random load. They were able to calculate the mean square acceleration of the plate. Stanisic [46] developed a technique to determine the spectral density of a transverse displacement of a plate. Lindberg and Olson [47] were the first to use the finite element method for random response analysis of a multi-bay panel system. Afterward, a consistent finite element method for the random response analysis of complex structures was presented by Olson [48]. He computed the response of a five-bay continuous beam. A number of methods are available in the literature for predicting the response of structural elements to random excitation. For example, Powell [49] introduced the notion of an acceptance integral method for estimating the root mean square response of a structure excited by a random forcing function. More recently, Elishakoff and Zhu [50] developed an improved finite element formulation for beams subjected to stationary random loading.

As for shell structures, the problem of random response is more complicated because of the nature of the excitation and the multiplicity of natural modes in the frequency range of interest. The first study of cylindrical shells excited by a random

pressure field was carried out by Cottis and Jasonides [51]. They developed a general mathematical theory for simply-supported uniform thin cylindrical shells based on Reissner's simplified shallow shell equations of motion. They derived an expression for the space-time correlation function of the radial displacement of a thin cylinder due to a purely random pressure field. This work was later extended to orthotropic shells [52]. Nemat-Nasser [53] studied the correlation function of the radial displacement of a simply supported cylindrical panel under a purely random pressure field. Elishakoff [54] investigated the role of cross correlations in random vibration of a spherical panel analytically and numerically. Stationary linear random vibration response of cooling towers was studied by Yang and Kapania [55] using a thin shell element.

1.2.3 Shell structures subjected to turbulent boundary layer pressure fields

In section 1.2.1, a brief review of the effect of a fluid at rest on the vibration of thin shell structures was presented. A stationary fluid has an inertial effect on the shell structure however a flowing fluid applies additional effects on the shell.

If the flow is turbulent, the shell is subjected to a random pressure field arising from a turbulent boundary layer. Flow velocity fluctuates randomly in the turbulent boundary layer and consequently gives rise to turbulent pressure fluctuations which can excite the shell at velocities lower than those which may cause fluidelastic instabilities [5]. Fluidelastic instability has large-amplitude vibration and can result in rapid failure,

however random pressures cause small vibration amplitudes, which in long term lead to structural fatigue. Study of the random vibration response of shell structures has long been of primary interest to researchers and structural engineers.

For turbulent random pressure fields, experimental and theoretical investigations of wall pressure characteristics have been extensively carried out by many researchers and this case continues to be a subject of great interest. Early investigations on turbulent boundary-layer-induced random pressure fields and their interaction with elastic structures include works performed by Corcos [56, 57], Maestrello [58], Farabee [59], Ffowcs Williams [60], Farabee and Geib [61]. Investigations of the fluctuating wall pressure beneath a turbulent boundary layer have also been conducted by Bakewell [62] and Corcos [63] for fully-developed turbulent pipe flow. Turbulent boundary layers on flat plates have been studied by Willmarth and Wooldridge [64] and Bull [65]. Several models have been established to characterize turbulent boundary layer pressure exciting a plate [57, 64]. There is still much ongoing research in this field. For example, Leclercq and Bohineust [66] conducted an experimental investigation to obtain wall-pressure power spectral density in a turbulent boundary layer. A recent treatment of this problem was given by Lee, Blake and Farabee [67] who developed a methodology to predict the wall-pressure fluctuation spectrum based on time-mean flow characteristics of turbulent flow obtained from solving Reynolds averaged Navier-Stokes equations.

Theoretical investigations have concentrated on understanding how pressure fluctuations on the wall in a turbulent boundary layer result from turbulent velocity

fluctuations, while experimental works have mainly focused on measuring wall-pressure cross correlation function and power spectral density of the wall-pressure. Blake [68] gives a comprehensive overview of turbulent boundary layer excited vibrations in his book. A survey on structural excitation of a turbulent boundary layer was conducted by Leehey [69]. Most of the studies in the literature are devoted to investigating characteristics of pressure fluctuations beneath a turbulent boundary layer, and studies on the displacement response of an elastic structure to these excitations are scarce.

The excitation of a finite circular cylindrical shell by boundary layer pressure fluctuations in subsonic flow was studied by Cottis and Jasonides [70] using Green's function method. They assumed that pressure field space-time correlation is the product of a 0th-order Bessel function and an exponential. The response space-time correlation function was calculated, however they did not proceed to evaluate the mean square value of the response, nor did they undertake numerical solution.

The first effort to make a comparison of measured and predicted simply-supported thin cylindrical shell vibration when subjected to internal turbulent water flow at high frequencies was made by Clinch [71] using Powell's joint-acceptance method. Following Clinch's study, Lakis and Païdoussis [72] presented a theory using a cylindrical finite element to predict the mean square displacement response of a uniform or axially non-uniform thin cylindrical shell when subjected to an arbitrary random pressure field, or to a pressure field arising from a turbulent boundary layer caused by internal subsonic flow.

Strawderman and Brand [73] developed an analytical solution for the velocity spectra of simply supported, rectangular flat plates excited by turbulent flow. In their analysis, pressure fluctuations exerted on the plate surface were uniquely due to a turbulent boundary layer and the contribution of radiated acoustic pressure to plate excitation was neglected. They adopted the Corcos model to describe the turbulent boundary layer pressure field. Han, Bernhard and Mongeau [74] applied an energy flow analysis in order to obtain the velocity spectral density of a plate excited by turbulent boundary layer pressure fluctuations. In their study, the Smol'yakov-Tkachenko model was employed to estimate pressure fluctuations beneath a turbulent boundary layer.

Recently, innovative and fast solutions for the stochastic response of a plate or cylinder have been carried out by many researchers [75-79]. For example, Birgersson, Ferguson and Finnveden [75] used spectral finite element and dynamic stiffness methods to analyze the autospectral density of the velocity of a plate subjected to a pressure fluctuations originating from a turbulent boundary layer. They used an approach in which the cross spectral density of the response was determined by a single integration over all wavenumbers rather than double integrals over the surface. Finnveden, Birgersson, Ross and Kremer [78] investigated the vibration response of a plate excited by a turbulent boundary layer experimentally and numerically. The vibration response of the velocity of a thin-walled plate was measured and then predicted based on wall pressure models. Mazzoni [79] proposed a deterministic model based on an analytical wavenumber integration procedure to predict the response of a thin elastic plate subjected to both a turbulent flow of fluid at a low Mach number and

acoustic noise. The power spectrum of the acceleration of the fluid-loaded plate excited by a turbulent boundary layer was obtained and compared with that obtained with using a classic random approach. Vitiello, De Rosa and Franco [76] developed a procedure to evaluate the aeroelastic response of a flat plate subjected to a turbulent boundary layer. De Rosa and Franco [77] presented an exact and predictive response to evaluate the power spectral density of acceleration of a simply-supported plate wetted on one side subjected to a turbulent boundary layer. Birgersson, Finnveden and Robert [80] predicted the power spectral density of velocity of thin cylindrical shells excited by turbulent flow using Arnold-Warburton theory and the spectral finite element method, however the effect of fluid-structure coupling was not accounted for in their analysis. Autospectral velocity of thin plates excited by a low-speed turbulent boundary layer flow was analyzed numerically and experimentally by Hambric, Hwang and Bonness [81]. All these investigations deal with auto spectral density of response with no attempt to obtain root mean square displacement response.

In analytical works, both wavenumber-frequency [74, 75, 82] and space-frequency domains [72, 83] were utilized in order to analyze structural response due to turbulent boundary layer pressure fields. In this thesis, calculations are conducted in the space-frequency domain because it is more adapted to the physical understanding of experimental measurements.

1.2.4 Shortcomings of previous works

As the discussion in the previous sections has shown, there is significant interest in a prediction method for the response of thin structures to boundary layer pressure fluctuations generated by turbulent flow. However, it is clear that current models are insufficient to determine the total root mean square displacement response of the structure. The primary issue that must first be resolved is to precisely model dynamic behavior of such structures in contact with stationary fluid, since the dynamic characteristics of these structures are needed as an input to determine the structural response to turbulent flow.

Thin shells encountered in practice are mostly composed of plates and cylinders. For this reason many research studies on fluid-structure interaction problems have been devoted to modeling these structures and consequently, the developed finite elements are solely applicable to these structures. In fact, analyses of three-dimensional thin shell structures subjected to stationary fluid are scarce in the literature. Some simplifications are often applied to consider 3D shells as 2D structures. It is therefore necessary to develop an element to correctly model the behavior of curved thin shell structures in contact with fluid. The method developed in this thesis is capable of predicting the dynamic behavior of thin plates and shells and is generally applicable to three-dimensional structures such as turbine blades in a vacuum and in contact with fluid. Since the pressure imposed by a stationary fluid is calculated individually for each

finite element, structures that are partially submerged in fluid or partially-filled can be modeled.

Beyond the abovementioned issue, the flow-induced vibration problem needs to be addressed. Numerous works in the literature have been devoted to investigating pressure fluctuations beneath a turbulent boundary layer. Characteristics of a turbulent boundary layer such as wall-pressure power spectral density and cross correlation functions have been extensively studied and well established. Furthermore, much research effort has been invested in evaluating the auto spectral density of the response of a plate due to a turbulent boundary layer pressure field, but no attempt to calculate total root mean square displacement response has been undertaken. In the literature survey it appears that studies predicting the total root mean square displacement response of thin cylindrical shells to random pressure fluctuations beneath a turbulent boundary layer are few. For example, an investigation was carried out by Lakis and Païdoussis [72] to determine the total root mean square displacement response of cylindrical shells, however their work was restricted to cylindrical forms, since a cylindrical finite element was employed.

To the authors' knowledge, no exact treatment of the total root mean square displacement response of a thin plate excited by a turbulent boundary layer has been performed to date. In the foregoing analytical studies conducted on turbulent flow-induced vibration, shell structures were generally plate or cylinder and the excitation forces were generally purely random. Frequently some simplifying assumptions were considered in order to predict the response, such as considering unit power spectral

density of wall pressure, or neglecting the effects of fluid-structure coupling. Therefore for more complex shell geometries and more realistic random pressure fields, developing a method to predict total root mean square displacement response is desirable.

1.3 Objectives

The first objective of this work is to model dynamic behavior of three-dimensional thin elastic curved structures in a vacuum and subjected to inviscid incompressible quiescent fluid.

The second objective of the present study is to predict the response of a thin structure subjected to an arbitrary random pressure field and subsequently to a pressure field arising from a fully-developed turbulent boundary layer in subsonic flow. The ultimate goal of this study is to obtain an expression for the root mean square displacement response produced by the turbulent boundary-layer-induced pressure field.

1.4 Methods

A comprehensive understanding of fluid-structure interaction phenomenon is of primary importance in this study, because the characteristics of the structure in contact

with fluid are needed to predict the vibration amplitude of a thin structure to a fully-developed turbulent boundary layer random pressure field.

Assumptions introduced into the theory are briefly outlined here:

(i) the shell structure is assumed to be thin;

(ii) the structure has a linear elastic behavior;

(iii) weak coupling is assumed, i.e. the effect of structural vibration on fluid structure is neglected;

(iv) linear potential flow theory is used to describe fluid-structure interaction. In fact, the amplitude of shell displacements remain small enough for linear fluid mechanics to be adequate;

(v) the fluid behaves in an inviscid manner, i.e. shear forces in the fluid can be neglected and fluid pressure is normal to the shell;

(vi) it is assumed that free surface effects are neglected in the case of structures containing stationary fluid. Since the natural frequencies of the shell are much higher than those of free surface phenomenon, at least in the lowest modes, coupling between shell modes and the liquid free surface is weak;

(vii) influence of the structural vibration induced by the fluctuating pressure field on the boundary layer is neglected due to its sufficiently small amplitude.

(viii) the process is assumed to be ergodic and the turbulent pressure field spatially homogeneous;

(ix) the structural damping matrix is assumed to be proportional to mass and stiffness matrices;

(x) the structure is lightly damped ($\zeta_r << 1$);

(xi) the turbulent boundary layer is fully developed;

(xii) acoustic pressure fluctuations induced by flow at moderate speeds are very small compared to turbulent pressure fluctuations, therefore we assume that excitation only arises from pressure fluctuations in the turbulent boundary layer;

(xiii) the compressibility effect is ignored;

(xiv) the flow is subsonic and Mach number is below 0.3.

A general method to model a thin elastic curved structure in a vacuum and subjected to quiescent fluid is developed. This approach is then extended to predict the vibrational response of such structures to an arbitrary random pressure field and subsequently to a pressure field arising from a fully-developed turbulent boundary layer in subsonic flow.

To do so, the method developed here incorporates a finite element previously developed by our group [84, 85] to study dynamic behavior of three-dimensional thin curved structures in contact with stationary fluid. In this approach the structural finite element was developed using a combination of Sanders' thin shell theory and the finite element method, in which the finite elements are four-node flat rectangular shell elements with five degrees of freedom per node. Sanders' thin shell theory is based on Love's first approximation for thin shells. Love's first approximation or Kirchhoff-Love shell theory consists of the following four assumptions: (1) the shell is thin; (2)

displacements and rotations are small; (3) transverse normal stresses are negligible and (4) the normal to the shell reference surface before deformation remains normal after deformation. Sanders redefined the force and moment resultants based on the original hypotheses of Love in such a way that all strains vanish for rigid-body motion. This shell theory satisfies the convergence criteria of the finite element method.

Many numerical methods are available to study shell dynamics and carry out mathematical calculations, such as the finite difference, Galerkin, the Rayleigh-Ritz and finite element methods. In this study, the finite element method is used to calculate element mass and stiffness matrices by exact integration, since it has the capacity to precisely predict both high and low frequencies. It also overcomes the difficulties of other methods in dealing with various boundary conditions and relatively complex shapes. It does not present drawbacks such as taking boundary conditions into account to define displacement functions.

As stated above, a mixed combination of classic thin shell theory and the finite element method is chosen, which makes this method more accurate than the conventional finite element method. Moreover, the finite element used in this study is not limited to a specific geometry; it is versatile to model sophisticated three-dimensional structures such as turbine blades. This element is capable of calculating low and high frequencies with high precision and can take into account various boundary conditions of the structure without altering the displacement field.

The development of shell elements from classic shell theory is complex whereas flat shell elements are easier to formulate using previously available theories

for membrane and plate bending. Both membrane and bending effects are taken into consideration in this theory. Flat shell elements are developed by superimposing the stiffness of membrane and bending elements. The solution of membrane displacements is assumed to be a bilinear polynomial. The transverse displacement component is modeled using an exponential function derived from Sanders' thin shell theory. The structural mass and stiffness matrices in local coordinates are determined by exact analytical integration. Transformation between global and local coordinates is required to generate the element mass and stiffness matrices in global coordinates. The transformation matrix for nodal displacement of the element is established using direction cosines (to model curved structures such as turbine blades) or two successive rotations about the x- and y- axes (to model reservoirs). This local-global transformation increases the number of degrees of freedom. This is a consequence of the absence of rotational stiffness associated with the 6th degree of freedom about the local axis, which can cause singularity. To prevent numerical singularity problems, weak fictitious rigidity and mass in diagonal terms associated with the local normal rotation are inserted at each node of the finite element.

Since the transverse displacement function is derived from thin shell theory this method may be easily adapted to take hydrodynamic effects into account. To accomplish this, linear potential flow theory is applied to describe fluid-structure interaction. In fact, the amplitude of shell displacements remained small enough for linear fluid mechanics to be adequate. The velocity potential function, Bernoulli's equation and the impermeability condition are used to determine the fluid pressure

acting on the structure. The velocity potential function must satisfy boundary conditions at the fluid-structure interface and the fluid extremity. In general, three boundary conditions exist: fluid free surface, rigid wall and impermeability.

Fluid pressure is expressed as a function of the acceleration of the transverse displacement of the element, the fluid density and the boundary conditions of the fluid. The product of fluid pressure and the developed structural shape function is integrated analytically over the fluid-structure interface to evaluate the inertial effect of the fluid and is interpreted as the virtual added mass of the stationary fluid.

This method is used to study dynamic behavior of thin elastic structures partially or completely filled with or submerged in stationary fluid. Dynamic behavior of thin structures in a vacuum and subjected to stationary fluid is now modeled. An in-house program is developed to obtain natural frequencies, mode shapes and other characteristics of the thin structure in a vacuum and in contact with stationary fluid. The dynamic characteristics of the structure in a vacuum and in contact with quiescent fluid are needed as an input to the calculation of the response of the structure to pressure fluctuations in turbulent flow. As mentioned earlier, this method is capable of calculating both high and low frequencies with high accuracy which is of considerable significance for determining the response of structures subjected to random pressure fields such as those generated by turbulent flow.

A numerical approach is proposed to determine the magnitude of the response of thin structures to a turbulent boundary-layer-induced random pressure field.

Structural response to turbulence-induced excitation forces is calculated using random vibration theory. The following procedures are taken:

The nodal displacements of the structure are expressed as a normal mode expansion in terms of the generalized coordinates and the modal matrix. Equilibrium equations are decoupled by assuming that structural damping is linearly related to the mass and stiffness matrices. We assume that the fluid behaves in an inviscid manner, therefore fluid pressure fluctuations are normal to the surface of the shell. The random fluctuating pressure field on the surface of the shell element is translated into equivalent lateral force field acting at an arbitrary point by integrating over the surface. This lateral force is then approximated using a finite set of discrete force and moments acting at each node of the finite element. Since a turbulent boundary layer is intrinsically random, the statistical properties of the turbulent flow must be employed. Statistical properties of wall-pressure fluctuations of turbulent boundary layers are utilized to obtain vibration amplitude. We assume the random process is stationary ergodic and the random pressure fluctuation is homogeneous. Therefore mean square displacement response can be expressed in terms of the cross spectral density (CSD) of the pressure field. The wall-pressure CSD is approximated by semi-empirical models. The Corcos model for the CSD of the pressure fluctuations is adopted to describe the turbulent pressure field. This model agrees well with experimental results. The Corcos model was used due to its simplicity compared to other wall-pressure models. In the Corcos model the CSD of the pressure is formulated as the product of the power spectral density (PSD) of the pressure and the wall-pressure cross correlation function.

Wall-pressure PSD is the most significant characteristic of turbulent flow. Fluctuating wall-pressure beneath a turbulent boundary layer for various velocities has been measured for different structures subjected to various fluids. The non-dimensional wall-pressure PSD as a function of Strouhal number has been proposed by several investigators. The wall-pressure PSDs obtained by Bakewell et al. in pipe airflow, by Clinch in pipe water flow, by Willmarth and Wooldridge over a flat plate boundary layer, and in a straight flow channel were reproduced by Au-Yang [86] and are presented for different Strouhal numbers in Figure 1.1.

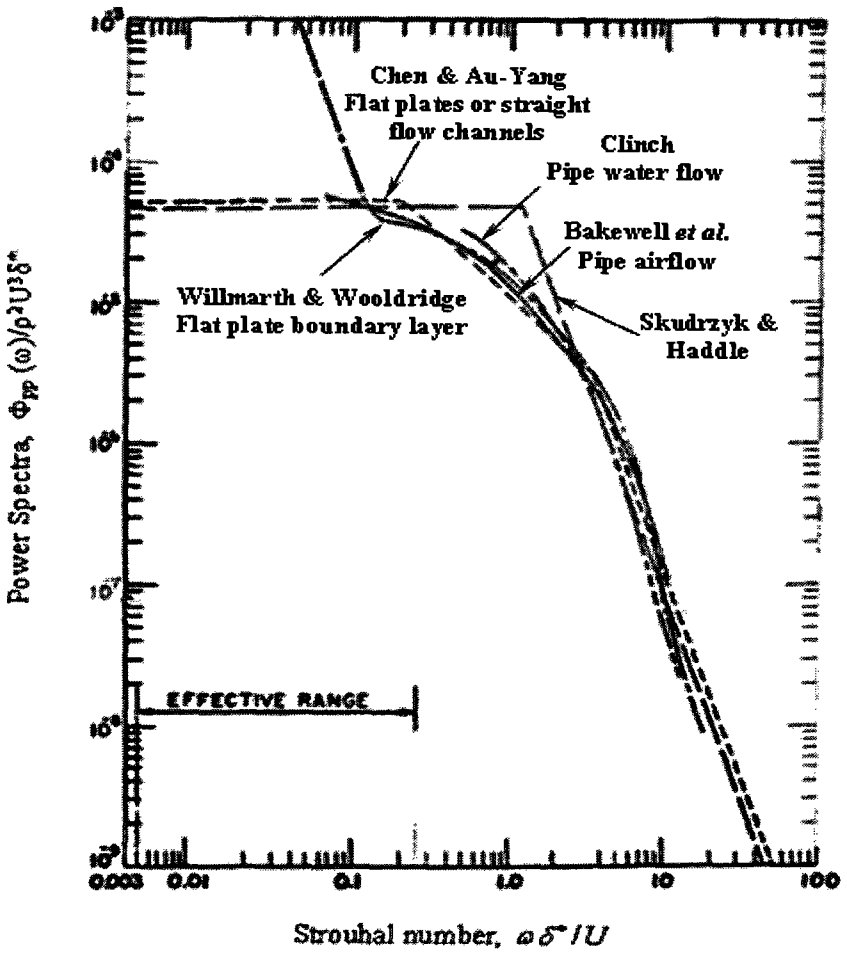

Figure 1.1 Wall-pressure power spectral densities versus Strouhal number [86]

Even though there are differences in investigations, namely fluid properties, flow velocity and even the geometry of structures, the general features and magnitude of the wall-pressure PSD are nevertheless similar as observed in Figure 1.1. Therefore, it seems that the proposed expression by Lakis based on Bakewell's measurements in pipe airflow is applicable to a thin plate. Figure 1.2 [72] depicts Bakewell's

measurements of the mean square pressure per unit bandwidth, i.e. the power spectral density, versus Strouhal number. Lakis' curve of best fit is also shown in Figure 1.2.

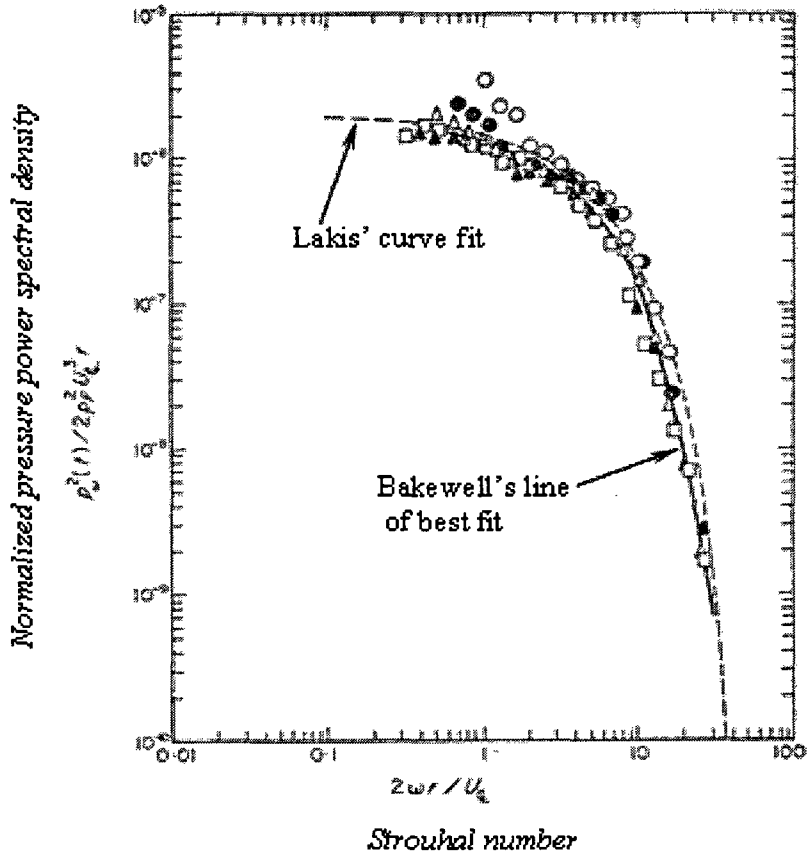

Figure 1.2 Bakewell measurements of mean square pressure per unit bandwidth vs. Strouhal number. Solid line: Bakewell, Dashed line: Lakis' curve fit. Reynolds number: ◦ 100000; • 150000; Δ 200000; ▲ 250000; □ 300000. [72]

Corcos postulated that the cross correlation function could be represented as the product of the lateral and longitudinal correlation functions. The longitudinal and

lateral correlations in the Corcos model are presented as an exponentially decaying oscillating function in the flow direction and a simple exponentially decaying function in the cross-flow direction, respectively. It is worth mentioning that different empirical expressions for different structures have been suggested for longitudinal and lateral correlations; however these expressions are approximately the same.

The expressions of the wall-pressure PSD, longitudinal and lateral correlations are introduced into the mean square displacement expression. Exact integrations over surface and frequency are carried out analytically and an expression for the mean square displacement response is obtained in terms of the wetted natural frequencies, undamped mode shapes, generalized mass of the system and other characteristics of the structure and flow.

These sophisticated expressions are implemented in an in-house program to predict the total root mean square displacement response of thin structures. The input damping ratio and parameters related to the flow field are assumed to be known from experimental data while the virtual added mass and wetted natural frequency effects due to hydraulic loading of the structure are included in the analysis.

1.5 Organization of the thesis

The following articles have been submitted for publication during the course of my PhD studies:

Esmailzadeh, M., Lakis, A. A., Thomas, M., Marcouiller, L. Three-Dimensional Modeling of Curved Structures Containing and/or Submerged in Fluid. Journal of Finite Elements in Analysis and Design. 2008; 44(6-7): 334-345.

Esmailzadeh, M., Lakis, A. A., Thomas, M., Marcouiller, L. Prediction of the response of a thin structure subjected to a turbulent boundary-layer-induced random pressure field. Journal of Sound and Vibration. Revised Article submitted March 2009.

CHAPTER II

ARTICLE 1: THREE-DIMENSIONAL MODELING OF CURVED STRUCTURES CONTAINING AND/OR SUBMERGED IN FLUID

M. Esmailzadeh [a], A. A. Lakis [a,*], M. Thomas [b], L. Marcouiller [c]

[a] *Mechanical Engineering Department, École Polytechnic of Montréal, C.P. 6079, Succursale Centre-ville, Montréal, Québec, Canada, H3C 3A7, Tel: +1 514 340 4711, ext: 4906, Fax: +1 514 340 4172, E-mail: aouni.lakis@polymtl.ca*

[b] *Mechanical Engineering Dept., École de Technologie Supérieure, 1100, Notre-Dame Ouest, Montréal, Québec, Canada, H3C 1K3*

[c] *Institut de Recherche d'Hydro Québec, 1800, Lionel-Boulet Varennes, Québec, Canada, J3X 1S1*

Article published in

Journal of Finite Elements in Analysis and Design

2008; 44(6-7): 334-345

Keywords: Fluid structure interaction, FEM, Thin shell, Blade

2.1 Abstract

The dynamic behavior of a three-dimensional thin flexible structure in inviscid incompressible stationary fluid is studied numerically. A finite element is developed using a combination of classical thin plate theory and finite element analysis, in which the finite elements are rectangular four-noded flat shells with five degrees of freedom per node. The displacement functions are derived from Sanders' thin shell equations. The velocity potential function and Bernoulli's equation for liquid yield an expression for fluid pressure as a function of nodal displacement of the element and inertial force of the quiescent fluid. An analytical integration of the fluid pressure over the element produces the virtual added-mass matrix of fluid. Calculations are presented to illustrate the dynamic behavior of a rectangular reservoir containing fluid as well as a completely submerged blade.

2.2 Introduction

The presence of fluid in the vicinity of a shell has an important influence on the dynamic behavior of the structure and can cause damage to the structure. The effect of the surrounding medium on the vibration of plates and shells is of primary interest to scientist and engineers working in aerospace, marine and reactor technology. In the design of fluid-structure interaction, calculation of the natural frequencies of the system

is a preliminary step in dynamic analysis. There are many ways in which the fluid may be coupled to the motions of the shell. In the case of a shell filled with compressible fluid, the compressibility of the fluid affects the effective stiffness of the system in addition to the straining effects it imposes on the shell through pressurization. In the case of shells partially filled with liquid, free surface motion may be coupled to shell motion (sloshing). Other effects of coupled fluid-shell motion occur when the fluid is flowing, such as flutter instability at high velocities. Recent books by Païdoussis provide a comprehensive treatment of the subject as well as a complete bibliography of all important works in the field [1, 2]. Methods for describing fluid-structure interaction have been studied theoretically by Axisa [3]. Numerical modeling of linear vibrations of elastic structures coupled with internal fluids, such as hydroelasticity has been described by Morand [4].

Even though there have been numerous studies done on fluid interaction effects, most of these concern cylindrical tanks [5-7] and plates [8-11] in contact with fluid. Several studies exist on the dynamic response of rectangular containers; however the flexibility of the structure is not completely taken into account. This may be due to the fact that rectangular fluid containers are usually made of reinforced concrete and may be considered quite rigid. In most of these studies some simplifications have been made to enable treatment of a 3D structure using 2D modeling. Kim et al. [12] presented an analytic solution to study dynamic behavior of a rectangular reservoir partially filled with fluid using the Rayleigh-Ritz method. However, in their study, only a pair of walls is assumed to be flexible while the other pair and bottom remain rigid, which is similar

to the case of two parallel plates. Kim and Lee [13] investigated hydro-elastic analysis of a rectangular tank completely filled with liquid using NASTRAN program and compared results with analytic solutions. In their study, they considered the tank as two parallel plates because it was composed of a rigid bottom and two parallel walls. Bauer and Eidel [14] conducted investigative research on a two-dimensional rectangular container of infinite width partially covered with an elastic plate (beam) and partially filled with fluid. Soedel [15] studied free and forced vibration of a simply supported rectangular plate with reservoir conditions at its edges, carrying liquid with a free-sloshing surface. The free surface effect, i.e. sloshing mode, is of importance in the propellant tanks of liquid-propelled rockets and has received considerable attention. Sloshing modes for a liquid-filled cylindrical and rectangular tank have been analytically and numerically investigated by several researchers [16-21]. The effect created by compressibility of the fluid, i.e. the acoustic mode, has been taken into account in many research works. For example, the linear free vibration of a circular cylindrical shell filled with compressible fluid has been analytically investigated by Jeong and Kim [22]. Hernandez [23] has numerically computed vibration modes of an elastic thin structure in contact with a compressible fluid.

In this work the liquid is assumed to be incompressible and it is also assumed that the effect of internal static pressure is small; this means that we do not consider pressurized shells. Moreover, free surface effects are neglected. This may be justified as follows: the natural frequencies of the shells in a vacuum in the modes under consideration are likely to be high, whereas the natural frequencies of free surface

phenomena are likely to be low, at least in the lowest modes. Accordingly, coupling between the shell modes and the liquid free surface modes may be expected to be weak. Actually, there is a possibility of non-linear coupling between the low-frequency free surface modes and the shell modes, but we will not attempt to take this phenomenon into account here since linear theory will be used in any case. Under these assumptions, it is clear that the only effect that the stationary fluid will have on motions of the shell will be that of inertial hydrodynamic loading. The dynamic effect of the fluid may be taken into account by incorporating the virtual mass of the fluid into the analysis.

A cylindrical finite element was developed by one of the authors of this article, in which displacement functions were derived from shell's equations of motion instead of using polynomial displacement functions [24, 25]. Prior to the work presented herein, this element could only be applied to cylindrical [5, 21, 26-30], conical [31] or spherical [32] shells, since it is a cylindrical frustum. We developed a more accurate and general method to model any kind of thin elastic curved structure in a vacuum and subjected to a quiescent fluid. In the present work a model was generated using a more efficient approach combining the finite element method and classical thin shell theory. The displacement functions were derived from Sanders' thin shell equations. Linear potential flow theory was applied to describe the fluid-structure interaction; in fact the amplitude of shell displacements remained small enough for linear fluid mechanics to be adequate. The velocity potential function and Bernoulli's equation were used to determine the distribution of pressure over the wall of the structure. The product of the

pressure and the developed structural shape function was integrated over the fluid-structure interface to assess the virtual added mass of the fluid.

This method will be extended to study the dynamic behavior of thin shells subjected to turbulent flow. Since the transverse displacement function is derived from thin plate theory, this method may be easily adapted to take hydrodynamic effects into account. Moreover, this method is capable of calculating both high and low frequencies with high accuracy. Although this capability is normally of little interest in free vibration analysis, it is of considerable importance for determining the response of curved structures subjected to random pressure fields such as those generated by turbulent flow [33].

An in-house program was developed to calculate natural frequencies and mode shapes of a 3D thin shell structure. In order to demonstrate the applicability of the proposed method, empty and fluid-filled rectangular reservoirs under different boundary conditions were investigated as well as a submerged turbine blade. The accuracy of the proposed numerical method was also verified.

2.3 Structural Modeling

This theory is an extension of that expounded by Lakis and Païdoussis [24, 25]. It is a finite element method in which normal displacement is determined from the plate's equation of motion instead of the usual and more arbitrary interpolating

polynomials. The geometry of structure shell element used in this analysis is shown in Figure 2.1. A rectangular flat shell element consists of four nodes, each of which has five degrees of freedom that represent the in-plane and out-of-plane displacement components and spatial derivatives of normal displacement (i.e. two rotations about in-plane axes).

2.3.1 Equations of motion

To establish the equilibrium equations of the thin plate, Sanders' equations for thin cylindrical shells are used, assuming the radius of the shell to be infinite. Sanders based his equations on Love's first approximation for thin shells and demonstrated that all strains vanish for any rigid-body motion. This shell theory satisfies convergence criteria of the finite element method stating that all strains within the element should vanish when the nodal displacements are generated by rigid body motions. The equilibrium equations of an orthotropic plate in terms of displacement components at the plate mean surface based on Sanders' shell theory are written as [34]

$$P_{11}\frac{\partial^2 U}{\partial y^2}+P_{12}\frac{\partial^2 V}{\partial x\,\partial y}+P_{33}\left(\frac{\partial^2 V}{\partial x\,\partial y}+\frac{\partial^2 U}{\partial y^2}\right)=0,$$

$$P_{22}\frac{\partial^2 V}{\partial y^2}+P_{21}\frac{\partial^2 U}{\partial x\,\partial y}+P_{33}\left(\frac{\partial^2 U}{\partial x\,\partial y}+\frac{\partial^2 V}{\partial x^2}\right)=0,$$

$$P_{44}\frac{\partial^4 W}{\partial x^4}+(P_{45}+P_{54}+2P_{66})\frac{\partial^4 W}{\partial x^2\,\partial y^2}+P_{55}\frac{\partial^4 W}{\partial y^4}=0, \qquad (2.1)$$

where U and V are in-plane displacement components, W represents the displacement component normal to the middle surface and P_{ij} are terms of the elasticity matrix for the case of orthotropic material [35].

The first two equations describe the membrane's behavior and the third equation specifies the bending of a rectangular plate.

2.3.2 Displacement Functions

Exact solution of the equations of motion is very complicated and many simplification approximations are required. By comparison, flat shell elements are easier to formulate using previously available theories of membrane and plate bending elements. We assume the solution of membrane displacements to be a bilinear polynomial and the normal displacement will be determined from the plate's equation of motion. Therefore, the displacement functions will be written as follows:

$$U(x,y,t) = C_1 + C_2\frac{x}{A} + C_3\frac{y}{B} + C_4\frac{xy}{AB}, \tag{2.2}$$

$$V(x,y,t) = C_5 + C_6\frac{x}{A} + C_7\frac{y}{B} + C_8\frac{xy}{AB}, \tag{2.3}$$

$$W(x,y,t) = \sum_{j=9}^{20} C_j e^{i\pi(\frac{x}{A}+\frac{y}{B})+i\omega t}, \tag{2.4}$$

where A and B are the plate length and width in the x and y directions, respectively, C_j are unknown constants, i is the complex number $i^2 = -1$ and ω is the natural frequency of the plate in rad/s.

The exponential solution of normal deflection W can be expanded into a Taylor series as follows:

$$W(x,y,t) = C_9 + C_{10}\frac{x}{A} + C_{11}\frac{y}{B} + C_{12}\frac{x^2}{2A^2} + C_{13}\frac{xy}{AB} + C_{14}\frac{y^2}{2B^2} + C_{15}\frac{x^3}{6A^3} + C_{16}\frac{x^2y}{2A^2B} + C_{17}\frac{xy^2}{2AB^2} + C_{18}\frac{y^3}{6B^3} + C_{19}\frac{x^3y}{6A^3B} + C_{20}\frac{xy^3}{6AB^3}. \tag{2.5}$$

We can write the displacements U, V and W in matrix form:

$$\{U \quad V \quad W\}^{\mathrm{T}} = [\mathbf{R}][\mathbf{A}]^{-1}\{\boldsymbol{\delta}\} = [\mathbf{N}]\{\boldsymbol{\delta}\}, \tag{2.6}$$

where matrix [**N**] is the shape function of the finite element, matrices [**R**] and $[\mathbf{A}]^{-1}$ are given in the Appendix and $\{\boldsymbol{\delta}\}$ is the nodal displacement vector of the element given as:

$$\{\boldsymbol{\delta}\} = \left\{\{\boldsymbol{\delta}_i\}^{\mathrm{T}}, \{\boldsymbol{\delta}_j\}^{\mathrm{T}}, \{\boldsymbol{\delta}_k\}^{\mathrm{T}}, \{\boldsymbol{\delta}_l\}^{\mathrm{T}}\right\}^{\mathrm{T}}. \tag{2.7}$$

Each node, i.e. "node i", possesses a nodal displacement vector composed of the following terms:

$$\{\boldsymbol{\delta}_i\} = \{U_i \quad V_i \quad W_i \quad \partial W_i/\partial x \quad \partial W_i/\partial y\}^{\mathrm{T}}. \tag{2.8}$$

2.3.3 Kinematics relationship

The strain vector in terms of displacements is given by [34]

$$\{\boldsymbol{\varepsilon}\} = \{\varepsilon_x \quad \varepsilon_y \quad 2\varepsilon_{xy} \quad \kappa_x \quad \kappa_y \quad \kappa_{xy}\}^{\mathrm{T}} = \left\{\frac{\partial U}{\partial x} \quad \frac{\partial V}{\partial y} \quad \frac{\partial U}{\partial y}+\frac{\partial V}{\partial x} \quad \frac{-\partial^2 W}{\partial x^2} \quad \frac{-\partial^2 W}{\partial y^2} \quad \frac{-2\partial^2 W}{\partial x \partial y}\right\}^{\mathrm{T}}. \tag{2.9}$$

Substituting the displacements defined in Eq. (2.6) into Eq. (2.9), we obtain the strain vector in terms of nodal displacements:

$$\{\boldsymbol{\varepsilon}\} = [\mathbf{Q}][\mathbf{A}]^{-1}\{\boldsymbol{\delta}\} = [\mathbf{B}]\{\boldsymbol{\delta}\}, \tag{2.10}$$

where matrix [**Q**] is given in the Appendix.

2.3.4 Constitutive equations

The stress-strain relationships for an anisotropic material may be expressed as follows:

$$\{\boldsymbol{\sigma}\} = [\mathbf{P}]\{\boldsymbol{\varepsilon}\} = [\mathbf{P}][\mathbf{B}]\{\boldsymbol{\delta}\}, \tag{2.11}$$

where [**P**] is the elasticity matrix. The non-zero terms of the elasticity matrix for an isotropic plate are defined as

$$P_{11} = P_{22} = D, \quad P_{44} = P_{55} = K, \quad P_{12} = P_{21} = \nu D, \quad P_{45} = P_{54} = \nu K,$$

$$P_{33} = (1-\nu)D/2, \; P_{66} = (1-\nu)K/2, \tag{2.12}$$

where

$$D=\frac{Eh}{1-\nu^2} \quad , \quad K=\frac{Eh^3}{12(1-\nu^2)} \tag{2.13}$$

E is the modulus of elasticity, ν is Poisson's coefficient and h is the plate thickness.

The rigidity and mass matrices of one rectangular finite element in its local coordinates are given by finite element theory:

$$[\mathbf{K}]_e = \iint_A [\mathbf{B}]^{\mathrm{T}}[\mathbf{P}][\mathbf{B}]\mathrm{d}A, \tag{2.14a}$$

$$[\mathbf{M}]_e = \rho_s h \iint_A [\mathbf{N}]^{\mathrm{T}}[\mathbf{N}]\mathrm{d}A, \tag{2.14b}$$

where ρ_s is the material density of shell and $\mathrm{d}A$ is the element surface area.

Substituting matrices [**B**] and [**N**] into Eqs. (2.14a) and (2.14b), we obtain

$$[\mathbf{K}]_e = [\mathbf{A}]^{-\mathrm{T}}\left(\int_0^{y_e}\int_0^{x_e}[\mathbf{Q}]^{\mathrm{T}}[\mathbf{P}][\mathbf{Q}]\mathrm{d}x\mathrm{d}y\right)[\mathbf{A}]^{-1}, \tag{2.15a}$$

$$[\mathbf{M}]_e = [\mathbf{A}]^{-\mathrm{T}}\left(\rho_s h\int_0^{y_e}\int_0^{x_e}[\mathbf{R}]^{\mathrm{T}}[\mathbf{R}]\mathrm{d}x\mathrm{d}y\right)[\mathbf{A}]^{-1}, \tag{2.15b}$$

where x_e and y_e are the element dimensions in x and y directions, respectively. The matrices $[\mathbf{M}]_e$ and $[\mathbf{K}]_e$ were obtained analytically by carrying out the necessary matrix operations and integration over x and y.

2.3.5 Mass and stiffness matrices in global coordinates

Flat shell elements are developed by superimposing the stiffness of membrane and bending elements. The membrane and bending forces are totally independent of each other in the flat shell element itself; however, this separation is no longer possible in folded plates or curved shells. The behavior of a continuously curved surface can be adequately represented by a surface built using small flat elements. Transformation between global and local coordinates is required to generate the element stiffness matrix in global coordinates. This local-global transformation increases the number of degrees of freedom. It is a consequence of the absence of rotational stiffness associated with the 6th degree of freedom about the local axis, which can cause singularity. To prevent singularity problems a weak fictitious rigidity associated with a local normal rotation has been inserted.

The transformation matrix for nodal displacement of the element was established using direction cosines or two successive rotations about x- and y- axes and by considering that the rotations about in-plane axes for a thin flat rectangular shell element are expressed as [36]

$$\theta_x = \partial W / \partial y \quad , \quad \theta_y = -\partial W / \partial x , \tag{2.16}$$

where θ_x and θ_y are rotations about x- and y- axes, respectively. Accordingly, stiffness and mass matrices in global coordinates could be computed [36].

2.4 Fluid Modeling

Linear potential flow is an idealized method of modeling flow. In our mathematical model the fluid is assumed inviscid, incompressible and its motion non-rotational. We assume that shell displacements remain small enough for linear fluid mechanics to be adequate. Figure 2.2 shows the fluid-structure element.

The velocity potential function ϕ must satisfy the Laplace equation throughout the fluid domain. This relation is expressed in the Cartesian coordinate system by

$$\nabla^2\phi = \frac{\partial^2\phi}{\partial x^2} + \frac{\partial^2\phi}{\partial y^2} + \frac{\partial^2\phi}{\partial z^2} = 0, \tag{2.17}$$

where x, y and z are in-plane and normal directions of a plate, respectively.

A fluid velocity vector can be expressed as a gradient of the velocity potential function as

$$V_x = U_x + \frac{\partial\phi}{\partial x}, \quad V_y = \frac{\partial\phi}{\partial y}, \quad V_z = \frac{\partial\phi}{\partial z}, \tag{2.18}$$

where U_x is the unperturbed flow velocity along the shell in the x-direction. The remaining components of velocity, V_x, V_y and V_z are disturbance or perturbation fluid velocities in three directions as shown in Figure 2.2.

The dynamic condition at the fluid-shell interface can be determined using the Bernoulli's equation. Introducing velocity into the Bernoulli's equation and taking into account only the linear terms, this equation at the wall of shell element could be expressed as

$$\frac{\partial \phi}{\partial t} + U_x \frac{\partial \phi}{\partial x} + \frac{P}{\rho_f} = 0, \tag{2.19}$$

where ρ_f is the density of fluid. Therefore, hydrodynamic pressure at the fluid-shell interface for a stationary fluid ($U_x = 0$) is obtained:

$$P\Big|_{\text{at the wall}} = -\rho_f \frac{\partial \phi}{\partial t}. \tag{2.20}$$

The impermeability condition of the structure's surface requires that the out-of-plane velocity component of the fluid on the plate surface matches the instantaneous rate of change of the plate transversal displacement. This condition implies permanent contact between the plate surface and the peripheral fluid layer, which is

$$V_z\Big|_{\text{at the wall}} = U_x \frac{\partial W}{\partial x} + \frac{\partial W}{\partial t}. \tag{2.21}$$

For a stationary fluid, using Eq. (2.18) the impermeability condition can be written as

$$\frac{\partial \phi}{\partial z}\Big|_{\text{at the wall}} = \frac{\partial W}{\partial t}, \tag{2.22}$$

where W is the lateral displacement of the shell element.

The velocity potential function can be expressed as two separate functions:

$$\phi(x, y, z, t) = F(z) S(x, y, t), \tag{2.23}$$

where $F(z)$ and $S(x, y, t)$ are the two separate functions to be determined.

The velocity potential function on upper and lower surfaces of the element can be expressed by introducing Eq. (2.23) into Eq. (2.22) and then substituting $S(x, y, t)$ into Eq. (2.23):

$$\phi(x,y,z,t)=\frac{F(z)}{\mathrm{d}F(0)/\mathrm{d}z}\frac{\partial W}{\partial t} \quad , \quad \phi(x,y,z,t)=\frac{F(z)}{\mathrm{d}F(-h)/\mathrm{d}z}\frac{\partial W}{\partial t}, \tag{2.24}$$

where h is the thickness of the shell.

Substituting W from Eq. (2.4) into Eq. (2.24) and then introducing ϕ into the Laplace equation yields:

$$\frac{\mathrm{d}^2F(z)}{\mathrm{d}z^2}-\mu^2F(z)=0, \tag{2.25}$$

where

$$\mu^2=\pi^2\left(\frac{1}{A^2}+\frac{1}{B^2}\right). \tag{2.26}$$

The general solution of Eq. (2.25) is given as

$$F(z)=A_1\mathrm{e}^{\mu z}+A_2\mathrm{e}^{-\mu z}, \tag{2.27}$$

where A_1 and A_2 are constants to be specified.

By introducing Eq. (2.27) into Eq. (2.24) one gets the following expressions for the velocity potential function:

$$\phi(x,y,z,t)=\left(\frac{A_1\mathrm{e}^{\mu z}+A_2\mathrm{e}^{-\mu z}}{\mathrm{d}F(0)/\mathrm{d}z}\right)\frac{\partial W}{\partial t} \quad , \quad \phi(x,y,z,t)=\left(\frac{A_1\mathrm{e}^{\mu z}+A_2\mathrm{e}^{-\mu z}}{\mathrm{d}F(-h)/\mathrm{d}z}\right)\frac{\partial W}{\partial t}. \tag{2.28}$$

Total pressure imposing on the shell element from the fluid can be obtained by introducing Eq. (2.24) into Eq. (2.20) as follows:

$$P=-\rho_{\mathrm{f}}\left(\frac{F(0)}{\mathrm{d}F(0)/\mathrm{d}z}-\frac{F(-h)}{\mathrm{d}F(-h)/\mathrm{d}z}\right)\frac{\partial^2 W}{\partial t^2}. \tag{2.29}$$

2.4.1 Boundary conditions of a fluid bound in a reservoir

The velocity potential function must satisfy the boundary conditions at the fluid-structure interface and the fluid extremity as well. In general, three boundary conditions exist; fluid free surface, rigid wall and impermeability. To obtain an overall understanding of the problem we studied a flexible rectangular reservoir containing fluid where the following conditions should be considered:

2.4.1.1 Fluid over a plate with a free surface condition

Consider fluid over a plate as shown in Figure 2.3, which can represent the bottom of a reservoir. At the fluid-structure interface the impermeability condition, Eq. (2.22), is imposed.

The free surface behavior of the fluid is expressed by [37]

$$\frac{\partial \phi}{\partial z}\Big|_{z=h_1} = -\frac{1}{g}\frac{\partial^2 \phi}{\partial t^2}, \tag{2.30}$$

where g is the gravitational acceleration and h_1 is the height of fluid over the plate.

Substituting these boundary conditions into Eq. (2.28) we obtain the following expression for the potential function:

$$\phi(x,y,z,t) = \frac{1+Ce^{2\mu h_1}}{\mu(1-Ce^{2\mu h_1})}\frac{\partial W}{\partial t}, \tag{2.31}$$

where $C = (\mu g - \omega^2)/(\mu g + \omega^2)$ and tends to a value of -1. The fluid pressure applying on the bottom plate of the reservoir is obtained by introducing the above relationship into the Bernoulli's equation:

$$P = -\rho_f \left(\frac{1 + Ce^{2\mu h_1}}{\mu(1 - Ce^{2\mu h_1})} \right) \frac{\partial^2 W}{\partial t^2}. \tag{2.32}$$

2.4.1.2 Fluid bound between two parallel plates

Figure 2.4 illustrates fluid enclosed between two parallel plates, which depict the side walls of a reservoir.

Boundary conditions for both plates at z=0 and z=h_2 include an impermeability condition. By introducing these boundary conditions into Eq. (2.28) we obtain the potential function as follows:

$$\phi(x, y, z, t) = \frac{1 - 2e^{\mu h_2} + e^{2\mu h_2}}{\mu(1 - e^{2\mu h_2})} \frac{\partial W}{\partial t}, \tag{2.33}$$

where h_2 is the distance between the two plates.

The fluid pressure applying on each wall is obtained by introducing Eq. (2.33) into Bernoulli's equation:

$$P = -\rho_f \left(\frac{1 - 2e^{\mu h_2} + e^{2\mu h_2}}{\mu(1 - e^{2\mu h_2})} \right) \frac{\partial^2 W}{\partial t^2}. \tag{2.34}$$

2.4.2 Fluid boundary conditions imposed on a submerged blade

Consider a blade completely submerged in fluid as shown in Figure 2.5. A free surface and rigid wall are considered as fluid boundary conditions. The heights of fluid over and under an arbitrary element and at the origin of the blade are h_1, h_2, h_{o1} and h_{o2}, respectively as shown in Figure 2.5. The free surface behavior is obtained from Eq. (2.30) and the rigid wall behavior is expressed by

$$\left.\frac{\partial \phi}{\partial z}\right|_{z=-h-h_2} = 0, \tag{2.35}$$

where h is the thickness of blade. The total pressure applied on each element is obtained by introducing these boundary conditions into Eqs. (2.28) and (2.29) as follows:

$$P = -\rho_f \left(\frac{1-e^{2\mu h_1}}{\mu(1+e^{2\mu h_1})} - \frac{1+e^{2\mu h_2}}{\mu(e^{2\mu h_2}-1)} \right) \frac{\partial^2 W}{\partial t^2}. \tag{2.36}$$

The total pressure in these cases can be expressed as follows:

$$P = -\rho_f Z_f \frac{\partial^2 W}{\partial t^2}, \tag{2.37}$$

where the coefficient Z_f depends on the fluid-structure contact model.

2.4.3 Calculation of fluid-induced force

The fluid-induced force vector can be obtained by performing the following integration:

$$\{\mathbf{F}\}_e = \int_A [\mathbf{N}]^{\mathrm{T}} \{\mathbf{P}\} \mathrm{d}A, \tag{2.38}$$

where [**N**] is the shape function matrix of the finite element, {**P**} is a vector expressing the pressure applied by the fluid on the shell element and dA is the fluid-structure interface area of the element.

By introducing displacement functions from Eq. (2.6) into relation (2.37) and then substituting pressure into Eq. (2.38), the force vector is obtained as follows:

$$\{\mathbf{F}\}_e = \rho_{\mathrm{f}} Z_{\mathrm{f}} [\mathbf{A}]^{-\mathrm{T}} \left(\int_0^{y_e} \int_0^{x_e} [\mathbf{R}]^{\mathrm{T}} [\mathbf{R}_{\mathrm{f}}] \mathrm{d}x \, \mathrm{d}y \right) [\mathbf{A}]^{-1} \{\ddot{\boldsymbol{\delta}}\}. \tag{2.39}$$

The fluid force of a stationary fluid represents fluid inertial force and leads us to the fluid virtual added mass matrix of the finite element,

$$[\mathbf{M}_{\mathrm{f}}]_e = \rho_{\mathrm{f}} Z_{\mathrm{f}} [\mathbf{A}]^{-\mathrm{T}} \left(\int_0^{y_e} \int_0^{x_e} [\mathbf{R}]^{\mathrm{T}} [\mathbf{R}_{\mathrm{f}}] \mathrm{d}x \, \mathrm{d}y \right) [\mathbf{A}]^{-1}, \tag{2.40}$$

where matrices $[\mathbf{R}_{\mathrm{f}}]$, [**R**] and $[\mathbf{A}]^{-1}$ are given in the Appendix.

2.5 Dynamic Behavior of Fluid-Structure Interaction

The dynamic responses of a shell are affected by the presence of fluid. Generally, the fluid pressure acting upon a structure is expressed as a function of displacement and its derivatives: velocity and acceleration. These three terms represent, respectively, stiffness, Coriolis and inertial effects of the fluid forces. The fluid force matrices are superimposed onto the structural matrices to form the dynamic equations of a coupled fluid-structure system.

The dynamic behavior of a shell subjected to flowing fluid can be represented as follows [24]:

$$\left[\left[\mathbf{M}_s\right]-\left[\mathbf{M}_f\right]\right]\left\{\ddot{\boldsymbol{\delta}}_T\right\}-\left[\mathbf{C}_f\right]\left\{\dot{\boldsymbol{\delta}}_T\right\}+\left[\left[\mathbf{K}_s\right]-\left[\mathbf{K}_f\right]\right]\left\{\boldsymbol{\delta}_T\right\}=\left\{\mathbf{0}\right\}, \qquad (2.41)$$

where displacement vector $\left\{\boldsymbol{\delta}_T\right\}$ contains the nodal displacement vector of every element, $\left\{\dot{\boldsymbol{\delta}}_T\right\}$ and $\left\{\ddot{\boldsymbol{\delta}}_T\right\}$ are velocity and acceleration vectors of the entire structure, $\left[\mathbf{M}_s\right]$ and $\left[\mathbf{K}_s\right]$ are, respectively, the global mass and stiffness matrices of the shell structure in a vacuum and $[\mathbf{M}_f]$, $[\mathbf{C}_f]$ and $[\mathbf{K}_f]$ represent the inertial, Coriolis and centrifugal forces, which are induced by potential flow [33]. It is noted that in the case of fluid at rest the fluid velocity related terms will be null; therefore, the global equations of motion of a shell interacting with a stationary fluid can be reduced to the following system:

$$\left[\left[\mathbf{M}_s\right]-\left[\mathbf{M}_f\right]\right]\left\{\ddot{\boldsymbol{\delta}}_T\right\}+\left[\mathbf{K}_s\right]\left\{\boldsymbol{\delta}_T\right\}=\left\{\mathbf{0}\right\}. \qquad (2.42)$$

It should be recalled that the effects induced by the fluid free surface have been ignored in Eq. (2.42) and the inertial loading of the fluid is the only fluid effect on the motion of the shell.

Note that matrix $[\mathbf{M}_f]$ might be a symmetric positive definite and may be calculated using the kinetic energy of the fluid, but in our method we obtained the three matrices $[\mathbf{M}_f]$, $[\mathbf{C}_f]$ and $[\mathbf{K}_f]$ using the Laplace equation (Eq. (2.17)), Bernoulli's equation (Eq. (2.20)) and the boundary conditions of the fluid.

2.6 Numerical results and discussions

2.6.1 Fluid-filled reservoir

On the basis of the preceding analysis, natural frequencies of a rectangular reservoir in a vacuum and completely filled with fluid are calculated by the program developed in-house for this purpose. Consider a lidless rectangular tank whose geometry is 0.5, 0.7 and 0.4 m in x, y and z directions, respectively, as shown in Figure 2.6. Its thickness is $h = 0.005$ m and the material properties are Young's modulus $E = 2\times10^{11}$ Pa, Poisson's ratio $\nu = 0.3$ and density $\rho_s = 7970\,\text{kg/m}^3$. Water is used as the containing fluid with a density of $\rho_f = 1000\,\text{kg/m}^3$. Two cases of boundary conditions

have been studied: (a) the bottom and facing walls of the reservoir are simply supported at all edges and (b) the bottom is clamped.

In order to check the validity of the calculations, a finite element analysis was carried out using ANSYS [38]. The three dimensional ANSYS model is built using a 3D contained fluid element (FLUID80) and an elastic shell element (SHELL63). The four-noded quadrilateral shell element (SHELL63) has six degrees of freedom at each node; translations in three directions and rotations about three axes. The FLUID80 element is defined by eight nodes with three translations in each direction and it is well suited for calculating hydrostatic pressure and fluid-structure interactions. The FLUID80 element is used to model fluid contained within vessels having no flow rate. The fluid element at the interface should not be attached directly to structural element but should have separate coincident nodes that are coupled only in the direction normal to the interface. The reservoir is meshed and divided into 131 elastic shell elements and the fluid region consists of 140 (5×7×4) fluid elements with connectivity to the shell elements, in which fluid-solid mesh is similar along the fluid-solid interface. The same solid mesh used in ANSYS is also used in our program.

The main difference between our proposed shell model compared with ANSYS is that compatibility between our shell element and the fluid element is totally respected. In a typical ANSYS analysis, FLUID80 or FLUID30 elements are modifications of 3D structural solid elements. It appears that ANSYS uses the fluid element as a solid in order to couple it with structural elements.

The first few natural frequencies of the empty and fluid-filled simply supported rectangular reservoir are listed and compared with ANSYS results in Tables 2.1 and 2.2 (case a). Tables 2.3 and 2.4 present the natural frequencies of the empty and fluid-filled bottom-clamped rectangular reservoir, respectively (case b). The Tables show good agreement between the presented theory and that of ANSYS. It should be underlined that the natural frequencies of a fluid-filled reservoir are significantly lower than those of the reservoir in a vacuum.

2.6.2 Partially-filled reservoir

Natural frequency variations as a function of fluid level variation under two different boundary conditions for the same reservoir have been depicted in Figures 2.7 and 2.8, in which the frequencies have been denoted as —◆— 1st, —■— 2nd and —▲— 3rd frequencies.

As we expected, the frequencies of the fluid-filled reservoir are substantially lower than those of the reservoir in a vacuum. It is observed in these figures that the natural frequencies decrease as fractional filling increases; however, different behaviors of natural frequencies are observed under different reservoir boundary conditions. The effect of fluid depth on the first three frequencies of a lidless reservoir with a rigid core and two simply supported facing walls is demonstrated in Figure 2.7. It is observed that the influence of fluid below 1/4 fractional filling on the first and second natural

frequencies is insignificant but afterward the reservoir undergoes a substantial change in natural frequencies for all modes between 1/4 and 3/4. The frequencies of all the modes remain almost constant with an increase in liquid level between 3/4 and 1. Figure 2.8 indicates frequency variations versus fluid level for a lidless reservoir simply supported at all edges. As presented, the natural frequencies of the first mode decrease rapidly in the range of 0 to 1/4 and then the effect of the fluid becomes insignificant. For the 2nd and 3rd frequencies a substantial reduction is observed over the range of 0 to 3/4, after which the frequencies are almost constant.

2.6.3 Submerged blade

To demonstrate the applicability of the proposed method, a clamped-free blade in a vacuum and a submerged blade in fluid are investigated. The blade has the same material properties as the reservoir in the previous sections and its length, width and thickness are 20, 10 and 1 cm, respectively. The blade has been discretized to 40×20 elements as shown in Figure 2.5 and water has been used as the fluid. Natural frequencies of the blade in a vacuum were obtained and compared with ANSYS as listed in Table 2.5.

The level of fluid over and under the blade as well as the boundary conditions of the fluid (free surface, rigid wall or elastic object) affect the dynamic behavior of the blade until a certain height of fluid is reached. To clarify this phenomenon, variations

of the first three frequencies as a function of variations of fluid height over and under the blade are investigated individually. Figure 2.9 demonstrates the frequency variations versus variations of the ratio of fluid height over blade-to-blade length while the blade is sufficiently far from a rigid wall. As shown in this figure, as the height of fluid over the blade increases the frequency decreases; however, this reduction ceases when the fluid height to blade length ratio (h_{o1}/L) reaches 50%.

Figure 2.10 illustrates the frequency variations versus variations of the ratio of the height of fluid under blade-to-blade length while the blade is sufficiently far from the free surface. Note that when the height of fluid under the blade increases the frequency increases as well, but this increase stops when fluid level (h_{o2}) reaches 50% of the blade length (L).

Because of geometry restrictions of the blade, the ratio of height of fluid over and under the blade-to-blade length could not be reduced less than 16% in order to have a completely submerged blade. It is also important to note that structures with different boundary conditions behave differently under the influence of fluid, therefore the level of fluid at which the frequency stops changing varies from one structure to another.

Dynamic analysis was performed to determine the frequencies and mode shapes of the blade in a vacuum as well as submerged in fluid using our in-house program. The first mode shapes of the blade in a vacuum at 236.2 Hz and submerged in water at 190.4 Hz (where h_{o1}=4 cm and h_{o2} is large enough) were visualized using TECPLOT and compared with the undeformed blade as shown in Figure 2.11.

2.7 Conclusion

A rectangular flat shell element is developed using Sanders' thin shell theory and the finite element method. This element is applied in a model to study the dynamic behavior of thin elastic structures partially or completely filled with or submerged in stationary fluid. The structural mass and stiffness matrices were determined by exact analytical integration. The fluid pressure applied on the structure was determined by combining potential flow theory and an impermeability condition, and is expressed as a function of the acceleration of the normal displacement of the structure. Consequently, it could be interpreted as the virtual added mass of a stationary fluid. This method is able to predict the natural frequencies and mode shapes of three-dimensional thin structures containing and/or submerged in fluid. An in-house program was developed to calculate eigenvalues and eigenvectors of a structure in a vacuum and in the vicinity of a fluid. A rectangular reservoir partially and completely filled with fluid as well as a submerged blade was studied and the results agreed well with those of the commercial finite element software, ANSYS.

The developed flat shell element can be utilized to investigate non-uniform structures under various boundary conditions. The method can be extended to study the dynamic behavior of thin shells subjected to flowing fluid. In a further study, we plan to extend our approach to investigate the vibration of a hydraulic turbine ('n' blades) in a vacuum, submerged in quiescent fluid or subjected to turbulent flow.

As for future development, a theory capable of predicting the response of thin shells (such as a channel and hydraulic turbine blades) subjected to an arbitrary random pressure field as well as a pressure field arising from pressure fluctuations in the turbulent boundary layer in subsonic flow will be investigated using the present method. The eigenvalues and eigenvectors of the coupled fluid-structure will be employed in the theory to obtain the root mean square response of the system subjected to random pressure. An analytical-numerical method will be developed based on the present element to obtain random response.

2.8 Appendix

This appendix contains some of the matrices which are referred to in this work.

Matrix **[R]** (3 × 20):

$$[\mathbf{R}] = \begin{bmatrix} 1 & \frac{x}{A} & \frac{y}{B} & \frac{xy}{AB} & 0 & 0 & 0 & 0 & 0 & 0 & 0 & 0 & 0 & 0 & 0 & 0 & 0 & 0 & 0 & 0 \\ 0 & 0 & 0 & 0 & 1 & \frac{x}{A} & \frac{y}{B} & \frac{xy}{AB} & 0 & 0 & 0 & 0 & 0 & 0 & 0 & 0 & 0 & 0 & 0 & 0 \\ 0 & 0 & 0 & 0 & 0 & 0 & 0 & 0 & 1 & \frac{x}{A} & \frac{y}{B} & \frac{x^2}{2A^2} & \frac{xy}{AB} & \frac{y^2}{2B^2} & \frac{x^3}{6A^3} & \frac{x^2y}{2A^2B} & \frac{xy^2}{2AB^2} & \frac{y^3}{6B^3} & \frac{x^3y}{6A^3B} & \frac{xy^3}{6AB^3} \end{bmatrix}$$

Matrix $[\mathbf{Q}]$ (6×20):

$$[\mathbf{Q}] = \begin{bmatrix} 0 & \frac{1}{A} & 0 & \frac{y}{AB} & 0 & 0 & 0 & 0 & 0 & 0 & 0 & 0 & 0 & 0 & 0 & 0 & 0 & 0 & 0 & 0 \\ 0 & 0 & 0 & 0 & 0 & 0 & \frac{1}{B} & \frac{x}{AB} & 0 & 0 & 0 & 0 & 0 & 0 & 0 & 0 & 0 & 0 & 0 & 0 \\ 0 & 0 & \frac{1}{B} & \frac{x}{AB} & 0 & \frac{1}{A} & 0 & \frac{y}{AB} & 0 & 0 & 0 & 0 & 0 & 0 & 0 & 0 & 0 & 0 & 0 & 0 \\ 0 & 0 & 0 & 0 & 0 & 0 & 0 & 0 & 0 & 0 & 0 & \frac{-1}{A^2} & 0 & 0 & \frac{-x}{A^3} & \frac{-y}{A^2B} & 0 & 0 & \frac{-xy}{A^3B} & 0 \\ 0 & 0 & 0 & 0 & 0 & 0 & 0 & 0 & 0 & 0 & 0 & 0 & 0 & \frac{-1}{B^2} & 0 & 0 & \frac{-x}{AB^2} & \frac{-y}{B^3} & 0 & \frac{-xy}{AB^3} \\ 0 & 0 & 0 & 0 & 0 & 0 & 0 & 0 & 0 & 0 & 0 & 0 & \frac{-2}{AB} & 0 & 0 & \frac{-2x}{A^2B} & \frac{-2y}{AB^2} & 0 & \frac{-x^2}{A^3B} & \frac{-y^2}{AB^3} \end{bmatrix}$$

Matrix $[\mathbf{R}_f]$ (3×20):

$$[\mathbf{R}_f] = \begin{bmatrix} 0 & 0 & 0 & 0 & 0 & 0 & 0 & 0 & 0 & 0 & 0 & 0 & 0 & 0 & 0 & 0 & 0 & 0 & 0 & 0 \\ 0 & 0 & 0 & 0 & 0 & 0 & 0 & 0 & 0 & 0 & 0 & 0 & 0 & 0 & 0 & 0 & 0 & 0 & 0 & 0 \\ 0 & 0 & 0 & 0 & 0 & 0 & 0 & 0 & 1 & \frac{x}{A} & \frac{y}{B} & \frac{x^2}{2A^2} & \frac{xy}{AB} & \frac{y^2}{2B^2} & \frac{x^3}{6A^3} & \frac{x^2y}{2A^2B} & \frac{xy^2}{2AB^2} & \frac{y^3}{6B^3} & \frac{x^3y}{6A^3B} & \frac{xy^3}{6AB^3} \end{bmatrix}$$

Matrix $[\mathbf{A}]^{-1}$ (20×20):

$$[A]^{-1} =$$

$$\begin{bmatrix}
1 & 0 & 0 & 0 & 0 & 0 & 0 & 0 & 0 & 0 & 0 & 0 & 0 & 0 & 0 & 0 & 0 & 0 & 0 & 0 \\
\frac{-A}{x_e} & 0 & 0 & 0 & 0 & \frac{A}{x_e} & 0 & 0 & 0 & 0 & 0 & 0 & 0 & 0 & 0 & 0 & 0 & 0 & 0 & 0 \\
\frac{-B}{y_e} & 0 & 0 & 0 & 0 & 0 & 0 & 0 & 0 & 0 & 0 & 0 & 0 & 0 & 0 & \frac{B}{y_e} & 0 & 0 & 0 & 0 \\
\frac{AB}{x_e y_e} & 0 & 0 & 0 & 0 & \frac{-AB}{x_e y_e} & 0 & 0 & 0 & 0 & \frac{AB}{x_e y_e} & 0 & 0 & 0 & 0 & \frac{-AB}{x_e y_e} & 0 & 0 & 0 & 0 \\
0 & 1 & 0 & 0 & 0 & 0 & 0 & 0 & 0 & 0 & 0 & 0 & 0 & 0 & 0 & 0 & 0 & 0 & 0 & 0 \\
0 & \frac{-A}{x_e} & 0 & 0 & 0 & 0 & \frac{A}{x_e} & 0 & 0 & 0 & 0 & 0 & 0 & 0 & 0 & 0 & 0 & 0 & 0 & 0 \\
0 & \frac{-B}{y_e} & 0 & 0 & 0 & 0 & 0 & 0 & 0 & 0 & 0 & 0 & 0 & 0 & 0 & 0 & \frac{B}{y_e} & 0 & 0 & 0 \\
0 & \frac{AB}{x_e y_e} & 0 & 0 & 0 & 0 & \frac{-AB}{x_e y_e} & 0 & 0 & 0 & 0 & \frac{AB}{x_e y_e} & 0 & 0 & 0 & 0 & \frac{-AB}{x_e y_e} & 0 & 0 & 0 \\
0 & 0 & 1 & 0 & 0 & 0 & 0 & 0 & 0 & 0 & 0 & 0 & 0 & 0 & 0 & 0 & 0 & 0 & 0 & 0 \\
0 & 0 & 0 & A & 0 & 0 & 0 & 0 & 0 & 0 & 0 & 0 & 0 & 0 & 0 & 0 & 0 & 0 & 0 & 0 \\
0 & 0 & 0 & 0 & B & 0 & 0 & 0 & 0 & 0 & 0 & 0 & 0 & 0 & 0 & 0 & 0 & 0 & 0 & 0 \\
0 & 0 & \frac{-6A^2}{x_e^2} & \frac{-4A^2}{x_e} & 0 & 0 & 0 & \frac{6A^2}{x_e^2} & \frac{-2A^2}{x_e} & 0 & 0 & 0 & 0 & 0 & 0 & 0 & 0 & 0 & 0 & 0 \\
0 & 0 & \frac{-AB}{x_e y_e} & \frac{-AB}{y_e} & \frac{-AB}{x_e} & 0 & 0 & \frac{AB}{x_e y_e} & 0 & \frac{AB}{x_e} & 0 & 0 & \frac{-AB}{x_e y_e} & 0 & 0 & 0 & 0 & \frac{AB}{x_e y_e} & \frac{AB}{y_e} & 0 \\
0 & 0 & \frac{-6B^2}{y_e^2} & 0 & \frac{-4B^2}{y_e} & 0 & 0 & 0 & 0 & 0 & 0 & 0 & 0 & 0 & 0 & 0 & 0 & \frac{6B^2}{y_e^2} & 0 & \frac{-2B^2}{y_e} \\
0 & 0 & \frac{12A^3}{x_e^3} & \frac{6A^3}{x_e^2} & 0 & 0 & 0 & \frac{-12A^3}{x_e^3} & \frac{6A^3}{x_e^2} & 0 & 0 & 0 & 0 & 0 & 0 & 0 & 0 & 0 & 0 & 0 \\
0 & 0 & \frac{6A^2B}{x_e^2 y_e} & \frac{4A^2B}{x_e y_e} & 0 & 0 & 0 & \frac{-6A^2B}{x_e^2 y_e} & \frac{2A^2B}{x_e y_e} & 0 & 0 & 0 & \frac{6A^2B}{x_e^2 y_e} & \frac{-2A^2B}{x_e y_e} & 0 & 0 & 0 & \frac{-6A^2B}{x_e^2 y_e} & \frac{-4A^2B}{x_e y_e} & 0 \\
0 & 0 & \frac{6AB^2}{x_e y_e^2} & 0 & \frac{4AB^2}{x_e y_e} & 0 & 0 & \frac{-6AB^2}{x_e y_e^2} & 0 & \frac{-4AB^2}{x_e y_e} & 0 & 0 & \frac{6AB^2}{x_e y_e^2} & 0 & \frac{-2AB^2}{x_e y_e} & 0 & 0 & \frac{-6AB^2}{x_e y_e^2} & 0 & \frac{2AB^2}{x_e y_e} \\
0 & 0 & \frac{12B^3}{y_e^3} & 0 & \frac{6B^3}{y_e^2} & 0 & 0 & 0 & 0 & 0 & 0 & 0 & 0 & 0 & 0 & 0 & 0 & \frac{-12B^3}{y_e^3} & 0 & \frac{6B^3}{y_e^2} \\
0 & 0 & \frac{-12A^3B}{x_e^3 y_e} & \frac{-6A^3B}{x_e^2 y_e} & 0 & 0 & 0 & \frac{12A^3B}{x_e^3 y_e} & \frac{-6A^3B}{x_e^2 y_e} & 0 & 0 & 0 & \frac{-12A^3B}{x_e^3 y_e} & \frac{6A^3B}{x_e^2 y_e} & 0 & 0 & 0 & \frac{12A^3B}{x_e^3 y_e} & \frac{6A^3B}{x_e^2 y_e} & 0 \\
0 & 0 & \frac{-12AB^3}{x_e y_e^3} & 0 & \frac{-6AB^3}{x_e y_e^2} & 0 & 0 & \frac{12AB^3}{x_e y_e^3} & 0 & \frac{6AB^3}{x_e y_e^2} & 0 & 0 & \frac{-12AB^3}{x_e y_e^3} & 0 & \frac{6AB^3}{x_e y_e^2} & 0 & 0 & \frac{12AB^3}{x_e y_e^3} & 0 & \frac{-6AB^3}{x_e y_e^2}
\end{bmatrix}$$

2.9 References

[1] M.P. Païdoussis, Fluid-Structure Interactions: Slender Structures and Axial Flow, vol. I, Academic Press, London, 1998.

[2] M.P. Païdoussis, Fluid-Structure Interactions: Slender Structures and Axial Flow, vol. II, Elsevier, Amsterdam, 2004.

[3] F. Axisa, J. Antunes, Modelling of Mechanical Systems, vol. 3: Fluid-Structure Interaction, Elsevier, 2006.

[4] H.J.P. Morand, R. Ohayon, Fluid-Structure Interaction: Applied Numerical Methods, Wiley, New York, 1995.

[5] M. Amabili, M.P. Païdoussis, A.A. Lakis, Vibrations of partially filled cylindrical tanks with ring-stiffeners and flexible bottom, J. Sound Vib. 213 (2) (1998) 259-298.

[6] M. Chiba, Free vibration of a partially liquid-filled and partially submerged, clamped-free circular cylindrical shell, J. Acoust. Soc. Am. 100 (4 pt 1) (1996) 2170.

[7] K.H. Jeong, S.C. Lee, Fourier series expansion method for free vibration analysis of either a partially liquid-filled or a partially liquid-surrounded circular cylindrical shell, Comput. Struct. 58 (5) (1996) 937-946.

[8] M. Amabili, Effect of finite fluid depth on the hydroelastic vibrations of circular and annular plates, J. Sound Vib. 193 (4) (1996) 909-925.

[9] Y. Fu, W.G. Price, Interaction between a partially or totally immersed vibrating cantilever plate and the surrounding fluid, J. Sound Vib. 118 (3) (1987) 495-513.

[10] M.K. Kwak, S.-B. Han, Effect of fluid depth on the hydroelastic vibration of free-edge circular plate, J. Sound Vib. 230 (1) (2000) 171-185.

[11] U.S. Lindholm, D.D. Kana, W.H. Chu, H.N. Abramson, Elastic vibration characteristics of cantilever plates in water, J. Ship Res. 9 (1) (1965) 11-22.

[12] J.K. Kim, H.M. Koh, I.J. Kwahk, Dynamic response of rectangular flexible fluid containers, J. Eng. Mech. 122 (9) (1996) 807-817.

[13] M.C. Kim, S.S. Lee, Hydroelastic analysis of a rectangular tank, in: MSC Aerospace User's Conference, Newport Beach, CA, 1997, pp. 17-20.

[14] H.F. Bauer, W. Eidel, Hydroelastic vibrations in a two-dimensional rectangular container filled with frictionless liquid and a partly elastically covered free surface, J. Fluids Struct. 19 (2) (2004) 209-220.

[15] S.M. Soedel, W. Soedel, On the free and forced vibration of a plate supporting a freely sloshing surface liquid, J. Sound Vib. 171 (2) (1994) 159-171.

[16] Y.W. Kim, Y.S. Lee, Coupled vibration analysis of liquid-filled rigid cylindrical storage tank with an annular plate cover, J. Sound Vib. 279 (1-2) (2005) 217-235.

[17] J.F. Sigrist, S. Garreau, Dynamic analysis of fluid-structure interaction problems with modal methods using pressure-based fluid finite elements, Finite Elem. Anal. Des. 43 (4) (2007) 287-300.

[18] J.R. Cho, H.W. Lee, S.Y. Ha, Finite element analysis of resonant sloshing response in 2-D baffled tank, J. Sound Vib. 288 (4-5) (2005) 829-845.

[19] C.J.K. Lee, H. Noguchi, S. Koshizuka, Fluid-shell structure interaction analysis by coupled particle and finite element method, in: Fourth MIT Conference on Computational Fluid and Solid Mechanics: Comput. Struct. 85 (11-14) (2007) 688-697.

[20] H.M. Koh, J.K. Kim, J.H. Park, Fluid-structure interaction analysis of 3-D rectangular tanks by a variationally coupled BEM-FEM and comparison with test results, Earthquake Eng. Struct. Dyn. 27 (2) (1998) 109-124.

[21] A.A. Lakis, S. Neagu, Free surface effects on the dynamics of cylindrical shells partially filled with liquid, J. Sound Vib. 207 (2) (1997) 175-205.

[22] K.H. Jeong, K.J. Kim, Free vibration of a circular cylindrical shell filled with bounded compressible fluid, J. Sound Vib. 217 (2) (1998) 197-221.

[23] E. Hernandez, Approximation of the vibration modes of a plate and shells coupled with a fluid, J. Appl. Mech. Trans. ASME, 73 (6) (2006) 1005-1010.

[24] A.A. Lakis, M.P. Païdoussis, Free vibration of cylindrical shells partially filled with liquid, J. Sound Vib. 19 (1971) 1-15.

[25] A.A. Lakis, M.P. Païdoussis, Dynamic analysis of axially non-uniform thin cylindrical shells, J. Mech. Eng. Sci. 14 (1972) 49-71.

[26] M.H. Toorani, A.A. Lakis, Dynamics behavior of axisymmetric and beam-like anisotropic cylindrical shells conveying fluid, J. Sound Vib. 259 (2) (2003) 265-298.

[27] M.H. Toorani, A.A. Lakis, Large amplitude vibrations of anisotropic cylindrical shells, Comput. Struct. Technol. Comput. Struct. 82 (23-26) (2004) 2015-2025.

[28] A. Selmane, A.A. Lakis, Vibration Analysis of Anisotropic Open Cylindrical Shells Subjected to a Flowing Fluid, J. Fluids Struct. 11 (1) (1997) 111-134.

[29] M.H. Toorani, A.A. Lakis, Dynamic analysis of anisotropic cylindrical shells containing flowing fluid, in: 2001 ASME Pressure Vessels and Piping Conference, July 22-26 2001, Atlanta, GA, USA, American Society of Mechanical Engineers, New York, NY 10016-5990, USA, 2001, pp.165-174.

[30] A. Selmane, A.A. Lakis, Non-linear dynamic analysis of orthotropic open cylindrical shells subjected to a flowing fluid, J. Sound Vib. 202 (1) (1997) 67-93.

[31] A.A. Lakis, P. Van Dyke, H. Ouriche, Dynamic analysis of anisotropic fluid-filled conical shells, J. Fluid Struct. 6 (2) (1992) 135-162.

[32] A.A. Lakis, N. Tuy, A. Laveau, A. Selmane, Analysis of axially non-uniform thin spherical shells, in: International Symposium on STRUCOPT-COMPUMAT, Paris, France, 1989 pp. 80-85.

[33] AA. Lakis, M.P. Païdoussis, Prediction of the response of a cylindrical shell to arbitrary or boundary-layer-induced random pressure fields, J. Sound Vib. 25 (1) (1972) 1-27.

[34] J.L. Sanders, An improved First Approximation Theory for Thin Shells, NASA TR-24, 1959.

[35] M.H. Toorani, A.A. Lakis, General equations of anisotropic plates and shells including transverse shear deformations, rotary inertia and initial curvature effects, J. Sound Vib. 237 (4) (2000) 561-615.

[36] R.D. Cook, D.S. Malkus, M.E. Pelsha, R.J. Witt, Concepts and Applications of

Finite Element Analysis, fourth ed., Wiley, New York, 2002.

[37] H. Lamb, Hydrodynamics, Dover, New York, NY, USA, 1945.

[38] ANSYS Release 9.0, ANSYS Inc., Canonsburg, PA, USA, November 2004.

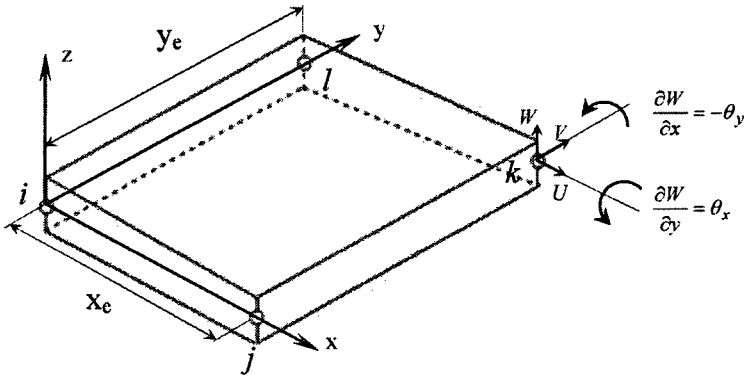

Figure 2.1 Flat rectangular shell element.

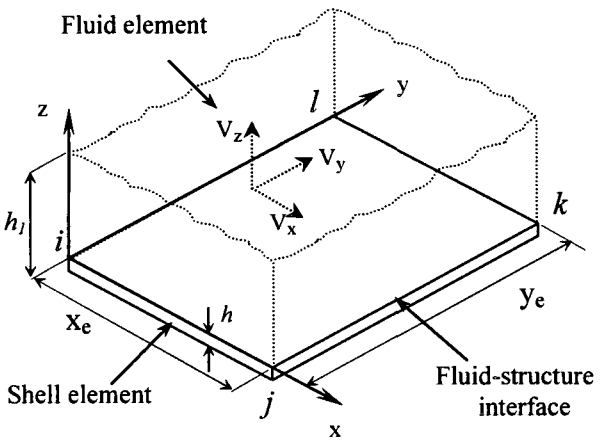

Figure 2.2 Fluid-structure element.

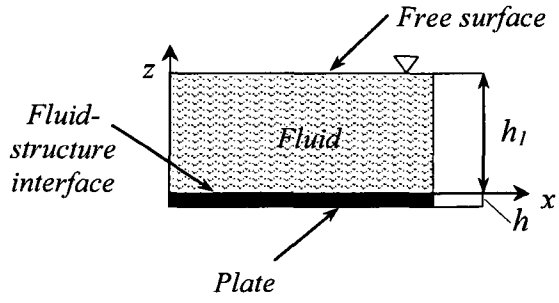

Figure 2.3 Fluid-structure element representing fluid over plate having free surface at $z=h_1$.

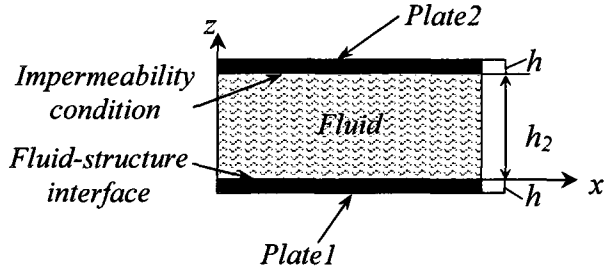

Figure 2.4 Fluid-structure element representing two identical plates coupled with bounded fluid.

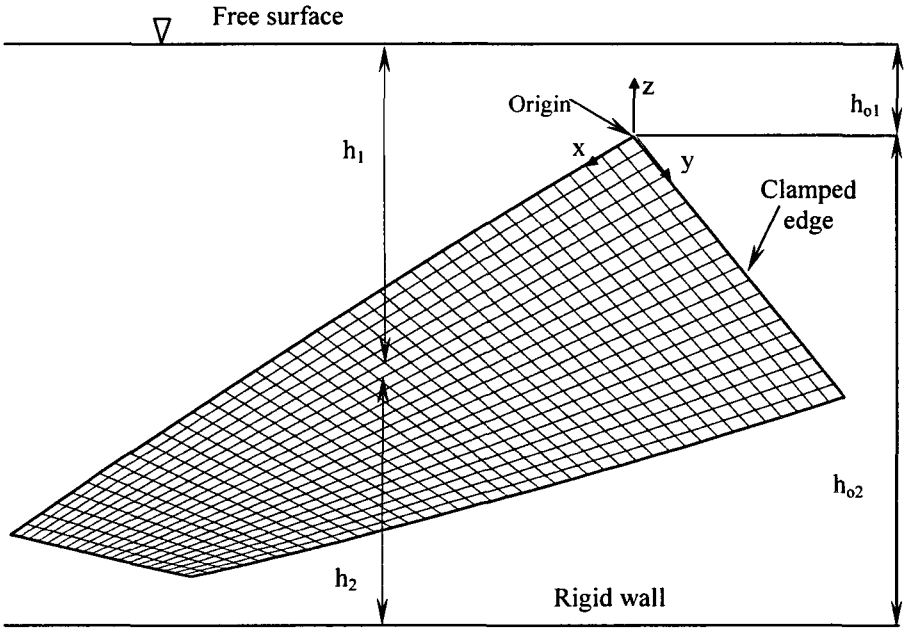

Figure 2.5 Submerged blade.

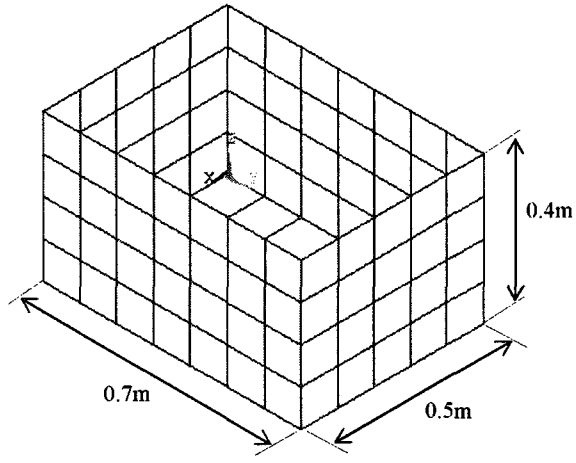

Figure 2.6 Rectangular reservoir.

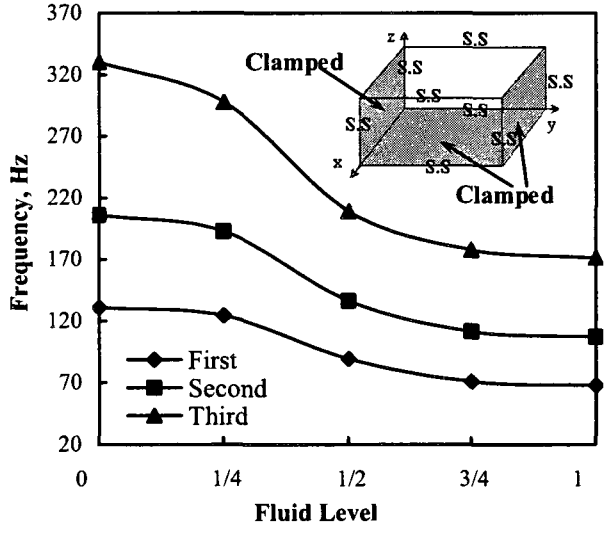

Figure 2.7 Frequency variations of a reservoir with a rigid core and two simply supported walls versus fluid level variations.

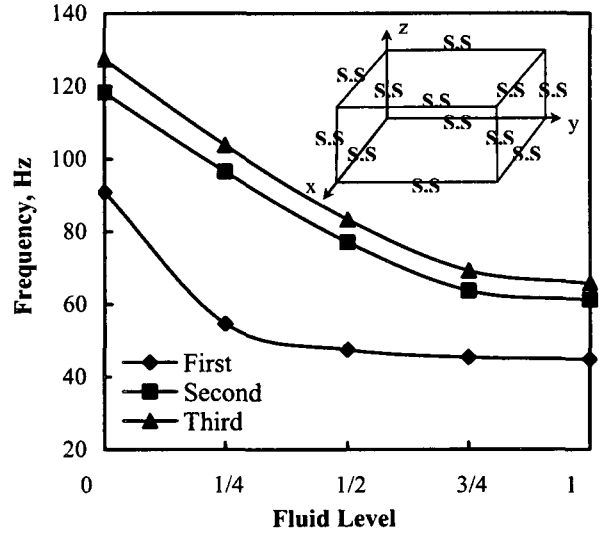

Figure 2.8 Frequency variations of a simply supported reservoir versus fluid level variations.

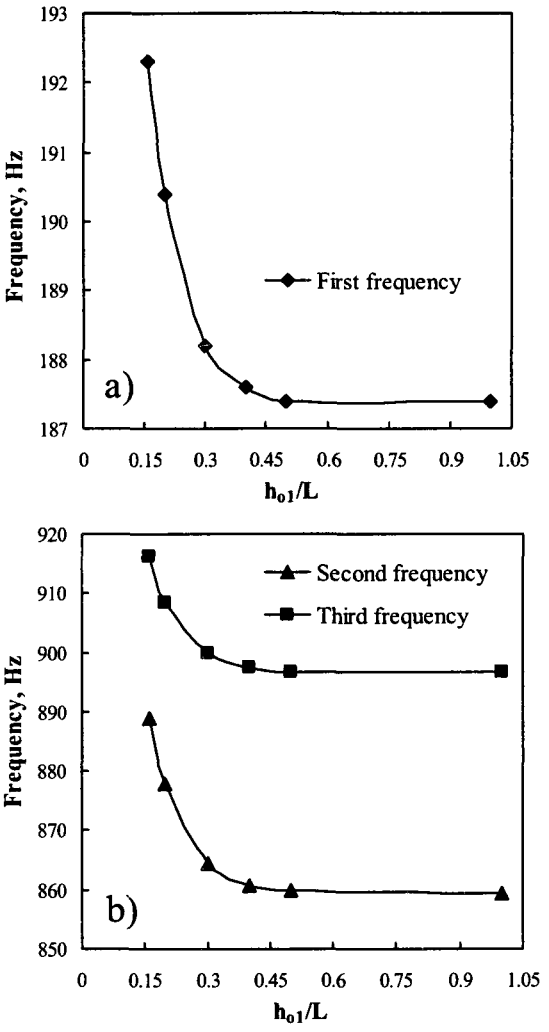

Figure 2.9 Frequency variations of a submerged blade as a function of h_{o1}/L variations at sufficiently large h_{o2}: (a) 1st frequency and (b) 2nd and 3rd frequencies.

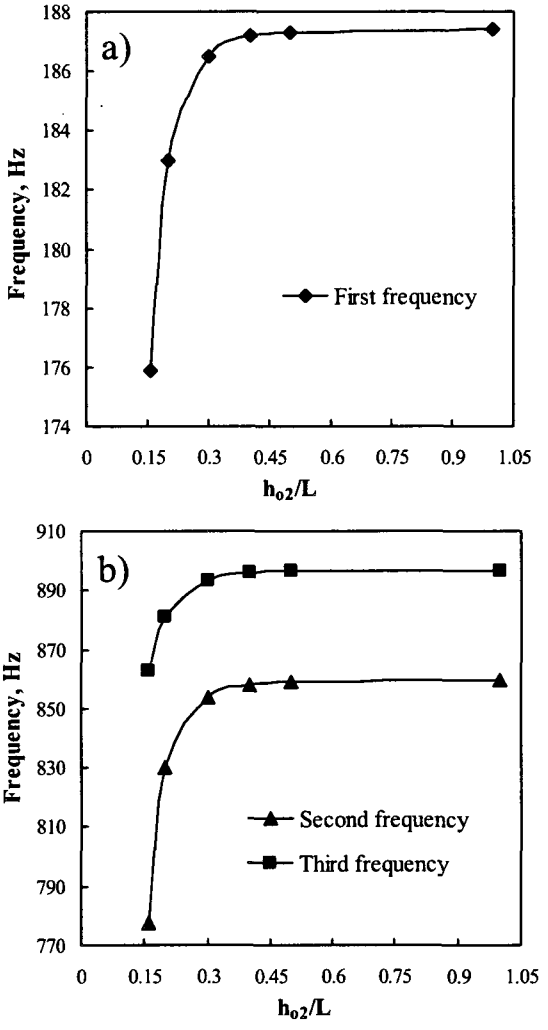

Figure 2.10 Frequency variations of a submerged blade as a function of h_{o2}/L variations at sufficiently large h_{o1}: (a) 1st frequency and (b) 2nd and 3rd frequencies.

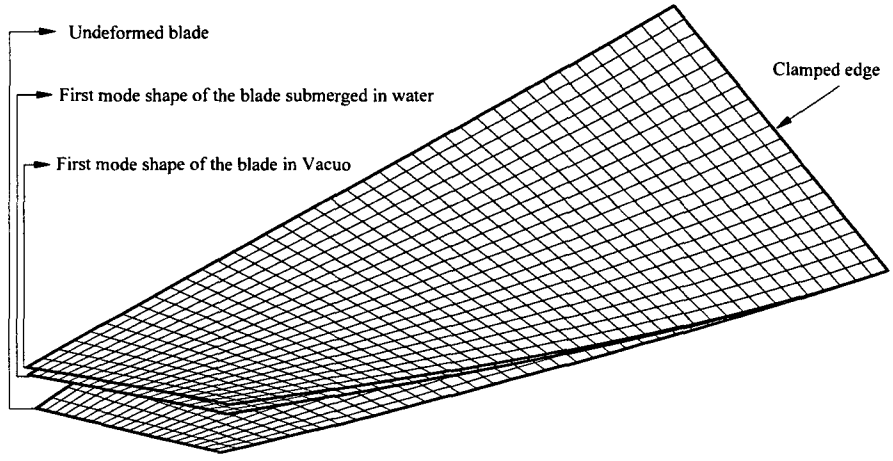

Figure 2.11 First mode shapes of a blade in vacuo and submerged in water (where h_{o1}=4 cm and h_{o2} is large enough), as compared with the undeformed blade.

Table 2.1

Comparison of natural frequencies of the simply supported reservoir in a vacuum (case a)

Natural frequency (Hz)		Discrepancy (%)
ANSYS	Present method	
91.62	91.00	0.68
119.11	118.30	0.68
128.01	127.50	0.40
143.97	142.40	1.09
157.61	156.00	1.02

Table 2.2

Comparison of natural frequencies of the fluid-filled simply supported reservoir (case a)

Coupled natural frequency (Hz)		Discrepancy (%)
ANSYS	Present method	
38.99	44.92	13.19
53.24	61.24	13.07
57.51	65.80	12.60
70.99	74.63	4.88
72.50	82.46	12.08

Table 2.3

Comparison of natural frequencies of the bottom-clamped rectangular reservoir in a vacuum (case b)

Natural frequency (Hz)		Discrepancy (%)
ANSYS	Present method	
53.44	52.98	0.86
59.68	59.12	0.93
85.98	85.08	1.05
100.34	99.48	0.86
136.19	134.90	0.95

Table 2.4

Comparison of natural frequencies of the fluid-filled bottom-clamped rectangular reservoir (case b)

Coupled natural frequency (Hz)		Discrepancy (%)
ANSYS	Present method	
26.519	27.61	3.95
29.917	30.69	2.52
45.05	45.30	0.55
45.32	52.98	14.46
73.31	70.15	4.50

Table 2.5

Comparison of natural frequencies of a clamped-free blade (10 cm × 20 cm × 1cm) in a vacuum

Natural frequency (Hz)		Discrepancy (%)
ANSYS	Present method	
212.47	236.20	10.05
1045.80	1087.00	3.79
1050.50	1123.00	6.46
2166.50	2148.00	0.86
3207.90	3251.00	1.33

CHAPTER III

ARTICLE 2: PREDICTION OF THE RESPONSE OF A THIN STRUCTURE SUBJECTED TO A TURBULENT BOUNDARY-LAYER-INDUCED RANDOM PRESSURE FIELD

M. Esmailzadeh [a], A. A. Lakis [a,*], M. Thomas [b], L. Marcouiller [c]

[a] *Mechanical Engineering Department, École Polytechnic of Montréal, C.P. 6079, Succursale Centre-ville, Montréal, Québec, Canada, H3C 3A7, Tel: +1 514 340 4711, ext: 4906, Fax: +1 514 340 4172, E-mail: aouni.lakis@polymtl.ca*

[b] *Mechanical Engineering Dept., École de Technologie Supérieure, 1100, Notre-Dame Ouest, Montréal, Québec, Canada, H3C 1K3*

[c] *Institut de Recherche d'Hydro Québec, 1800, Lionel-Boulet Varennes, Québec, Canada, J3X 1S1*

Revised Article Submitted in

Journal of Sound and Vibration

March 2009

Keywords: Thin plate; Random vibration; Turbulent boundary layer; Subsonic flow; Fluid-structure interaction; Finite element method.

3.1 Abstract

A method capable of predicting the root mean square displacement response of a thin structure subjected to a turbulent boundary-layer-induced random pressure field is presented. The basic formulation of the dynamic problem is an efficient approach combining classic thin shell theory and the finite element method, in which the finite elements are flat rectangular elements with six degrees of freedom per node. The displacement functions are derived from thin shell theory. Description of the turbulent pressure field is based on the Corcos formulation for cross spectral density of pressure fluctuations. A numerical approach is proposed to obtain the total root mean square displacements of the structure. Exact integration over surface and frequency leads to an expression for the response in terms of the characteristics of the structure and flow. An in-house program based on the presented method was developed. The total root mean square displacements of a thin plate under different boundary conditions subjected to a turbulent boundary layer were calculated and illustrated as a function of free stream velocity and damping ratio and the effects of flow direction on the response were also investigated. In addition, the power spectral densities of the displacements of an SFSF plate subjected to a fully-developed turbulent flow were studied. The total root mean square radial displacement of a thin cylindrical shell was obtained and compared favorably with that in the literature.

3.2 Introduction

Responses of structures subjected to turbulent boundary layer excitation have long been of great practical importance in engineering. Some examples are; marine applications, aircraft structures and power plants. Random pressure induced by a fully-developed turbulent boundary layer is a frequent source of excitation and can cause low-amplitude vibration and eventually long-term structural fatigue. For this reason, determination of the response of structures subjected to boundary layer pressure fields is of importance.

Experimental and theoretical investigations of induced random pressure fields have been carried out by many researchers including Corcos [1, 2], Maestrello [3], Farabee and Casarella [4], etc. Investigations of the fluctuating wall pressure beneath a turbulent boundary layer have also been conducted by many researchers for fully-developed turbulent pipe flow [5, 6] and for turbulent boundary layers on flat plates [7, 8]. Blake [9] includes a chapter on structural response to turbulent wall flow in his book. He determined relationships for the mean-square modal velocity and displacement of one single mode of a panel in terms of the auto-spectral density of modal pressure.

Experimental works have mainly concentrated on the power spectral density of the pressure and space-time cross correlation functions. Most of the studies in the literature are devoted to investigating pressure fluctuations beneath a turbulent boundary layer, and studies on the displacement response of an elastic structure to these

excitations are scarce. A simply supported uniform thin cylindrical shell subjected to a turbulent boundary layer was modeled theoretically by Cottis and Jasonides [10]. They derived a general expression for the space-time correlation of the response for both arbitrary and boundary-layer-induced pressure fields but they did not proceed to evaluate the mean square value of response, nor did they undertake numerical solution of the problem. Their work was later extended to orthotropic shells [11]. To our knowledge, the first attempt to make a comparison of measured and predicted pipe vibration was made by Clinch [12]. He considered simply supported thin cylindrical shells which he analyzed using Powell's joint-acceptance method. In the analysis he assumed that the areas over which the wall pressure fluctuations are correlated are small compared with pipe dimensions. More importantly, he considered the response only in the high modes of the shell, where resonances are so close to one another that a continuous curve of response versus frequency may be assumed. He then compared his theoretical results to his own experimental data for a long, slender, thin cylinder conveying water. The average root mean square wall displacement displayed good agreement between theory and experiment at high frequencies. The limitation of his theory is that it applies only for high frequencies. However, it is worth mentioning that only the first resonance frequencies of the shell make a significant contribution to the response due to turbulent flow. Following Clinch's study, Lakis and Païdoussis presented [13] a theory to predict the displacement response of a uniform or axially non-uniform thin cylindrical shell to an arbitrary random pressure field, and to a pressure field arising from the turbulent boundary layer of an internal subsonic flow.

They obtained the root mean square (r.m.s.) displacements of the shell for a pressure field originating from the turbulent boundary layer of a subsonic internal flow at a specific circumferential wavenumber as well as the total displacement response by summation over all circumferential modes. Curling and Païdoussis [14] investigated an analytical solution to obtain the power spectral density (PSD) of the displacements of bundles of cylinders in turbulent axial flow. They calculated PSD of mid-cylinder displacements and compared results with experimental measurements obtained by Gagnon and Païdoussis.

Innovative and fast solutions for the stochastic response of a plate have been carried out by many researchers [15-19]. Birgersson, Ferguson and Finnveden [15] used spectral finite element and dynamic stiffness methods to analyze the autospectral density of the velocity of a plate due to a turbulent boundary layer. They utilized an approach in which the cross spectral density of the response was determined by a single integration over all wavenumbers rather than double integrals over the surface. Finnveden, Birgersson, Ross and Kremer [16] investigated the vibration response of a plate excited by a turbulent boundary layer experimentally and numerically. The vibration response of the velocity of a thin-walled plate was measured and then predicted using wall pressure models. The measured response agreed with existing models in a low frequency regime. Mazzoni [17] proposed a deterministic model based on an analytical wavenumber integration procedure to predict the response of a thin elastic plate subjected to both a turbulent flow of fluid at a low Mach number and acoustic noise. The power spectrum of the acceleration of the fluid-loaded plate

subjected to a turbulent boundary layer was obtained and compared with that obtained with using a classical random approach. Vitiello, De Rosa and Franco [18] developed a procedure to evaluate the aeroelastic response of a flat plate excited by a turbulent boundary layer. De Rosa and Franco [19] presented an exact and predictive response for a simply supported plate wetted on one side subjected to a turbulent boundary layer. Autospectral velocity of thin plates excited by low-speed turbulent boundary layer flow was analyzed numerically and experimentally by Hambric, Hwang and Bonness [20].

A cylindrical finite element was developed by one of the authors of this article, in which displacement functions were derived from shell equations of motion instead of using polynomial displacement functions [21, 22]. Prior to the work presented herein this element could only be applied to cylindrical, conical or spherical shells since it is a cylindrical frustum. Based on this element, another work has been developed by one of the authors of this paper to predict the response of a thin cylindrical shell subjected to random pressure fluctuations arising from a turbulent boundary layer [13].

In this paper we develop a general method to model any kind of thin elastic structure subjected to an arbitrary random pressure field and subsequently to a pressure field arising from a fully-developed turbulent boundary layer. The finite element used in this study is based on a previously developed method to study dynamic behavior of a thin structure subjected to stationary fluid [23, 24]. In this approach a flat rectangular element with six degrees of freedom per node was developed using a combination of Sanders' thin shell theory and the finite element method. Since the transverse displacement function is derived from thin plate theory this method may be easily

adapted to take hydrodynamic effects into account. Moreover, this method is capable of calculating both high and low frequencies with high accuracy. This capability is normally of little interest in free vibration analysis, but it is of considerable importance for determining the response of structures subjected to random pressure fields such as those generated by turbulent flow. A continuous random pressure field is transformed into a discrete force field acting at each node of the finite element. Structural response to turbulence-induced excitation forces is calculated using random vibration theory. Corcos formulation for cross spectral density of the pressure fluctuations was adopted to describe the turbulent pressure field. A numerical approach is proposed to obtain the magnitude of the random response. Exact integration over surface and frequency was carried out analytically and an expression for the root mean square displacement response was obtained in terms of the characteristics of the structure and flow.

An in-house program was developed to predict the root mean square displacement response of a thin structure to a random pressure field arising from a turbulent boundary layer. In order to demonstrate the applicability of the proposed method, a thin plate under different boundary conditions was investigated. Accuracy of the proposed method was also verified for a cylindrical shell case. A thin cylindrical shell was analyzed and compared with the results obtained by Lakis and Païdoussis [13]. In our proposed method, the Corcos lateral and longitudinal correlations were used, but in Lakis' results Bakewell correlations were employed. Even though different correlations were adapted in the numerical calculation, good agreement was found. It should be noted that Lakis validated his results by verifying with Clinch's experimental

measurements and good agreement was obtained [13]. In other words, comparison with Clinch's experimental measurements shows that our method is sound. It seems that their work is the only case in the literature that calculates the total r.m.s. displacement of a shell subjected to a random pressure field arising from a boundary layer induced by turbulent flow. Comparisons with experimental measurements are scarce in the literature. Thus, this case study is undertaken in order to validate our method. As mentioned earlier, research has been conducted on auto-spectral density of the response of a plate but the vibration amplitude (total r.m.s. displacement) was not investigated.

Assumptions introduced into the theory are as follows: (1) the plate is assumed to be thin; (2) the pressure field is assumed to be stationary, ergodic and homogeneous; (3) the damping matrix is assumed to be proportional to mass and stiffness matrices in order to uncouple the equations of motion; (4) the turbulent boundary layer is fully developed; (5) acoustic pressure fluctuations induced by flow at moderate speeds are very small compared to turbulent pressure fluctuations, therefore we assume excitation only arises from pressure fluctuations in the turbulent boundary layer; (6) the compressibility effect is negligible; (7) flow is subsonic and Mach number is below 0.3; (8) pressure drop over the length of the plate is sufficiently small for the mean pressure to be considered constant over this length; (9) influence of the structural vibration induced by the fluctuating pressure field on the boundary layer is neglected due to its sufficiently small amplitude; (10) non-inertial dynamic effects of the flow are negligible.

3.3 Equation of motion

Dynamic behavior of a structure subjected to arbitrary loads is governed by the following equation:

$$[\mathbf{M}]\{\ddot{\boldsymbol{\delta}}\}+[\mathbf{C}]\{\dot{\boldsymbol{\delta}}\}+[\mathbf{K}]\{\boldsymbol{\delta}\}=\{\mathbf{F}(x,y,t)\}, \tag{3.1}$$

where **M**, **C** and **K** are the global mass, damping and stiffness matrices of the system, respectively, $\boldsymbol{\delta}$, $\dot{\boldsymbol{\delta}}$ and $\ddot{\boldsymbol{\delta}}$ are the global displacement, velocity and acceleration vectors, respectively and $\mathbf{F}(x,y,t)$ is a vector of external forces as a function of space and time.

Eq. (3.1) is quite general. In this paper we base our theory on a developed method for analysis of a thin plate in a vacuum and in inviscid incompressible stationary fluid [23, 24]. Global mass and stiffness matrices were determined using this method to obtain the free vibration characteristics of such plates. To briefly summarize; this theory was developed using a combination of classic thin plate theory and finite element analysis in which the finite elements were four-noded flat rectangular elements with six degrees of freedom per node, representing the in-plane and out-of-plane displacements and their spatial derivatives. The displacement functions were derived from Sanders' thin shell equations instead of the usual and more arbitrary interpolating polynomials. To establish the equilibrium equations for rectangular thin plates, Sanders' equations for cylindrical shells are used assuming the radius to be infinite. Both membrane and bending effects are taken into account in this theory to enable the

element to model curved structures as well. It is worth mentioning that Sanders based his equations on Love's first approximation theory but he demonstrated that all strains vanish for rigid body motion, which satisfies the convergence criteria of the finite element. The structural mass and stiffness matrices were determined by exact analytical integration. The fluid pressure applied on the structure was determined by combining the velocity potential function, Bernoulli's equation and the impermeability condition and was expressed as a function of acceleration of the normal displacement of the structure and the inertial force of the quiescent fluid. An analytical integration of the fluid pressure over the element produced the virtual added-mass matrix of stationary fluid.

The geometry of the structure element used in this analysis is shown in Figure 3.1. The nodal displacement vector at node i, $\boldsymbol{\delta}_i$ is defined by:

$$\left\{\boldsymbol{\delta}_i\right\} = \left\{U_i \quad V_i \quad W_i \quad \partial W_i/\partial x \quad \partial W_i/\partial y \quad \partial^2 W_i/\partial x\partial y\right\}^{\mathrm{T}}, \tag{3.2}$$

where U_i and V_i are the in-plane displacements of the plate reference surface in the x- and y- directions, respectively, W_i represents the radial displacement of the plate middle surface, $\partial W_i/\partial x$ and $\partial W_i/\partial y$ are the first derivatives of the radial displacement with respect to x and y, respectively, and $\partial^2 W_i/\partial x\partial y$ is the cross derivative of the radial displacement with respect to x and y at node i.

The displacement vector $\boldsymbol{\delta}$, for a plate subdivided into finite elements having n nodes has the form:

$$\{\delta\} = \left\{ \{\delta_1\}^T, \{\delta_2\}^T, ..., \{\delta_n\}^T \right\}^T. \tag{3.3}$$

3.4 Uncoupling the equations of motion

All the terms in Eq. (3.1) have now been defined except for the damping matrix, which will not be given an explicit form for reasons to become obvious below. Before proceeding with a discussion of the response of the plate to random pressure fields we need to uncouple the equation of motion.

The plate response $\delta(x,y,t)$ at any point x, y and at any time t may be expressed as a normal mode expansion in terms of the generalized coordinates $\{\mathbf{q}(t)\}$ and the modal matrix as follows:

$$\{\delta(x,y,t)\} = \left[\{\Phi_1\}, \{\Phi_2\}, ..., \{\Phi_N\} \right] \{\mathbf{q}(t)\} = \left[\Phi(x,y) \right] \{\mathbf{q}(t)\}, \tag{3.4}$$

where $[\Phi(x,y)]$ is the modal matrix in a vacuum, which consists of the orthogonal eigenvectors $\{\Phi_i\}$, and N is the number of mode shapes to be used in the analysis.

Substituting the above relationship into the equation of motion and pre-multiplying by Φ^T, the following is obtained:

$$[\bar{\mathbf{M}}]\{\ddot{\mathbf{q}}\} + [\bar{\mathbf{C}}]\{\dot{\mathbf{q}}\} + [\bar{\mathbf{K}}]\{\mathbf{q}\} = [\Phi]^T \{\mathbf{F}\}, \tag{3.5}$$

where $\bar{\mathbf{M}} = \Phi^T \mathbf{M} \Phi$ and $\bar{\mathbf{K}} = \Phi^T \mathbf{K} \Phi$ are the generalized mass and stiffness matrices, respectively. Due to orthogonality of the normal modes, $\bar{\mathbf{M}}$ and $\bar{\mathbf{K}}$ are diagonal matrices and the generalized damping matrix $\bar{\mathbf{C}} = \Phi^T \mathbf{C} \Phi$ will be a diagonal matrix if it

is taken to be proportional to $\bar{\mathbf{M}}$ and $\bar{\mathbf{K}}$, or a linear combination of these. The viscous damping type of structural damping is adopted in the equation of motion. Denoting the rth diagonal term of $\bar{\mathbf{C}}$ by $\bar{C}_r = 2\zeta_r\sqrt{\bar{K}_r\bar{M}_r}$, $\bar{M}_r$ and $\bar{K}_r$ being the corresponding terms of $\bar{\mathbf{M}}$ and $\bar{\mathbf{K}}$, and ζ_r being the rth generalized damping ratio and introducing these into Eq. (3.1) leads to the uncoupled set of equations:

$$\ddot{q}_r + 4\pi\zeta_r f_r \dot{q}_r + 4\pi^2 f_r^2 q_r = \frac{1}{\bar{M}_r}\{\mathbf{\Phi}\}_r^{\mathrm{T}}\{\mathbf{F}\}, \qquad r = 1,2,...,N, \tag{3.6}$$

where f_r is the rth natural frequency in Hz, $\bar{M}_r$ is the rth element of the generalized mass matrix and N is the number of mode shapes chosen for evaluation.

Upon solving the above equation the response at a typical node g, $\boldsymbol{\delta}_g$ in terms of the generalized coordinates is found:

$$\{\boldsymbol{\delta}_g(x,y,t)\} = \sum_{r=1}^{N}\{\mathbf{\Phi}_{gr}(x,y)\}\, q_r(t), \tag{3.7}$$

where $\mathbf{\Phi}_{gr}(x,y)$ is the rth mode shape at node g with $q_r(t)$ being the associated generalized coordinates. This is the instantaneous response due to an arbitrary force vector.

3.5 Representation of a continuous random pressure field at the nodal points

The continuous random pressure field of the deformable body will be approximated using a finite set of discrete forces and moments acting at the nodal points. The plate is divided into finite elements, each of which is a rectangular flat element. A pressure field is considered to be acting on an area S_c surrounding the node c of the coordinates l_c and d_c as shown in Figure 3.2. This area S_c is delimited by the positions l_c' and l_c'' with respect to the origin in the x-direction and d_c' and d_c'' with respect to the origin in the y-direction. It is therefore possible to determine the pressure distribution acting over the area S_c in terms of a lateral force. The lateral force acting at an arbitrary point, A, on the area S_c is given by (see Figure 3.2):

$$F_A(t) = \int_{d_c'}^{d_c''} \int_{l_c'}^{l_c''} P(x,y,t)\mathrm{d}x\,\mathrm{d}y\,, \tag{3.8}$$

where $P(x,y,t)$ is the instantaneous pressure on the surface. The force $F_A(t)$ acting at point A is transformed into one force and two moments acting at node c, as illustrated in Figure 3.2.

The external load vector acting at a typical node c, $\mathbf{F}_c$ associated with the nodal displacements can be written in the following form:

$$\mathbf{F}_c(t)=\begin{Bmatrix}0\\0\\F_n\\M_y\\M_x\\0\end{Bmatrix}=\begin{Bmatrix}0\\0\\-\int_{d_i'}^{d_i''}\int_{l_i'}^{l_i''}P(x_i,y_i,t)\mathrm{d}x_i\,\mathrm{d}y_i\\-\int_{d_p'}^{d_p''}\int_{l_p'}^{l_p''}(x_p-l_p)P(x_p,y_p,t)\mathrm{d}x_p\,\mathrm{d}y_p\\-\int_{d_j'}^{d_j''}\int_{l_j'}^{l_j''}(y_j-d_j)P(x_j,y_j,t)\mathrm{d}x_j\,\mathrm{d}y_j\\0\end{Bmatrix}, \tag{3.9}$$

where F_n is the lateral force in the z-direction, M_x and M_y are the moments in the x- and y- directions acting at node c, respectively and $l_i''=l_p''=l_j''=l_c''$, $l_i'=l_p'=l_j'=l_c'$, $d_i''=d_p''=d_j''=d_c''$, $d_i'=d_p'=d_j'=d_c'$, $l_p=l_c$ and $d_j=d_c$. This particular indicial notation is introduced for convenience in subsequent manipulations.

3.6 Response to an arbitrary random pressure field

If the pressure field is deterministic, the response as expressed by Eq. (3.7) is the solution. In the case of a random field however, we must proceed differently. First we express the mean square of the response in terms of the spectral density of an arbitrary random pressure field. This is followed by presentation of the response to an arbitrary homogeneous random pressure field.

3.6.1 Mean square displacements in terms of the cross spectral density of an arbitrary random pressure

As mentioned earlier, a random process can only be described in statistical terms. Here, we assume that the random pressure is stationary in time and homogeneous in space, so the response can be expressed in terms of the cross-spectral density of the pressure. Assuming that we are dealing with an ergodic process and using the correlation theorem, the mean square displacement response at node g, $\overline{\boldsymbol{\delta}_g^2(x_g, y_g, t)}$ can be expressed as follows:

$$\overline{\boldsymbol{\delta}_g^2(x_g, y_g, t)} = \lim_{T\to\infty} \frac{1}{T} \int_0^{+\infty} \boldsymbol{\Delta}_g^*(x_g, y_g, f, T)\boldsymbol{\Delta}_g(x_g, y_g, f, T)\mathrm{d}f\,, \tag{3.10}$$

where $\boldsymbol{\Delta}$ and $\boldsymbol{\Delta}^*$ are the finite Fourier transforms of the nodal displacement and its complex conjugate, respectively, f is the frequency in Hz and T is the period. It should be stated that $\lim_{T\to\infty} \frac{\boldsymbol{\Delta}_g^* \boldsymbol{\Delta}_g}{T}$ is the one-sided auto spectral density of displacement.

Taking the Fourier transform of Eq. (3.6), we obtain the Fourier transform of the generalized coordinates as follows:

$$Q_r(f,T) = \frac{H_r(f)\boldsymbol{\Phi}_r^{\mathrm{T}}\mathbf{F}(f,T)}{4\pi^2 f_r^2 \bar{M}_r}, \tag{3.11}$$

where $\mathbf{F}(f,T)$ is the Fourier transform of the force vector and $H_r(f)$ is the frequency response function for the rth mode defined as follows:

$$H_r(f)=\left\{1-\left(\frac{f}{f_r}\right)^2+2\mathrm{i}\zeta_r\left(\frac{f}{f_r}\right)\right\}^{-1}=\left|H_r(f)\right|\mathrm{e}^{-\mathrm{i}\theta_r(f)}, \tag{3.12}$$

where $\left|H_r(f)\right|$ and $\theta_r(f)$ are the magnification and phase factors, respectively, f is the forced frequency, f_r is the rth natural frequency and i^2=-1.

Substituting Eq. (3.11) into the Fourier transform of Eq. (3.7), the Fourier transform of the nodal displacement can be written as follows:

$$\mathbf{\Delta}_g(f,T)=\sum_{r=1}^{N}\mathbf{\Phi}_{gr}\frac{\left|H_r(f)\right|\mathrm{e}^{-i\theta_r(f)}}{4\pi^2 f_r^2\bar{M}_r}\mathbf{\Phi}_r^{\mathrm{T}}\mathbf{F}(f,T). \tag{3.13}$$

Introducing Eq. (3.13) and its complex conjugate into Eq. (3.10), the mean square response at node g is obtained:

$$\overline{\delta_g^2(x_g,y_g,t)}=\sum_{r=1}^{N}\sum_{s=1}^{N}\frac{\mathbf{\Phi}_{gr}(x_g,y_g)\mathbf{\Phi}_{gs}(x_g,y_g)}{(2\pi)^4 f_r^2 f_s^2\bar{M}_r\bar{M}_s}\lim_{T\to\infty}\frac{1}{T}\int_0^{\infty}\mathrm{e}^{\mathrm{i}(\theta_s-\theta_r)}\left|H_r(f)\right|\left|H_s(f)\right|\{\mathbf{\Phi}\}_s^{\mathrm{T}}\mathbf{F}^*(f,T)\{\mathbf{\Phi}\}_r^{\mathrm{T}}\mathbf{F}(f,T)\mathrm{d}f, \tag{3.14}$$

where $\mathbf{\Phi}_{gr}$ and $\mathbf{\Phi}_{gs}$ are the rth and sth mode shapes at node g, $\left|H_r(f)\right|$ and $\left|H_s(f)\right|$ are the magnification factors for the rth and sth modes, θ_r and θ_s are the phase lags between the force and the response, and $\mathbf{F}(f,T)$ and $\mathbf{F}^*(f,T)$ are the Fourier transforms of the force vector and its complex conjugate, respectively.

For a lightly damped multi-degree-of-freedom system with well separated natural frequencies, the cross-product terms are much smaller than the self-product terms; therefore the contribution of the cross-product terms to the mean square

displacement response can be ignored without significant loss of accuracy. Eq. (3.14) can then be rewritten as follows:

$$\overline{\delta_g^2(x_g,y_g,t)}=\sum_{r=1}^{N}\frac{\Phi_{gr}^2(x_g,y_g)}{16\pi^4 f_r^4 \bar{M}_r^2}\lim_{T\to\infty}\frac{1}{T}\int_0^{\infty}\left|H_r(f)\right|^2\{\Phi\}_r^{\mathrm{T}}\mathbf{F}(f,T)\{\Phi\}_r^{\mathrm{T}}\mathbf{F}^*(f,T)\mathrm{d}f\,. \tag{3.15}$$

Note that loads acting at each node have three components; one lateral force and two moments about the in-plane directions. Therefore the cross spectral density of the force between any two nodes has nine terms.

We next define the one-sided cross spectral density of pressure:

$$G_{pp}(x_i,y_i,x_j,y_j,f)=\lim_{T\to\infty}\frac{1}{T}\left[P^*(x_i,y_i,f,T)P(x_j,y_j,f,T)\right], \tag{3.16}$$

where P and P^* are the Fourier transforms of the pressure and its complex conjugate, respectively.

Substituting the Fourier transform of the external force vector from Eq. (3.9) into Eq. (3.15), transforming the vector by summation and then introducing Eq. (3.16) into Eq. (3.15), the mean square response at node g is obtained as follows:

$$\overline{\boldsymbol{\delta}_g^2(x_g,y_g,t)}=\sum_{r=1}^{N}\frac{\boldsymbol{\Phi}_{gr}^2}{16\pi^4 f_r^4 \bar{M}_r^2}\int_0^\infty |H_r(f)|^2$$

$$\{\sum_{i=1}^{n}\sum_{u=1}^{n}\Phi_{ir}\Phi_{ur}\int_{d_u'}^{d_u''}\int_{l_u'}^{l_u''}\int_{d_i'}^{d_i''}\int_{l_i'}^{l_i''}G_{pp}(x_i,y_i,x_u,y_u,f)\,dx_i\,dy_i\,dx_u\,dy_u+$$

$$\sum_{i=1}^{n}\sum_{v=1}^{n}\Phi_{ir}\Phi_{vr}\int_{d_v'}^{d_v''}\int_{l_v'}^{l_v''}\int_{d_i'}^{d_i''}\int_{l_i'}^{l_i''}(x_v-l_v)G_{pp}(x_i,y_i,x_v,y_v,f)\,dx_i\,dy_i\,dx_v\,dy_v+$$

$$\sum_{i=1}^{n}\sum_{k=1}^{n}\Phi_{ir}\Phi_{kr}\int_{d_k'}^{d_k''}\int_{l_k'}^{l_k''}\int_{d_i'}^{d_i''}\int_{l_i'}^{l_i''}(y_k-d_k)G_{pp}(x_i,y_i,x_k,y_k,f)\,dx_i\,dy_i\,dx_k\,dy_k+$$

$$\sum_{p=1}^{n}\sum_{u=1}^{n}\Phi_{pr}\Phi_{ur}\int_{d_u'}^{d_u''}\int_{l_u'}^{l_u''}\int_{d_p'}^{d_p''}\int_{l_p'}^{l_p''}(x_p-l_p)G_{pp}(x_p,y_p,x_u,y_u,f)\,dx_p\,dy_p\,dx_u\,dy_u+$$

$$\sum_{p=1}^{n}\sum_{v=1}^{n}\Phi_{pr}\Phi_{vr}\int_{d_v'}^{d_v''}\int_{l_v'}^{l_v''}\int_{d_p'}^{d_p''}\int_{l_p'}^{l_p''}(x_p-l_p)(x_v-l_v)G_{pp}(x_p,y_p,x_v,y_v,f)\,dx_p\,dy_p\,dx_v\,dy_v+$$

$$\sum_{p=1}^{n}\sum_{k=1}^{n}\Phi_{pr}\Phi_{kr}\int_{d_k'}^{d_k''}\int_{l_k'}^{l_k''}\int_{d_p'}^{d_p''}\int_{l_p'}^{l_p''}(x_p-l_p)(y_k-d_k)G_{pp}(x_p,y_p,x_k,y_k,f)\,dx_p\,dy_p\,dx_k\,dy_k+$$

$$\sum_{j=1}^{n}\sum_{u=1}^{n}\Phi_{jr}\Phi_{ur}\int_{d_u'}^{d_u''}\int_{l_u'}^{l_u''}\int_{d_j'}^{d_j''}\int_{l_j'}^{l_j''}(y_j-d_j)G_{pp}(x_j,y_j,x_u,y_u,f)\,dx_j\,dy_j\,dx_u\,dy_u+$$

$$\sum_{j=1}^{n}\sum_{v=1}^{n}\Phi_{jr}\Phi_{vr}\int_{d_v'}^{d_v''}\int_{l_v'}^{l_v''}\int_{d_j'}^{d_j''}\int_{l_j'}^{l_j''}(y_j-d_j)(x_v-l_v)G_{pp}(x_j,y_j,x_v,y_v,f)\,dx_j\,dy_j\,dx_v\,dy_v+$$

$$\sum_{j=1}^{n}\sum_{k=1}^{n}\Phi_{jr}\Phi_{kr}\int_{d_k'}^{d_k''}\int_{l_k'}^{l_k''}\int_{d_j'}^{d_j''}\int_{l_j'}^{l_j''}(y_j-d_j)(y_k-d_k)G_{pp}(x_j,y_j,x_k,y_k,f)\,dx_j\,dy_j\,dx_k\,dy_k\ \}\,df, \tag{3.17}$$

where $\overline{\boldsymbol{\delta}_g^2}$ is the mean square displacement response of node g, $\boldsymbol{\Phi}_{gr}$ is the rth mode shape at node g, f_r is the rth natural frequency in Hz, f is the excitation frequency in

Hz, $\bar{M}_r$ is the rth element of generalized mass matrix, $|H_r(f)|$ is the magnification factor for the rth mode, G_{pp} is the one-sided cross spectral density of pressure, N is the number of mode shapes chosen for evaluation, n is the number of nodes, l_i and d_i are the coordinates of a typical node i in the x- and y- directions, respectively, l_i' and l_i'' are the limits of the area surrounding the node i in the x-direction, d_i' and d_i'' are the limits of the area surrounding the node i in the y-direction (see Figure 3.2), and Φ_{ir}, Φ_{ur}, Φ_{pr}, Φ_{vr}, Φ_{jr}, Φ_{kr} represent the elements of the rth mode shape corresponding to the radial displacement, derivative of radial displacement with respect to x and derivative of radial displacement with respect to y, in respective pairs. We note that the indices i and u are associated with lateral forces, p and v with moments about y, and j and k with moments about x.

3.6.2 Power spectral density of displacements

As stated, one of the purposes of this study is to determine the total r.m.s. displacements. In addition, we are able to calculate PSD of displacements as a function of excitation frequency as follows:

$$G_{\delta_g\delta_g}(f)=\sum_{r=1}^{N}\frac{\Phi_{gr}^2}{16\pi^4 f_r^4 \bar{M}_r^2}|H_r(f)|^2$$

$$\{\sum_{i=1}^{n}\sum_{u=1}^{n}\Phi_{ir}\Phi_{ur}\int_{d_u'}^{d_u''}\int_{l_u'}^{l_u''}\int_{d_i'}^{d_i''}\int_{l_i'}^{l_i''}G_{pp}(x_i,y_i,x_u,y_u,f)\,dx_i dy_i dx_u dy_u +$$

$$\sum_{i=1}^{n}\sum_{v=1}^{n}\Phi_{ir}\Phi_{vr}\int_{d_v'}^{d_v''}\int_{l_v'}^{l_v''}\int_{d_i'}^{d_i''}\int_{l_i'}^{l_i''}(x_v-l_v)G_{pp}(x_i,y_i,x_v,y_v,f)\,dx_i dy_i dx_v dy_v +$$

$$\sum_{i=1}^{n}\sum_{k=1}^{n}\Phi_{ir}\Phi_{kr}\int_{d_k'}^{d_k''}\int_{l_k'}^{l_k''}\int_{d_i'}^{d_i''}\int_{l_i'}^{l_i''}(y_k-d_k)G_{pp}(x_i,y_i,x_k,y_k,f)\,dx_i dy_i dx_k dy_k +$$

$$\sum_{p=1}^{n}\sum_{u=1}^{n}\Phi_{pr}\Phi_{ur}\int_{d_u'}^{d_u''}\int_{l_u'}^{l_u''}\int_{d_p'}^{d_p''}\int_{l_p'}^{l_p''}(x_p-l_p)G_{pp}(x_p,y_p,x_u,y_u,f)\,dx_p dy_p dx_u dy_u +$$

$$\sum_{p=1}^{n}\sum_{v=1}^{n}\Phi_{pr}\Phi_{vr}\int_{d_v'}^{d_v''}\int_{l_v'}^{l_v''}\int_{d_p'}^{d_p''}\int_{l_p'}^{l_p''}(x_p-l_p)(x_v-l_v)G_{pp}(x_p,y_p,x_v,y_v,f)\,dx_p dy_p dx_v dy_v +$$

$$\sum_{p=1}^{n}\sum_{k=1}^{n}\Phi_{pr}\Phi_{kr}\int_{d_k'}^{d_k''}\int_{l_k'}^{l_k''}\int_{d_p'}^{d_p''}\int_{l_p'}^{l_p''}(x_p-l_p)(y_k-d_k)G_{pp}(x_p,y_p,x_k,y_k,f)\,dx_p dy_p dx_k dy_k +$$

$$\sum_{j=1}^{n}\sum_{u=1}^{n}\Phi_{jr}\Phi_{ur}\int_{d_u'}^{d_u''}\int_{l_u'}^{l_u''}\int_{d_j'}^{d_j''}\int_{l_j'}^{l_j''}(y_j-d_j)G_{pp}(x_j,y_j,x_u,y_u,f)\,dx_j dy_j dx_u dy_u +$$

$$\sum_{j=1}^{n}\sum_{v=1}^{n}\Phi_{jr}\Phi_{vr}\int_{d_v'}^{d_v''}\int_{l_v'}^{l_v''}\int_{d_j'}^{d_j''}\int_{l_j'}^{l_j''}(y_j-d_j)(x_v-l_v)G_{pp}(x_j,y_j,x_v,y_v,f)\,dx_j dy_j dx_v dy_v +$$

$$\sum_{j=1}^{n}\sum_{k=1}^{n}\Phi_{jr}\Phi_{kr}\int_{d_k'}^{d_k''}\int_{l_k'}^{l_k''}\int_{d_j'}^{d_j''}\int_{l_j'}^{l_j''}(y_j-d_j)(y_k-d_k)G_{pp}(x_j,y_j,x_k,y_k,f)\,dx_j dy_j dx_k dy_k\ \},$$

(3.18)

where $G_{\delta_g\delta_g}(f)$ is the power spectral density of the nodal displacement at node g.

3.6.3 Mean square displacements in terms of the cross spectral density of an arbitrary homogeneous random pressure

The cross spectral density of a homogeneous pressure field can be expressed in terms of distances of separation $\xi_x = |x_i - x_u|$ and $\xi_y = |y_i - y_u|$ instead of the coordinates themselves. Therefore, the one-sided cross spectral density of the pressure can be written as:

$$G_{pp}(\xi_x, \xi_y, f) = G_{pp}(x_i, y_i, x_u, y_u, f) = \lim_{T \to \infty} \frac{1}{T} P(x_i, y_i, f) P^*(x_u, y_u, f), \qquad (3.19)$$

Thus all the components of the cross spectral density of the wall pressure in Eq. (3.17) can be expressed in terms of $G_{pp}(\xi_x, \xi_y, f)$.

The one-sided cross spectral density of the wall pressure can be described by:

$$G_{pp}(\xi_x, \xi_y, f) = G_{pp}(f) \Psi(\xi_x, \xi_y, 0), \qquad (3.20)$$

where $G_{pp}(f)$ is the one-sided power spectral density of the pressure and $\Psi(\xi_x, \xi_y, 0)$ is the spatial correlation function between two points at the wall with a spatial separation of ξ_x and ξ_y, streamwise and spanwise, respectively. These spatial separations should be determined experimentally. Eqs. (3.17), (3.19) and (3.20) together express the response of a thin plate subjected to an arbitrary homogeneous random pressure field.

3.7 Response to a subsonic boundary layer pressure field

In the preceding section, expressions for the response of a thin plate subjected to an arbitrary homogeneous random pressure field were obtained, however the origin of the pressure field was left undefined. A model of the cross spectral density of the fluctuating pressure field $G_{pp}(\xi_x, \xi_y, f)$ is needed as an input to the numerical prediction algorithm.

Here we consider the particular case where the pressure field arises from pressure fluctuations in the subsonic, turbulent boundary layer of a flowing fluid. In the turbulent flow boundary layer, pressure fluctuates randomly so it cannot be described deterministically. Hence statistical methods should be employed to find the pressure.

3.7.1 Dynamics effects of a flow

We have indicated [25] how the inertial effects of a quiescent fluid contained by a shell or a shell partially or completely submerged in a stationary fluid may be taken into account. The salient point is given here; the fluid pressure applied on the structure is determined by combining potential flow theory, Bernoulli's equation and an impermeability condition and is expressed as a function of the acceleration of the normal displacement ($\partial^2 W / \partial t^2$) of the shell. Consequently, it can be interpreted as the virtual added mass of the fluid. However, when the fluid is flowing the shell is

subjected to additional terms such as centrifugal and Coriolis-type forces. The former is proportional to $U^2\partial^2 W/\partial x^2$ and considered as the stiffness of the fluid and has a diminishing effect on the natural frequencies of the system. The latter is proportional to $2U\partial^2 W/\partial x\partial t$ and has a damping effect on vibration. The magnitude of these effects depends on the dimensionless flow velocity $(U[(1-\nu^2)\rho/E]^{1/2})$, where U is the mean flow velocity, ν is Poisson's ratio, ρ is the fluid density and E is Young's modulus. The effect of these forces can be neglected unless we are dealing with very flexible shells, very heavy fluids, or very high velocities. In any case, for metal shells in the vicinity of fluid with flow velocity in the normal engineering range, damping and stiffness effects of the flow are negligible [13] and will not be taken into account in this paper. Therefore the effects of the flow on the shell can be considered the same as the effects of a stationary fluid in contact with the shell.

3.7.2 Statistical properties of fluctuating wall pressure in a turbulent boundary layer

3.7.2.1 Cross correlation function

Correlation decay in oblique directions, whether between points on the same plate or between points on different plates, is represented by the product of the lateral

and longitudinal decay functions. This independent-planes model of the pressure field for oblique directions was first suggested by Corcos [1] based on existing measurements. White [26] showed that the approximate separability does not introduce significant error. This theory was justified analytically by Curling and Païdoussis for clusters of cylinders [14] and was experimentally verified by Bakewell [27] for a body of revolution in a water medium. The cross correlation function can be written as follows:

$$\Psi(\xi_x, \xi_y, 0) = \Psi(\xi_x, 0, 0)\Psi(0, \xi_y, 0), \tag{3.21}$$

where $\Psi(\xi_x, 0, 0)$ and $\Psi(0, \xi_y, 0)$ are the streamwise and spanwise spatial correlation decay functions, respectively.

In the case of subsonic turbulent boundary-layer pressure fluctuations the longitudinal and lateral spatial correlation functions have been examined theoretically and experimentally by several investigators. For example, Clinch [28] measured the narrowband longitudinal and circumferential correlations in thin-walled pipes when influenced by the passage of fully-developed turbulent water flow.

Bakewell obtained lateral and longitudinal correlations in a turbulent boundary layer for a body of revolution in a water medium [27] and compared the results with the data obtained in flat plate boundary layers by Bull [8] and Willmarth and Wooldridge [7, 29], and with data from pipe flows which he generated himself [30]. The results showed that the statistical properties of fluctuating wall pressure in a turbulent boundary layer for a body of revolution were in good agreement with data obtained in flat plate boundary layers and also in pipe flows. This agreement was demonstrated for

the spectral density and the lateral and longitudinal correlation functions [27]. Different empirical expressions for different structures have been suggested for longitudinal and lateral correlations however these expressions are approximately the same.

Corcos postulated that the longitudinal and lateral correlations may be presented as an exponentially decaying oscillating function in the flow direction and a simple exponentially decaying function in the cross-flow direction, respectively as follows:

$$\Psi(\xi_x, 0, 0) = \mathrm{e}^{-\alpha_x 2\pi \left| S_{\xi x} \right|} \mathrm{e}^{\mathrm{i} 2\pi S_{\xi x}}, \tag{3.22a}$$

$$\Psi(0, \xi_y, 0) = \mathrm{e}^{-\alpha_y 2\pi \left| S_{\xi y} \right|}, \tag{3.22b}$$

where

$$S_{\xi x} = \frac{f \xi_x}{U_c}, \tag{3.22c}$$

$$S_{\xi y} = \frac{f \xi_y}{U_c}, \tag{3.22d}$$

α_x and α_y are empirically determined constants, $S_{\xi x}$ and $S_{\xi y}$ are the Strouhal numbers, f is the excitation frequency, ξ_x and ξ_y are streamwise and spanwise distances of separation, respectively and $\mathrm{i} = \sqrt{-1}$. The convection velocity U_c over smooth walls is assumed to be a constant given by $U_c = 0.6U_\infty$ [8] where U_∞ is the free stream velocity.

Blake recommends that $\alpha_x = 0.116$ and $\alpha_y = 0.7$ be used for smooth walls [9]. It is to be expected that these constants will be approximately the same for different fluids

at the same Strouhal number, at least for those with a sufficiently high Reynolds number.

It should be noted that mean square response is a real value, so the real part of the cross spectral density of the wall pressure should be taken into consideration. Putting all of these together and substituting Eqs. (3.22a) and (3.22b) into Eqs. (3.20) and (3.21), the wall pressure cross spectral density ($G_{pp}(\xi_x, \xi_y, f)$) in a fully-developed turbulent region can be written as follows:

$$G_{pp}(\xi_x, \xi_y, f) = G_{pp}(f) \mathrm{e}^{-\alpha_x 2\pi \left| S_{\xi_x} \right|} \mathrm{e}^{-\alpha_y 2\pi \left| S_{\xi_y} \right|} \cos(2\pi S_{\xi_x}), \tag{3.23}$$

where $G_{pp}(f)$ is the one-sided power spectral density of the wall pressure, S_{ξ_x} and S_{ξ_y} are the Strouhal numbers, f is the frequency in Hz, and α_x and α_y are constants describing the spatial coherence of the wall pressure field in longitudinal and lateral directions, respectively (see Eq. (3.17)).

3.7.2.2 Wall pressure power spectral density

The most significant characteristic of turbulent flow is the power spectral density. Fluctuating wall pressure beneath a turbulent boundary layer for various velocities has been measured for different structures and the non-dimensional wall-pressure PSD as a function of Strouhal number has been proposed by several investigators. Measurements of wall fluctuation, auto- and cross spectral, have been

made on the outside walls of cylinders with flow along the axis by Willmarth and Young [31]. The power spectral density of wall pressure fluctuations on smooth-walled pipe was measured by Clinch [32]. He illustrated the comparison between his results with those measured by Bakewell, Carey, Libuka, Schloemer and Von Winkle [5] for subsonic airflow in a smooth-walled pipe. Good agreement was found except at low Strouhal numbers due to the effects of extraneous noise, which increased the measured power spectral density. The power spectral density of turbulent wall pressure fluctuations on a body of revolution in a water medium was obtained by Bakewell [27] and the result was in good agreement with pressure data obtained on flat plates and in fully-developed turbulent pipe flow. Willmarth and Wooldridge measured the power spectral density of fluctuating pressure at a wall beneath a thick turbulent boundary layer [7]. Bakewell *et al.* [5] obtained measurements of the mean square pressure per unit bandwidth, i.e. the one-sided power spectral density versus Strouhal number for airflow at different Reynolds numbers in a pipe. The best curve fit for these measurements was obtained by Lakis [13].

Although there are differences in investigation characteristics, namely pipe radius, velocity and even the geometry of structure, the general features and magnitude of the spectral density are similar. The general trends of wall-pressure PSD obtained by Bakewell *et al.* in pipe airflow, by Clinch in pipe water flow, by Willmarth and Wooldridge over a flat plate boundary layer, and in a straight flow channel are similar as shown by Au-Yang [33]. Therefore, it seems that the proposed expression by Lakis is applicable to a thin plate as follows [13]:

$$G_{pp}(f) = k_2 \rho_f^2 \delta^* U_\infty^3 \, e^{-k_1 \delta^* f / U_\infty}, \tag{3.24}$$

where $G_{pp}(f)$ is the one-sided power spectral density of the pressure, k_1=0.25, k_2=2×10^{-6}, ρ_f is the density of the fluid, f is the frequency in Hz, δ^* is the boundary layer displacement thickness and U_∞ is the free stream velocity. It should be emphasized that the power spectral density of the pressure in Eq. (3.24) and all its implications apply to excitation frequencies above $f\delta^*/U_\infty$ of the order of 0.1 due to the absence of empirical data below that point [13].

The well-known Schlichting formula is used to estimate boundary layer thickness δ [34]:

$$\delta = 0.37x(\mathrm{Re}_x)^{-0.2}, \tag{3.25}$$

where $\mathrm{Re}_x = U_\infty x/\nu$ is the Reynolds number at the distance from the leading edge of the plate, ν is the kinematic viscosity, x is the distance from the leading edge of the plate and U_∞ is the free stream velocity. The boundary layer displacement thickness δ^* is approximated as 0.125 times the boundary layer thickness δ over smooth walls.

3.7.3 Mean square response

Substituting the power spectral density of the pressure from Eq. (3.24) into Eq. (3.23) and then introducing the cross spectral density of the pressure into Eqs. (3.17)

and (3.19) and taking integrations over surface and frequency, the mean square displacement response ($\overline{\delta_g^2}$) is obtained as follows:

$$\overline{\delta_g^2(x_g,y_g,t)}=\sum_{r=1}^{N}\frac{\Phi_{gr}^2}{16\pi^4 f_r^4 \bar{M}_r^2}\left[\begin{array}{l}\sum_{i=1}^{n}\sum_{u=1}^{n}\Phi_{ir}\Phi_{ur}|\Gamma_{iu}|+2\sum_{i=1}^{n}\sum_{v=1}^{n}\Phi_{ir}\Phi_{vr}|\Gamma_{iv}|+2\sum_{i=1}^{n}\sum_{k=1}^{n}\Phi_{ir}\Phi_{kr}|\Gamma_{ik}|+ \\ 2\sum_{p=1}^{n}\sum_{k=1}^{n}\Phi_{pr}\Phi_{kr}|\Gamma_{pk}|+\sum_{p=1}^{n}\sum_{v=1}^{n}\Phi_{pr}\Phi_{vr}|\Gamma_{pv}|+\sum_{j=1}^{n}\sum_{k=1}^{n}\Phi_{jr}\Phi_{kr}|\Gamma_{jk}|\end{array}\right], \tag{3.26}$$

where Φ_{ij}'s are the terms of the modal matrix, f_r is the rth natural frequency in Hz, $\bar{M}_r$ is the rth element of the generalized mass matrix and Γ's are complicated functions, too long to give here. Only Γ_{iu} is given in detail in the Appendix. If the total response is desired, the response must be summed over all significant modes of vibration.

3.8 Calculations and discussions

3.8.1 Computational method and computer program

To determine the response of a thin structure to a random pressure we must proceed as follows: i) the structure must be divided into a sufficient number of finite elements; ii) the mass and stiffness matrices for each finite element must be

determined; iii) the global mass and stiffness matrices must be constructed; iv) the eigenvalues and eigenvectors must be computed; v) the r.m.s. response must be calculated at each node.

We must proceed with Eq. (3.26) where a great deal of the computational task has already been carried out. An in-house program in FORTRAN language has been developed for carrying out the aforementioned steps and determining the response to turbulent boundary-layer pressure fields. The process is summarized by the flow chart given in Figure 3.3. The necessary time for calculation of the total r.m.s. displacement response for a plate composed of one hundred elements is approximately 20 minutes. This corresponds to the case in which numerous natural frequencies are utilized in the calculation of the total r.m.s. response. However, if only a few of the lowest natural frequencies are employed the total r.m.s. response can be calculated with an adequate degree of accuracy while computational costs can be considerably reduced. Moreover, the computer calculation includes determination of the total r.m.s. of all degrees of freedom at every node. A large amount of time may be saved if the response is not required at every node, or if only the total r.m.s. radial displacement is desired.

The present method and its associated computer program is capable of predicting the total r.m.s. response of a thin structure subjected to subsonic turbulent boundary layer pressure fluctuations with arbitrary boundary conditions. We are able to predict r.m.s. response at a given mode as well as total r.m.s. displacement over significant modes of vibration, which is the case in most applications.

3.8.2 Verification of the method

In order to check the validity of the method a long thin simply supported cylindrical shell having a length of 240 in, a radius of 3 in, and a thickness of 0.025 in, conveying water was studied. The material properties are; Young's modulus E = 28.5×10^{6} lb in^{-2}, Poisson's ratio ν = 0.305, density ρ = 0.749×10^{-3} lb s^{2} in^{-4} and damping ratio $\zeta = 2\times10^{-2}$. This shell was first studied by Clinch both theoretically and experimentally [12]. He obtained the mean square radial displacement in the frequency range of 100-1000 Hz. Lakis and Païdoussis then analyzed the cylindrical shell using cylindrical finite elements [13]. They developed a method to obtain the root mean square displacements associated with each circumferential wavenumber. Natural frequencies of the shell were calculated first and it was found that many of these natural frequencies were below 100 Hz. This indicates that the high frequency response as measured by Clinch will differ significantly from the total response. Lakis and Païdoussis obtained the high frequency response of the radial displacement by taking into account only the modes whose natural frequencies were in the range of 93-1000 Hz. Good agreement between their theoretical results and Clinch's experimental results was found and the results lend confidence that the values of the overall response of the shell obtained by them may also be reliable. They also calculated total response of the radial displacement of the axial mid-point by considering all frequency components. This was accomplished by summing the results with circumferential wavenumbers 2 to 6 at the flow velocities 248 and 520 in s^{-1} (see Table 1 and Figure 9 in reference [13]).

The total root mean square response of radial displacement was found to be much higher than the response in the frequency range of 93-1000 Hz. As expected, the contribution to the total response increases substantially with decreasing frequency.

To the author's knowledge, there is no reference in the literature for the total r.m.s. displacement of a plate or an open curved structure subjected to a random pressure field arising from a boundary layer induced by turbulent flow. Therefore, in order to verify our method at least qualitatively, the aforementioned shell was analyzed. First, natural frequencies were calculated using our method and we observed that there are frequencies lower than those associated with circumferential wavenumber n=2. These frequencies are associated with a beam-like mode of the cylinder (i.e. n=1), which was not taken into account in Lakis' work. It should be noted that in the case of a long slender cylinder some frequencies associated with the beam-like mode are the lowest natural frequencies of the system. The total r.m.s. radial displacement at the axial mid-point of a simply supported cylindrical shell was calculated for centerline velocities (U_{cl}) 248 and 520 in s^{-1} using our method developed in this work. The results are tabulated in Table 1 and compared with those obtained by Lakis. As seen in Table 3.1, the responses calculated by our method using flat shell elements are of the same order but higher than those obtained by Lakis and Païdoussis. The total responses obtained by Lakis were calculated by summing the results over circumferential modes from n=2 to n=6 only and the responses corresponding to the beam-like mode have not been taken into account. In our method, response calculation was carried out for all frequencies regardless of circumferential or axial modes, which could justify the higher

values. This discrepancy is attributed to the lower natural frequencies of the system that have been included in our method. It should be noted that because of the mixed combination of the low and high frequencies associated with the beam-like mode, we were not able to remove these frequencies from those calculated in our program. The power spectral density of the radial displacement at the axial mid-point of the abovementioned cylindrical shell for a centerline velocity of 248 in s^{-1} and a damping ratio of 0.02 is illustrated in Figure 3.4. It clearly demonstrates the significant contribution of the lower natural frequencies to the PSD of response.

3.8.3 Response of a plate subjected to a turbulent boundary-layer-induced random pressure field

The geometry and material properties of the plate chosen herein are taken from reference [35]. The steel plate has a length of 0.655 m, a width of 0.20165 m and a thickness of 0.00936 m. The material properties are; Young's modulus $E = 207\times10^9$ Pa, Poisson's ratio $\nu = 0.3$ and density $\rho = 7850$ kg m^{-3}.

The plate is discretized into 10×10 flat rectangular elements. Further refining of the mesh beyond this did not influence the free vibration characteristics of the system. The same mesh has been used for calculation of the response. Natural frequencies of a plate simply supported at its short sides and subjected to quiescent water from one side were calculated numerically using a flat rectangular element and the method outlined in

references [24, 25]. The first few natural frequencies of the aforementioned system compared well with corresponding analytical values in reference [35] and are listed in Table 3.2. For the sake of brevity we did not tabulate the natural frequencies of the plate under different boundary conditions wetted from one or both sides using our method. However, in all cases good agreement was found between our numerical results and those obtained in reference [35].

The same plate was used and we obtained its response to turbulent boundary layer pressure fluctuations under different boundary conditions. It should be mentioned that the root mean square response has not been studied in reference [35]. Here, the total r.m.s. displacement responses of the plate were obtained by summation over all significant modes of vibration (see Eq. (3.26)) at all nodes and then the maximum total r.m.s. response of the plate was calculated. Two sets of flow (i.e. fluid flowing over the plate and fluid flowing on both sides of the plate) and different boundary conditions of the plate were considered in this work. The effect of flow direction on the response was also investigated. The power spectral densities of the in-plane and out-of plane displacements of an SFSF plate were studied. In order to check the role of damping as revealed in Eq. (3.12), two damping ratios were considered in the calculation of the response.

3.8.3.1 SFSF plate

3.8.3.1.1 Response of an SFSF plate subjected to turbulent flow along its long sides from one side and both sides, respectively (Figures 3.5, 3.6 and 3.7, and Table 3.3)

The first case study is a plate which is simply supported at its short sides, over which water is flowing along the long side of the plate at a height more than 50% of the length of the plate. Based on previous analyses [24, 25] the natural frequencies of the plate in contact with quiescent water are calculated (see Table 3.2). As stated in section 3.7.1, solely the inertial effect of the fluid is taken into account in this work. It is worth mentioning that when the fluid height exceeds 50% of the length of the plate the boundary conditions of the fluid at the extremity and the height of the fluid are of no importance when considering natural frequency changes [25].

The maximum total r.m.s. displacement responses of the SFSF plate over which water is flowing along its long sides as a function of free stream velocity in the range of 5 to 30 m s^{-1} and for different damping ratios, namely $\zeta_r = 10^{-2}$ and 10^{-3} are shown in Figure 3.5. It is assumed that the turbulent boundary layer is fully developed over the entire plate. The results plotted in Figure 3.5 reveal that the total r.m.s. displacements are inversely proportional to the damping ratio and directly proportional to the free stream velocity. In order to demonstrate the behavior of r.m.s. responses, the maximum total r.m.s. membrane displacements (U and V) are also plotted in Figure 3.5. As

anticipated, the membrane displacements of the plate are minimal. The maximum total r.m.s. radial displacement is displayed on a secondary axis due to its higher value. The effects of the membrane responses are minimal for all boundary conditions of the plate. For this reason further studies will only consider radial displacement of the plate.

It is observed that lower natural frequencies contribute significantly to the response and as natural frequency increases the total r.m.s. response becomes insignificant quickly. It can be clearly seen from Eq. (3.26) that the response is inversely proportional to the square of the natural frequency. This therefore indicates that the first six natural frequencies suffice to calculate the total response for the plate studied here.

The power spectral density of the radial displacement (G_{WW}) of the aforementioned SFSF plate subjected to fully-developed turbulent flow from one side where flow is along its long sides is plotted against excitation frequency in Figure 3.6. The PSD of the radial displacement in Figure 3.6 is calculated for a free stream velocity of 30 m s^{-1} and a damping ratio of 0.001 at the node at which the maximum total r.m.s. radial displacement was obtained (see also Figure 3.5). As expected, it shows dominant peaks with coupled natural frequency values corresponding to those given in Table 3.2. Also as expected, the PSDs of the in-plane displacements (G_{UU} and G_{VV}) are minimal however for the sake of demonstration the power spectral densities of the in-plane displacements of the aforementioned SFSF plate subjected to fully-developed turbulent flow from one side where flow is along its long sides are illustrated against excitation frequency in Figure 3.7. The PSDs of the in-plane displacements in Figure 3.7 are

calculated for a free stream velocity of 30 m s^{-1} and a damping ratio of 0.001 at the node at which the maximum total r.m.s. radial displacement response was obtained. The same major peaks as those in Figure 3.6 are observed representing the natural frequencies of the system. It is observed that the lower natural frequencies contribute greatly to the PSD response.

The maximum total r.m.s. radial displacement of the SFSF plate with a damping ratio of $\zeta = 10^{-2}$ subjected to fully-developed turbulent flow from both sides was calculated for the case where water is flowing along the long sides of the plate. The results are tabulated in Table 3.3 for different free stream velocities and compared with those with flow on one side of the plate. As anticipated, the response of the plate wetted on both sides is higher than the response of the plate over which water is flowing due to its lower natural frequencies and larger virtual added mass [25].

3.8.3.1.2 Effects of flow direction on r.m.s. radial displacement response (W) of an SFSF plate (Figures 3.8 and 3.9)

The effects of flow direction on total r.m.s. radial displacement of an SFSF plate with water flowing on one or both sides were studied. Figure 3.8 shows the maximum total r.m.s. radial displacement versus free stream velocity and damping ratio for the same SFSF plate studied earlier (see Figure 3.5) but with water flowing over its short side. The results are also compared with those for the case of turbulent flow along

the long side of the plate. It is observed that the r.m.s. radial displacements for the case of flow along the long side of the plate is higher than those obtained for flow along the short side of the plate, except for the free stream velocity U_∞=5 m s^{-1}.

The maximum total r.m.s. radial displacement versus free stream velocity and damping ratio for an SFSF plate subjected to turbulent flow from both sides, where water is flowing along the short side of the plate is depicted in Figure 3.9 and compared with the results where flow is along the long side of the plate. Contrary to Figure 3.8, it is observed from Figure 3.9 that flow direction has almost no effect on the response of the SFSF plate subjected to turbulent flow from both sides for a given velocity and damping ratio.

3.8.3.2 Effects of flow direction on r.m.s. radial displacement (W) of a CFCF plate (Figure 3.10)

The second case study is a plate which is clamped at its short sides subjected to fully-developed turbulent flow from one side. In Figure 3.10 the effect of flow direction on the maximum total r.m.s. radial displacement is compared for two cases; water flowing over the short side of the CFCF plate, and water flowing over the long side of the CFCF plate. The maximum total r.m.s. radial responses of the CFCF plate with different damping ratios as a function of free stream velocity are also seen in Figure 3.10.

We observed that the maximum total r.m.s. radial response for the case of water flowing along the long side of the plate was lower than that obtained for the case of water flowing along the short side for free stream velocities 5 and 10 m s^{-1} and all damping ratios. On the other hand, the inverse behavior was observed for higher free stream velocities and all damping ratios.

As expected, the maximum total r.m.s. radial displacement is lower for the case of a CFCF plate than that obtained for an SFSF plate. This can be seen by comparing Figures 3.8 and 3.10.

3.8.3.3 Effects of flow direction on r.m.s. radial displacement of a CFFF plate (Figure 3.11)

A plate which is clamped at one short side subjected to fully-developed turbulent flow from one side was investigated as the last case study. Figure 3.11 illustrates the maximum total r.m.s. radial displacement versus free stream velocity and damping ratio for the aforementioned CFFF plate where water is flowing over its short side. The results are compared with those of an identically supported plate with turbulent flow along the long side. It was observed that the maximum total r.m.s. radial response for the case of water flowing along the long side of the plate is higher than that obtained for the case of water flowing along the short side for all velocities and damping ratios. The effect of flow direction on the maximum total r.m.s. radial

displacement versus free stream velocity and damping ratio for a CFFF plate subjected to turbulent flow from both sides shows the same behavior, however for the sake of brevity this case has not been plotted. It should be noted that in all the aforementioned cases the same behavior was observed i.e. the total r.m.s. radial displacement is inversely proportional to the damping ratio and directly proportional to the free stream velocity.

3.9 Conclusion

In this paper we have introduced a method capable of predicting the total r.m.s. displacement response of a thin structure to an arbitrary random pressure field. The method was then specialized for application to the case where the pressure field originates from a turbulent boundary layer of a subsonic flow. This work is based on a previously developed method to obtain the dynamic behavior of thin structures in contact with fluid. This method uses a combination of classic thin shell theory and finite element analysis in which the finite elements are flat rectangular elements with six degrees of freedom per node, representing the in-plane and out-of-plane displacements and their spatial derivatives. Since the transverse displacement function is derived from thin plate theory this method may be easily adapted to take hydrodynamic effects into account. This method is also capable of calculating both high and low frequencies with high accuracy. This capability is normally of little

interest in free vibration analysis but it is of great importance for determining the response of structures subjected to random pressure fields such as those generated by turbulent flow. Wetted natural frequencies and mode shapes in a vacuum, obtained using a previously developed method by the authors are incorporated into the calculation of random response. A random pressure field is estimated at each node of the finite element. Description of the turbulent pressure field is based on the Corcos formulation for the cross spectral density of pressure fluctuations. Root mean square displacement was found in terms of the cross spectral density of the pressure. A numerical approach is proposed to obtain the magnitude of the random response. Exact integration over surface and frequency leads to an expression for the response in terms of the wetted natural frequency of the system, undamped mode shapes, generalized mass matrix and other characteristics of the structure and flow.

An in-house program was developed to calculate the root mean square displacement response of a thin structure to random vibration due to the turbulent boundary layer of subsonic flow. The total r.m.s. displacement response was obtained by summation over all significant modes of vibration. To the author's knowledge, there is no reference in the literature for the total r.m.s. displacement of a plate or an open curved structure subjected to such random pressure. Therefore, in order to validate our method a cylindrical shell was analyzed and the total r.m.s. radial displacement was predicted and compared with that obtained by Lakis and Païdoussis. Although different expressions for correlations were adapted in the proposed method and in Lakis' work,

good agreement was found. Since Lakis validated his results using Clinch's experimental measurements, this result shows that our method is sound.

The total root mean square displacement of a thin plate under various boundary conditions (i.e. SFSF, CFCF and CFFF) subjected to a boundary-layer-induced random pressure field was studied and subsequently the maximum total r.m.s. displacement of the plate was predicted. The maximum total r.m.s. radial displacement responses as a function of free stream velocity for each set of flow and a given damping ratio were plotted for different boundary conditions of the plate. It was observed that they all have the same trend and the most sensitive case is the CFFF plate with higher magnitude.

The effect of flow direction on the response was also investigated. The effects of turbulent flow from one side and both sides of an SFSF plate on the r.m.s. radial displacement were investigated and higher responses in the case of the plate submerged in flow were obtained due to lower natural frequencies and larger virtual added mass, as expected. In all case studies it was observed that the maximum total r.m.s. displacement is directly proportional to free stream velocity and inversely proportional to the damping ratio. For each case study the same shift in response was observed as the damping ratio changed through all velocities. It is noted that the maximum total r.m.s. displacements are small for the set of calculations. Such small amplitudes are mainly of concern for fatigue considerations and must be below acceptable levels.

Furthermore, our method is capable of predicting the power spectral density of the displacement. The power spectral densities of the membrane and radial displacements of an SFSF plate subjected to fully-developed turbulent flow from one

side where flow is along the long sides of the plate versus excitation frequency were plotted. The spectrum shows the dominant peaks representing the coupled natural frequencies of the system. It was observed that lower natural frequencies contribute significantly to the PSD of the response.

This method can be applied to investigate parallel plates or a system of plates subjected to a fully-developed turbulent random pressure field. As a future study, this work could be extended to analyze three-dimensional thin curved structures subjected to a turbulent boundary layer random pressure field using a flat shell finite element with five degrees of freedom per node [25]. The same random vibration method is applicable and statistical properties such as power spectral density of pressure and correlations are more or less the same for different structures. Thin curved structures with discontinuities in thickness and material properties under different boundary conditions subjected to various boundary conditions of fluid can also be tackled.

3.10 Appendix A

A.1 Integration of the longitudinal correlations in the *x*-direction

Substituting Eqs. (3.22a) and (3.22c) into Eqs. (3.21), (3.20) and (3.19) and then introducing the result into Eq. (3.17) and integrating over x to eliminate the space variable leads to expressions for the longitudinal correlations.

A.2 Integration of the lateral correlations in the *y*-direction

Substituting Eqs. (3.22b) and (3.22d) into Eqs. (3.21), (3.20) and (3.19) and then introducing the result into Eq. (3.17) and integrating over y to eliminate the space variable gives us expressions for the lateral correlations.

A.3 Some statements used in Eq. (3.26)

After introducing the expressions obtained from A.1 and A.2 into Eq. (3.17) and integrating over frequency, Eq. (3.26) is obtained. Here for the reference only Γ_{iu} is given.

$$\Gamma_{iu}=\frac{K_2}{C^2(A^2+B^2)^2}\times$$

$$\left\{\begin{array}{l}
(B^2-A^2)\left[F_4^c(l_i',l_u',d_i',d_u')+F_4^c(l_i'',l_u'',d_i',d_u')-F_4^c(l_i',l_u'',d_i',d_u')-F_4^c(l_i'',l_u',d_i',d_u')\right]\\
-(2AB)\left[F_4^s(l_i',l_u',d_i',d_u')+F_4^s(l_i'',l_u'',d_i',d_u')-F_4^s(l_i',l_u'',d_i',d_u')-F_4^s(l_i'',l_u',d_i',d_u')\right]\\
+(B^2-A^2)\left[F_4^c(l_i',l_u',d_i'',d_u'')+F_4^c(l_i'',l_u'',d_i'',d_u'')-F_4^c(l_i',l_u'',d_i'',d_u'')-F_4^c(l_i'',l_u',d_i'',d_u'')\right]\\
-(2AB)\left[F_4^s(l_i',l_u',d_i'',d_u'')+F_4^s(l_i'',l_u'',d_i'',d_u'')-F_4^s(l_i',l_u'',d_i'',d_u'')-F_4^s(l_i'',l_u',d_i'',d_u'')\right]\\
-(B^2-A^2)\left[F_4^c(l_i',l_u',d_i'',d_u')+F_4^c(l_i'',l_u'',d_i'',d_u')-F_4^c(l_i',l_u'',d_i'',d_u')-F_4^c(l_i'',l_u',d_i'',d_u')\right]\\
+(2AB)\left[F_4^s(l_i',l_u',d_i'',d_u')+F_4^s(l_i'',l_u'',d_i'',d_u')-F_4^s(l_i',l_u'',d_i'',d_u')-F_4^s(l_i'',l_u',d_i'',d_u')\right]\\
-(B^2-A^2)\left[F_4^c(l_i',l_u',d_i',d_u'')+F_4^c(l_i'',l_u'',d_i',d_u'')-F_4^c(l_i',l_u'',d_i',d_u'')-F_4^c(l_i'',l_u',d_i',d_u'')\right]\\
+(2AB)\left[F_4^s(l_i',l_u',d_i',d_u'')+F_4^s(l_i'',l_u'',d_i',d_u'')-F_4^s(l_i',l_u'',d_i',d_u'')-F_4^s(l_i'',l_u',d_i',d_u'')\right]
\end{array}\right\},$$

where F_4^c and F_4^s are given as follows:

$$F_4^c(l_i',l_u',d_i',d_u')=\int_0^\infty \frac{e^{-\left[K_1+C\left|d_i'-d_u'\right|+B\left|l_i'-l_u'\right|\right]f}\cos(A\left|l_i'-l_u'\right|f)}{f^4\left[\frac{f^4}{f_r^4}+(\frac{4\zeta_r{}^2-2}{f_r^2})f^2+1\right]}df$$

$$=\frac{\pi}{8f_r^3}\left(5e^{-\gamma_1}\sin\gamma_2-5e^{-\gamma_3}\sin\gamma_4+\frac{1}{\zeta_r}\left(e^{-\gamma_1}\cos\gamma_2+e^{-\gamma_3}\cos\gamma_4\right)\right),$$

$$F_4^s(l_i',l_u',d_i',d_u')=\int_0^\infty \frac{e^{-\left[K_1+C\left|d_i'-d_u'\right|+B\left|l_i'-l_u'\right|\right]f}\sin(A\left|l_i'-l_u'\right|f)}{f^4\left[\frac{f^4}{f_r^4}+(\frac{4\zeta_r{}^2-2}{f_r^2})f^2+1\right]}df$$

$$=\frac{\pi}{8f_r^3}\left(-5e^{-\gamma_1}\cos\gamma_2+5e^{-\gamma_3}\cos\gamma_4+\frac{1}{\zeta_r}\left(e^{-\gamma_1}\sin\gamma_2+e^{-\gamma_3}\sin\gamma_4\right)\right),$$

and

$$\gamma_1(l_i',l_u',d_i',d_u')=\left[K_1+C\left|d_i'-d_u'\right|+(A\zeta_r+B)\left|l_i'-l_u'\right|\right]f_r,$$

$$\gamma_2(l_i', l_u', d_i', d_u') = \left[-K_1\zeta_r - C\zeta_r\left|d_i' - d_u'\right| + (A - B\zeta_r)\left|l_i' - l_u'\right|\right] f_r,$$

$$\gamma_3(l_i', l_u', d_i', d_u') = \left[K_1 + C\left|d_i' - d_u'\right| - (A\zeta_r - B)\left|l_i' - l_u'\right|\right] f_r,$$

$$\gamma_4(l_i', l_u', d_i', d_u') = \left[K_1\zeta_r + C\zeta_r\left|d_i' - d_u'\right| + (A + B\zeta_r)\left|l_i' - l_u'\right|\right] f_r,$$

where the constants are given as follows:

$$A = \frac{2\pi}{U_c},\ B = \frac{\alpha_x 2\pi}{U_c},\ C = \frac{\alpha_y 2\pi}{U_c},$$

$$K_1 = \frac{k_1 \delta^*}{U_\infty},\ K_2 = k_2 \rho_f^2 \delta^* U_\infty^3,$$

where f is the forced frequency in Hz, f_r is the rth natural frequency in Hz, ζ_r is the rth damping ratio, l_i' and l_i'' are the limits of the area surrounding the node i in the x-direction, d_i' and d_i'' are the limits of the area surrounding the node i in the y-direction, U_c is the convection velocity, U_∞ is the free stream velocity, ρ_f is the density of the fluid, δ^* is the boundary layer displacement thickness, k_1=0.25, k_2=2×10^{-6}, α_x = 0.116 and α_y = 0.7.

3.11 References

[1] G.M. Corcos, Resolution of pressure in turbulence, *Journal of the Acoustical Society of America* 35 (2) (1963) 192-199.

[2] G.M. Corcos, The resolution of turbulent pressures at the wall of a boundary layer, *Journal of Sound and Vibration* 6 (1) (1967) 59-70.

[3] L. Maestrello, Design criterion of panel structure excited by turbulent boundary layer, *Journal of Aircraft* 5 (4) (1968) 321-328.

[4] T.M. Farabee, M.J. Casarella, Spectral features of wall pressure fluctuations beneath turbulent boundary layers, *Physics of Fluids* 3 (1991) 2410-2420.

[5] H.P. Bakewell, G.F. Carey, J.J. Libuka, H.H. Schloemer, W.A. Von Winkle, Wall pressure correlations in turbulent pipe flow, U. S. Navy Underwater Sound Laboratory, Report No. 559, 1962.

[6] G.M. Corcos, Structure of turbulent pressure field in boundary-layer flows, *Journal of Fluid Mechanics* 18 (3) (1964) 353-378.

[7] W.W. Willmarth, C.E. Wooldridge, Measurements of fluctuating pressure at wall beneath thick turbulent boundary layer, *Journal of Fluid Mechanics* 14 (2) (1962) 187-210.

[8] M.K. Bull, Wall-pressure fluctuations associated with subsonic turbulent boundary layer flow, *Journal of Fluid Mechanics* 28 (4) (1967) 719-764.

[9] W.K. Blake, *Mechanics of Flow-Induced Sound and Vibration, Vol. II: Complex Flow-Structure Interaction*, Academic Press Inc., London, 1986.

[10] M.G. Cottis, J.G. Jasonides, The response of a finite thin cylindrical shell to random pressure fields, *Acoustical fatigue in Aerospace structures; Proceeding of the second international conference*, Dayton, Ohio, USA, April 29-May 1 1964, pp. 185-212.

[11] M.G. Cottis, On the dynamic response of an orthotropic finite cylindrical shell to an arbitrary pressure field, *Journal of Sound and Vibration* 7 (1) (1968) 31-38.

[12] J.M. Clinch, Prediction and measurement of the vibrations induced in thin-walled pipes by the passage of internal turbulent water flow, *Journal of Sound and Vibration* 12 (1970) 429-451.

[13] A.A. Lakis, M.P. Païdoussis, Prediction of the response of a cylindrical shell to arbitrary or boundary-layer-induced random pressure fields, *Journal of Sound and Vibration* 25 (1) (1972) 1-27.

[14] L.R. Curling, M.P. Païdoussis, Analyses for random flow-induced vibration of cylindrical structures subjected to turbulent axial flow, *Journal of Sound and Vibration* 264 (4) (2003) 795-833.

[15] F. Birgersson, N.S. Ferguson, S. Finnveden, Application of the spectral finite element method to turbulent boundary layer induced vibration of plates, *Journal of Sound and Vibration* 259 (4) (2003) 873-891.

[16] S. Finnveden, F. Birgersson, U. Ross, T. Kremer, A model of wall pressure correlation for prediction of turbulence-induced vibration, *Journal of Fluids and Structures* 20 (8) (2005) 1127-1143.

[17] D. Mazzoni, An efficient approximation for the vibro-acoustic response of a turbulent boundary layer excited panel, *Journal of Sound and Vibration* 264 (4) (2003) 951-971.

[18] P. Vitiello, S. De Rosa, F. Franco, Convected field analysis of flat panels response to turbulent boundary layer induced excitation, *Aerospace Science and Technology* 12 (1) (2008) 91-104.

[19] S. De Rosa, F. Franco, Exact and numerical responses of a plate under a turbulent boundary layer excitation, *Journal of Fluids and Structures* 24 (2) (2008) 212-230.

[20] S.A. Hambric, Y.F. Hwang, W.K. Bonness, Vibrations of plates with clamped and free edges excited by low-speed turbulent boundary layer flow, *Journal of Fluids and Structures* 19 (1) (2004) 93-110.

[21] A.A. Lakis, M.P. Païdoussis, Free vibration of cylindrical shells partially filled with liquid, *Journal of Sound and Vibration* 19 (1) (1971) 1-15.

[22] A.A. Lakis, M.P. Païdoussis, Dynamic analysis of axially non-uniform thin cylindrical shells, *Journal of Mechanical Engineering Science* 14 (1) (1972) 49-71.

[23] Y. Kerboua, A.A. Lakis, M. Thomas, L. Marcouiller, Hybrid method for vibration analysis of rectangular plates, *Nuclear Engineering and Design* 237 (8) (2007) 791-801.

[24] Y. Kerboua, A.A. Lakis, M. Thomas, L. Marcouiller, Vibration analysis of rectangular plates coupled with fluid, *Applied Mathematical Modelling* 32 (12) (2008) 2570-2586.

[25] M. Esmailzadeh, A.A. Lakis, M. Thomas, L. Marcouiller, Three-dimensional modeling of curved structures containing and/or submerged in fluid, *Finite Elements in Analysis and Design* 44 (6-7) (2008) 334-345.

[26] F.M. White, A unified theory of turbulent wall pressure fluctuations, USN Underwater Sound Laboratory, Report No. 629, 1964.

[27] H.P. Bakewell, Turbulent wall-pressure fluctuations on a body of revolution, *Journal of the acoustical society of America* 43 (6) (1968) 1358-1363.

[28] J.M. Clinch, Study of vibrations induced in thin-walled pipes under varying flow conditions, IIT Research Institute, Fluid Dynamics Section, NASA-CR-86659, 1967.

[29] W.W. Willmarth, C.E. Wooldridge, Measurements of correlation between fluctuating velocities and fluctuating wall pressure in thick turbulent boundary layer, North Atlantic Treaty Organization, Paris, Report No. 456, 1963.

[30] H.P. Bakewell, Narrow-band investigations of the longitudinal space-time correlation function in turbulent airflow, *Journal of the Acoustical Society of America* 36 (1) (1964) 146-148.

[31] W.W. Willmarth, C.S. Young, Wall pressure fluctuations beneath turbulent boundary layers on a flat plate and a cylinder, *Journal of Fluid Mechanics* 41 (1) (1970) 47-80.

[32] J.M. Clinch, Measurements of wall pressure field at surface of smooth-walled pipe containing turbulent water flow, *Journal of Sound and Vibration* 9 (3) (1969) 398-419.

[33] M.K. Au-Yang, *Flow-Induced Vibration of Power and Process Plant Components*, ASME Press, New York, 2001.

[34] H. Schlichting, *Boundary-Layer Theory*, McGraw-Hill, New York, 1979.

[35] M.R. Haddara, S. Cao, A study of the dynamic response of submerged rectangular flat plates, *Marine Structures* 9 (10) (1996) 913-933.

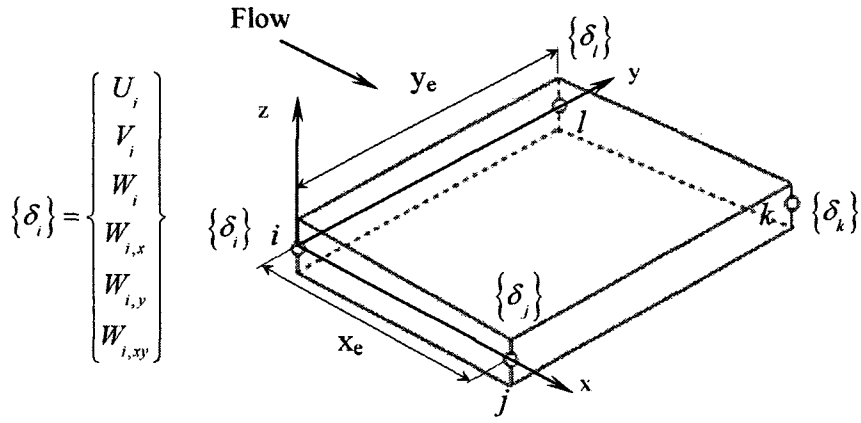

Figure 3.1 Flat rectangular element.

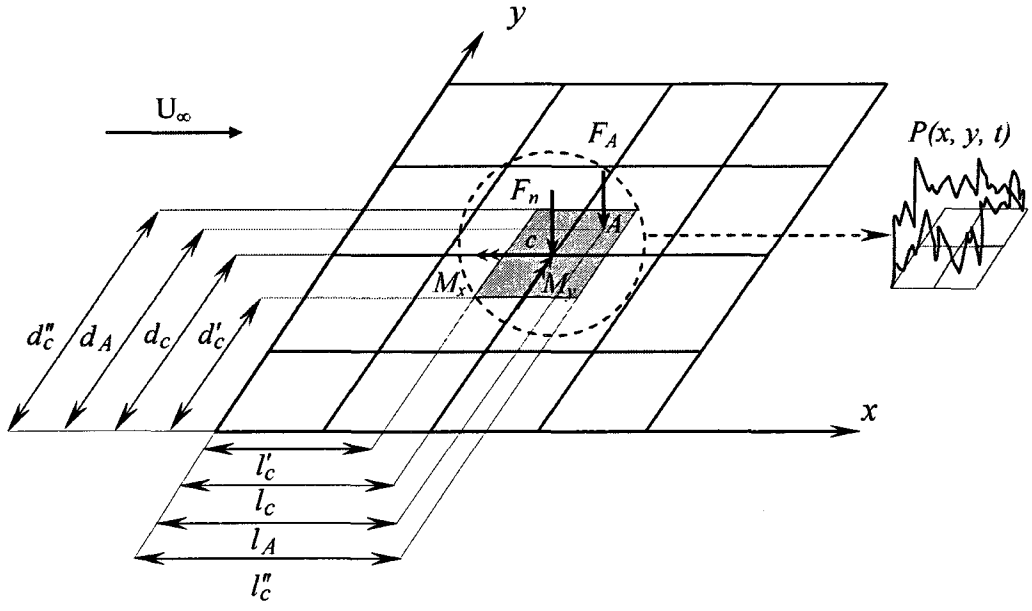

Figure 3.2 Transformation of a continuous pressure field to a discrete force field and the equivalent discrete force field acting at node *c*. Pressure fluctuations are also illustrated laterally on the area surrounding node *c*.

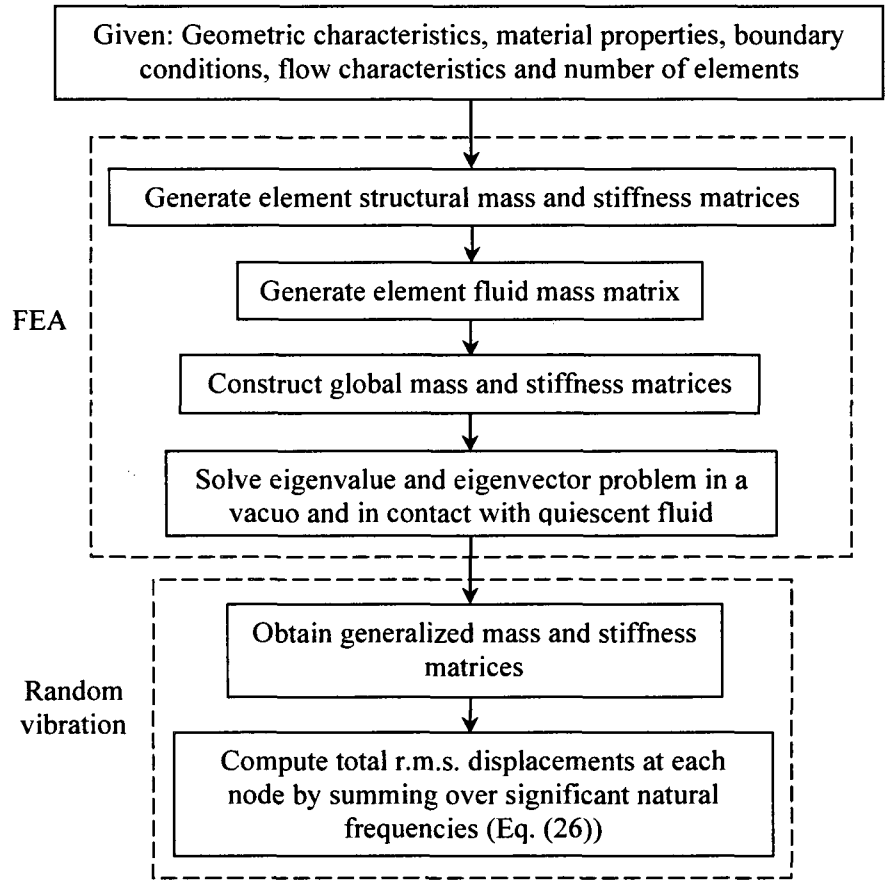

Figure 3.3 Flow chart of the in-house program for calculation of r.m.s. displacement response.

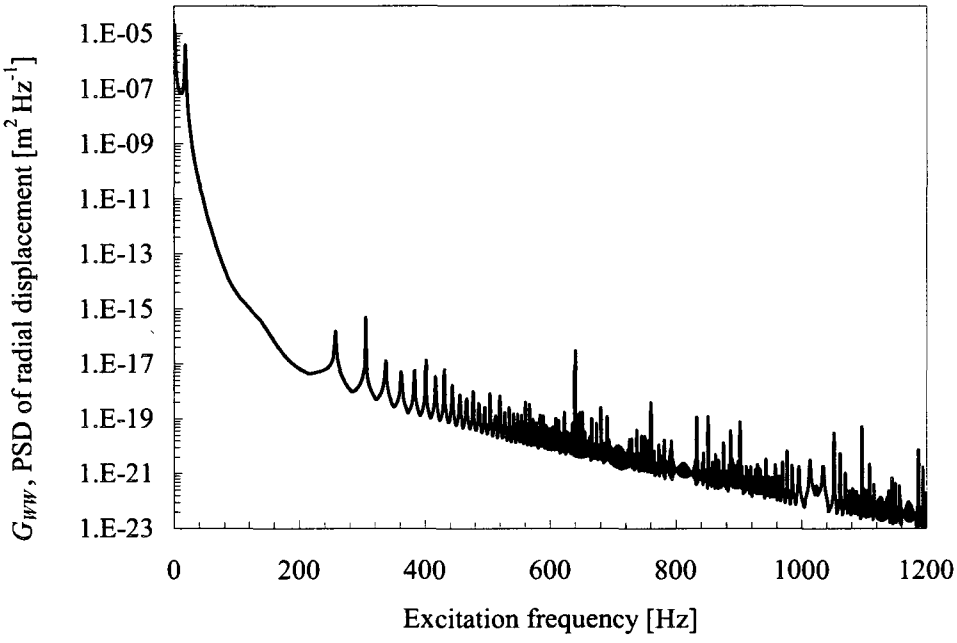

Figure 3.4 Power spectral density of radial displacement (G_{WW}) at the axial mid-point of a simply-supported cylindrical shell subjected to fully-developed turbulent internal flow versus excitation frequency for a centerline velocity of 248 in s^{-1} and a damping ratio of 0.02.

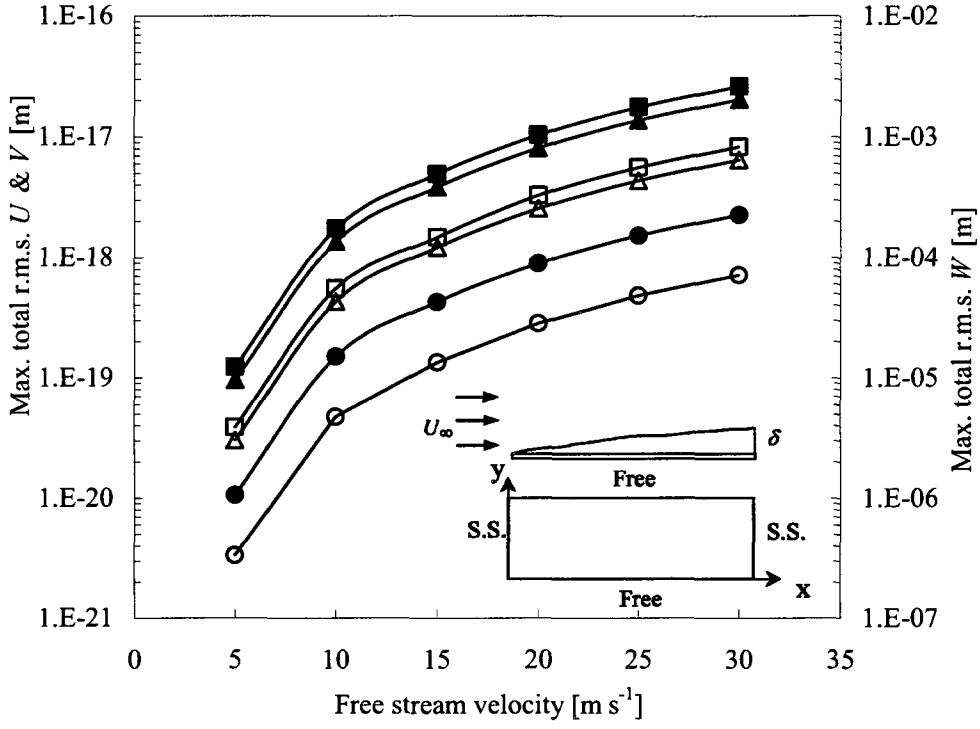

Figure 3.5 Maximum total r.m.s. displacement responses (U, V & W) versus free stream velocity and damping ratio (ζ) for an SFSF plate subjected to fully-developed turbulent flow from one side, where water is flowing along the long side of the plate; —■— U, $\zeta=10^{-3}$, —▲— V, $\zeta=10^{-3}$, —●— W, $\zeta=10^{-3}$, —□— U, $\zeta=10^{-2}$, —△— V, $\zeta=10^{-2}$, —○— W, $\zeta=10^{-2}$. The maximum total r.m.s. radial displacement (W) is plotted on secondary axis due to its higher value with comparison to the minimal r.m.s. membrane displacements (U & V). It is observed that the total r.m.s. displacements are inversely proportional to damping ratio and directly proportional to free stream velocity.

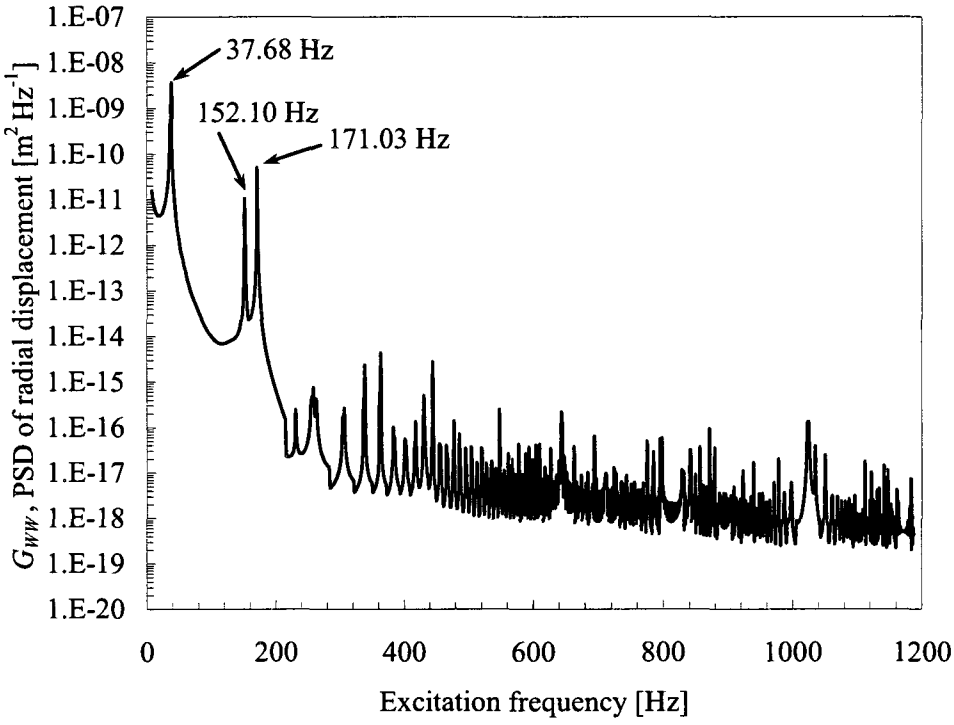

Figure 3.6 Power spectral density of radial displacement (G_{WW}) of an SFSF plate subjected to fully-developed turbulent flow from one side where flow is along its long sides against excitation frequency. The PSD of the radial displacement is calculated at the node at which the maximum total r.m.s. radial displacement response was obtained for a free stream velocity of 30 m s^{-1} and a damping ratio of 0.001 (see also Figure 3.5). The major peaks demonstrate the natural frequencies of the system given in Table 3.2. It is observed that the lower natural frequencies contribute significantly to the response.

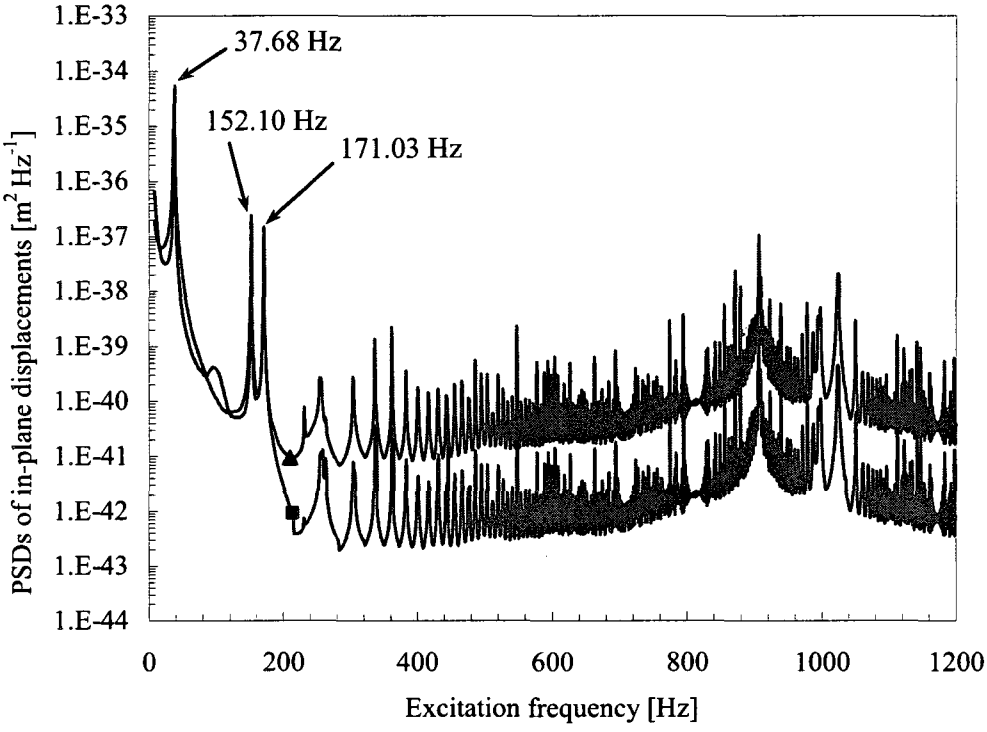

Figure 3.7 Power spectral densities of in-plane displacements of an SFSF plate subjected to fully-developed turbulent flow from one side where flow is along its long sides versus excitation frequency. The PSDs are calculated for a free stream velocity of 30 m s^{-1} and a damping ratio of 0.001 at the node at which the maximum total r.m.s. radial displacement response was obtained; —■— PSD of membrane displacement in the x-direction (G_{UU}), —▲— PSD of membrane displacement in the y-direction (G_{VV}). The PSDs of the in-plane displacements are minimal, however for the sake of demonstrating the behavior they are illustrated. The same major peaks as those in Figure 3.6 are observed representing the natural frequencies of the system.

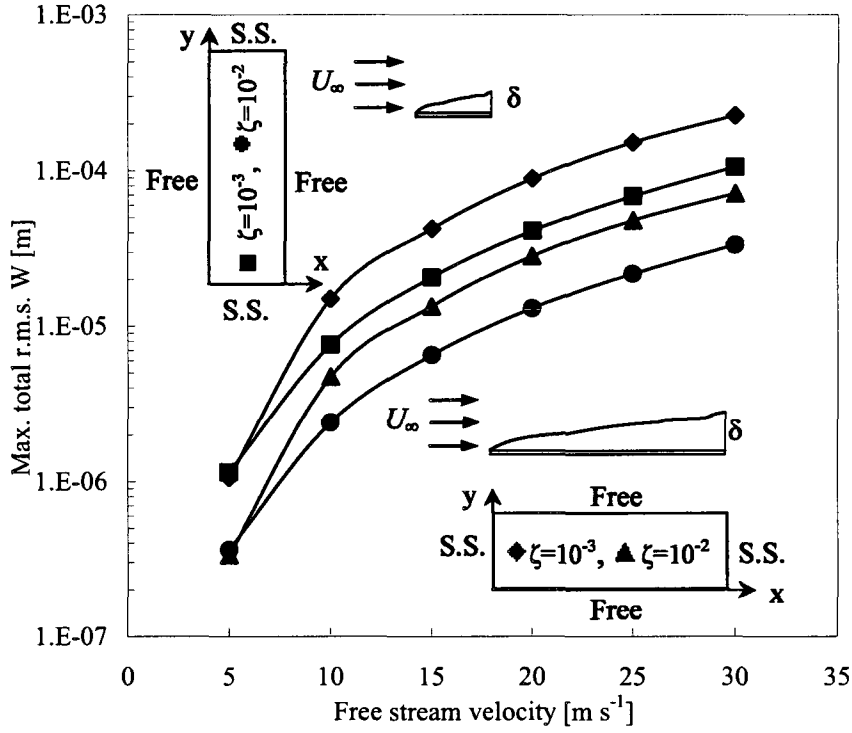

Figure 3.8 Comparison of the effect of flow direction on the maximum total r.m.s. radial displacement of an SFSF plate subjected to fully-developed turbulent flow from one side; —◆— flow along the long side of the SFSF plate with $\zeta=10^{-3}$, —■— flow along the short side of the SFSF plate with $\zeta=10^{-3}$, —▲— flow along the long side of the SFSF plate with $\zeta=10^{-2}$, —●— flow along the short side of the SFSF plate with $\zeta=10^{-2}$. Here, the maximum total r.m.s. radial displacements are illustrated against free stream velocity for different damping ratios. It is observed that the response for the case of flow along the long side of the plate is higher than that for the flow along the short side of the plate except for free stream velocity 5 m s^{-1}.

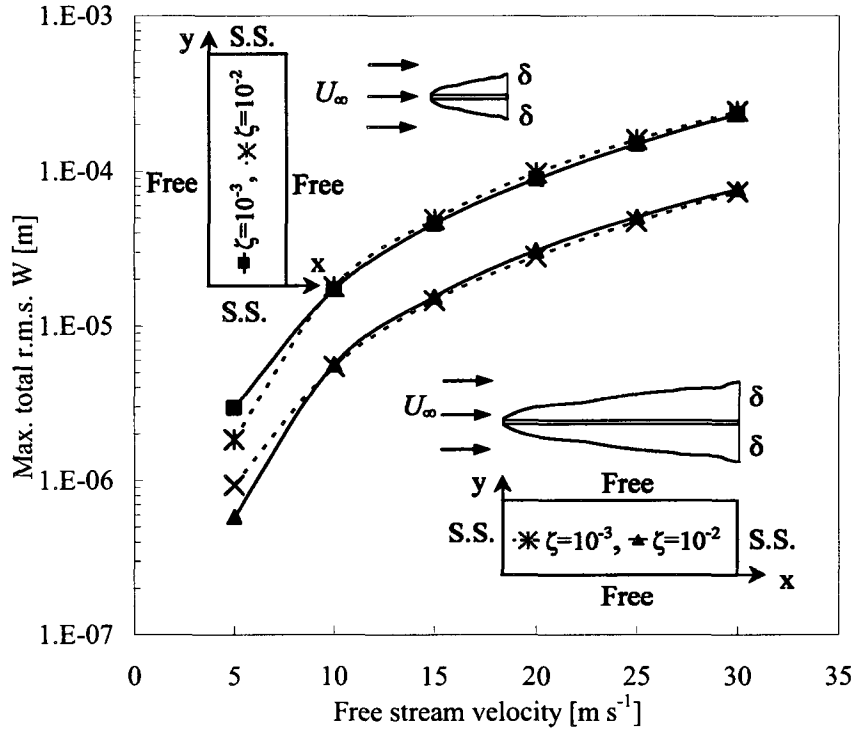

Figure 3.9 Comparison of the effect of flow direction on the maximum total r.m.s. radial displacement of an SFSF plate subjected to fully-developed turbulent flow from both sides; --✳- flow along the long side of the SFSF plate with $\zeta=10^{-3}$, —■— flow along the short side of the SFSF plate with $\zeta=10^{-3}$, —▲— flow along the long side of the SFSF plate with $\zeta=10^{-2}$, --✳- flow along the short side of the SFSF plate with $\zeta=10^{-2}$. The maximum total r.m.s. radial displacements are plotted against free stream velocity for different damping ratios, depicting that the response is relatively insensitive to flow direction.

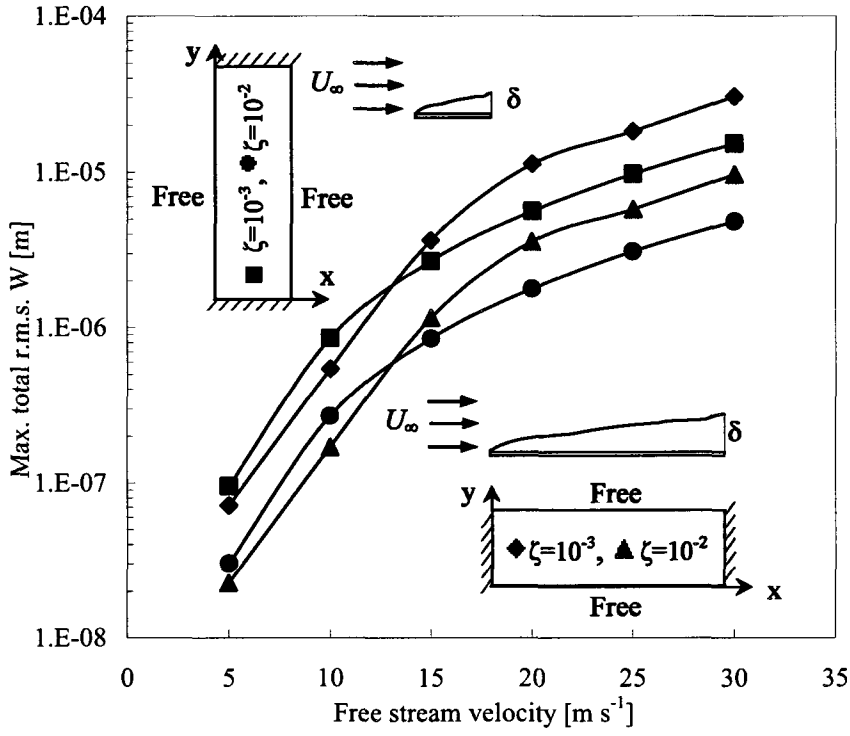

Figure 3.10 Comparison of the effect of flow direction on the maximum total r.m.s. radial displacement of a CFCF plate subjected to fully-developed turbulent flow from one side; —◆— flow along the long side of the CFCF plate with $\zeta=10^{-3}$, —■— flow along the short side of the CFCF plate with $\zeta=10^{-3}$, —▲— flow along the long side of the CFCF plate with $\zeta=10^{-2}$, —●— flow along the short side of the CFCF plate with $\zeta=10^{-2}$. The response is illustrated versus free stream velocity for different damping ratios. It is seen that the response for the case of flow along the long side of the plate is higher than that for the flow along the short side of the plate except for free stream velocities 5 and 10 m s^{-1}.

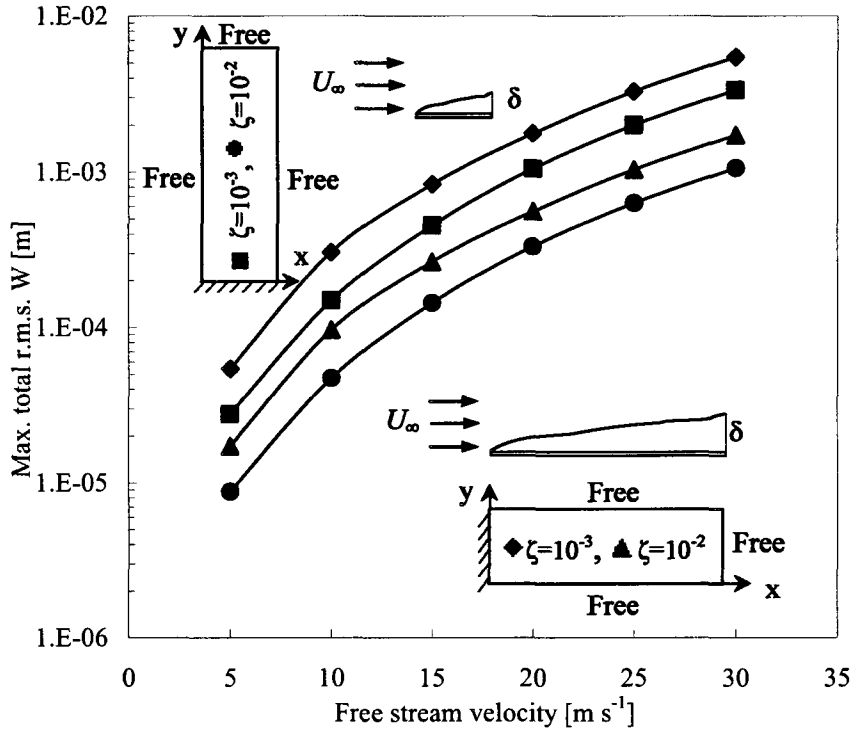

Figure 3.11 Comparison of the effect of flow direction on the maximum total r.m.s. radial displacement of a CFFF plate subjected to fully-developed turbulent flow from one side; —◆— flow along the long side of the CFFF plate with $\zeta=10^{-3}$, —■— flow along the short side of the CFFF plate with $\zeta=10^{-3}$, —▲— flow along the long side of the CFFF plate with $\zeta=10^{-2}$, —●— flow along the short side of the CFFF plate with $\zeta=10^{-2}$. The response is illustrated versus free stream velocity for different damping ratios. It shows that the response for the case of flow along the long side of the plate is higher than that for flow along the short side of the plate for a given velocity and damping ratio.

Table 3.1

Comparison of the total root mean square radial displacement (W) at the axial mid-point of a simply supported cylinder subjected to fully-developed turbulent internal flow

U_{cl} (in s^{-1})	Total root mean square radial displacement (in)	
	Lakis' theory, by summation over n=2 to 6 [13]	Present method
248	1.9238E-04	3.1146E-04
520	1.4389E-03	1.8627E-03

Table 3.2

Comparison of the natural frequencies of an SFSF plate subjected to stationary water from one side

Coupled natural frequency (Hz)		
Haddara & Cao (analytic) [35]	Present method	Discrepancy (%)
34.81	37.68	7.62
145.66	152.10	4.23
NA	171.03	NA
348.30	344.96	0.97
NA	367.39	NA

Table 3.3

Comparison of the maximum total r.m.s. radial displacement of an SFSF plate with a damping ratio of $\zeta=10^{-2}$ subjected to fully-developed turbulent flow from one and both sides for different free stream velocities, where water is flowing along the long side of the plate

U_∞ (m s^{-1})	Max. total r.m.s. radial displacement of a plate wetted on one side (m)	Max. total r.m.s. radial displacement of a plate wetted on both sides (m)
5	3.3552E-07	5.8416E-07
10	4.7501E-06	5.6450E-06
15	1.3484E-05	1.5456E-05
20	2.8316E-05	3.0860E-05
25	4.8085E-05	5.0640E-05
30	7.1533E-05	7.6949E-05

CHAPTER IV

GENERAL DISCUSSION

The three-dimensional finite element model developed in the first phase of this thesis was employed to analyze the dynamic behavior of various structures in a vacuum and in contact with stationary fluid.

A flexible rectangular reservoir under various boundary conditions in a vacuum, partially and completely filled with fluid was investigated. As we expected, the natural frequencies of the fluid-filled reservoir were significantly lower than those of the reservoir in a vacuum. The predicted natural frequencies of the empty and fluid-filled reservoir compared favorably with those obtained using ANSYS. The effect of fluid level variations on the coupled natural frequencies of the system was also investigated. It was observed that the natural frequencies decreased as fractional filling increased. However, different behaviors of natural frequencies were observed under different boundary conditions of the reservoir. The effect of fluid level above 3/4 fractional filling was found to have a negligible effect on the natural frequencies of the reservoir.

To demonstrate the applicability of the method, a blade in a vacuum and submerged in fluid was also studied. The predicted natural frequencies of the blade in a vacuum were compared with those obtained using ANSYS. As we expected the natural frequencies of the blade in contact with fluid diminished. The results indicated that the

level of fluid over and under the blade as well as the boundary conditions of the fluid at the extremities affected the dynamic behavior of the blade until fluid level reached 50% of the blade length. It was found that the frequency decreased as the height of fluid over the blade increased while the fluid boundary condition was a free surface and the blade was sufficiently far from the rigid wall. On the other hand, it was noted that as the height of fluid under the blade increased the frequency increased as well while the fluid boundary condition was a rigid wall and the blade was sufficiently far from the free surface. It was also demonstrated that the first mode shape of the submerged blade is the same as that in a vacuum.

The aforementioned results show that the method developed in this thesis is capable of determining the dynamic behavior of three-dimensional thin curved structures coupled with quiescent fluid.

In the second phase of this thesis the r.m.s. displacement response of a thin plate under various boundary conditions excited by a turbulent boundary layer was studied. The total response was obtained by summation over significant modes of vibration and subsequently the maximum total r.m.s. displacement of the plate was calculated. It was noted that the maximum total r.m.s. displacements were small for the set of calculations, as expected.

It was observed that the maximum total r.m.s. displacements of the plate are directly proportional to free stream velocity and inversely proportional to the damping ratio of the structure. The same behavior was observed for the plate under different

boundary conditions of the plate and flow. It can be concluded that damping is an effective means to minimize vibration amplitude.

The effects of turbulent flow from one and both sides of the plate on the total r.m.s. radial displacement were investigated and higher responses were obtained for the case of the plate submerged in flow due to lower natural frequencies and larger virtual added mass, as expected. Results for the displacement responses of the plate subjected to turbulent boundary-layer-induced pressure fluctuations indicated that only a limited number of modes need be included in the analysis, even though the PSD of the wall pressure contains a wide frequency spectrum.

No studies of the effects of turbulent boundary layer on the total r.m.s. radial displacement response of a thin plate have been documented and this prevented validation of the thin plate response to a random pressure field. To our best knowledge, there is no reference in the literature for the total r.m.s. displacement of a plate or an open curved structure subjected to this type of random pressure. Therefore, in order to validate our method a cylindrical shell was analyzed and the total r.m.s. radial displacement of the axial mid-point was predicted and compared with that obtained by Lakis and Païdoussis. Although different expressions for correlations were adapted in the proposed method and in Lakis' work, good agreement was found. Since Lakis validated his results using Clinch's experimental measurements, this result demonstrated that our method is sound and practicable.

The power spectral densities of the membrane and radial displacements of an SFSF plate subjected to fully-developed turbulent flow from one side where flow is

along the long sides of the plate were calculated. A study of the spectrum revealed that the peaks of the PSDs of displacements occur at the coupled natural frequencies of the system. The envelope of the peaks decays rapidly with frequency. The PSD curve is sharply peaked at the natural frequencies and shows clearly that only the frequencies in the vicinity of the natural frequencies are of interest and these contribute greatly to the response. It was observed that lower natural frequencies contribute significantly to the PSD of the response.

CHAPTER V

CONCLUSION AND RECOMMENDATION

5.1 Overview

A general method to model a thin elastic curved structure in a vacuum and subjected to quiescent fluid was developed. This approach was then extended to predict the response of such structures to an arbitrary random pressure field and subsequently to a pressure field arising from a fully-developed turbulent boundary layer in subsonic flow.

5.2 Concluding remarks

In the first part of this thesis, linear free vibration of three-dimensional thin shell structures in a vacuum and in the vicinity of stationary fluid was modeled. The structure could be partially or completely filled with or submerged in the fluid. The method used a combination of classical thin shell theory and the finite element method in which the finite elements were flat rectangular elements with five degrees of

freedom per node, representing the in-plane and out-of-plane displacements and two in-plane rotations. The structural mass and stiffness matrices were determined by exact analytical integration. In order to generate element stiffness and mass matrices in global coordinates, a transformation matrix was defined by applying a direction cosine for curved structures (such as turbine blades) and using two successive rotations about the x- and y- directions for a rectangular reservoir. This local-global transformation caused singularity which resulted from the absence of rigidity associated with the drilling degree of freedom. The numerical singularity was resolved by introducing fictitious mass and stiffness into the diagonal terms associated with the local normal rotation at each node of the element. Potential flow theory, Bernoulli's equation and the impermeability condition were employed to calculate the stationary fluid pressure exerted on each finite element. Fluid pressure was expressed as a function of the acceleration of the normal displacement of the structure, the fluid density and the boundary conditions of the fluid. An analytical integration of the product of the fluid pressure and shape function over the element produced the inertial effect of the stationary fluid and was interpreted as the virtual added-mass of fluid. This led to an increase in the total mass of the system and consequently resulted in a decrease in the natural frequencies. Since pressure imposed by stationary fluid was individually calculated for each finite element, structures partially containing or submerged in fluid can be modeled. This method is more accurate than conventional finite element methods because a combination of classic thin shell theory and the finite element method was employed. An in-house program was developed in order to obtain

eigenvalues and eigenvectors of the structure in a vacuum and in contact with fluid. This method was successfully applied to predict the dynamic behavior of a rectangular tank partially and completely filled with fluid. Satisfactory results for a submerged blade were also obtained using our method. Based on the results obtained by the presented method, it can be concluded that this developed method is a reliable tool to analyze the dynamic behavior of three-dimensional thin curved structures coupled with stationary fluid.

In the second part of this thesis we introduced a numerical method capable of predicting the total r.m.s. displacement response of a thin structure to an arbitrary random pressure field. The method was then specialized for application to the case where the pressure field originated from a turbulent boundary layer of a subsonic flow. In this approach a thin shell finite element formulation combined with the normal mode method and random vibration theory was employed to study random vibration response. First the structure in a vacuum and in contact with stationary fluid was analyzed based on the method developed in the first phase of this thesis, since the eigenvalues, eigenvectors and other characteristics of the system were needed as input to the random calculations. The random pressure field was approximated using a finite set of discrete forces and moments at each node of the finite element. The mean square displacement responses of the structure excited by a stationary ergodic random pressure were expressed in terms of the cross spectral density of the wall pressure. The mathematical model to describe the cross spectral density of pressure fluctuations was based on the Corcos model. An analytical expression was obtained for the total root mean square

displacement response of a thin shell structure excited by turbulent boundary layer pressure fluctuations in terms of the wetted natural frequency of the system, undamped mode shapes, generalized mass and other characteristics of the structure and flow. The total r.m.s. displacement response was obtained by summation over all significant modes of vibration. In addition, an expression was developed to predict the displacement power spectral density of the structure excited by turbulent flow. The solution was incorporated into the in-house program, which also determines the free vibration characteristics of the shell in a vacuum and in contact with quiescent fluid.

The method developed in this thesis benefits from the fact that the statistical properties of the turbulent boundary layer pressure field, such as the PSD of wall pressure, longitudinal and lateral correlation functions are similar for different structures. Therefore the same formulations and proposed method are applicable to predict the r.m.s. displacement response of various structures. It should be emphasized that the method developed in this thesis, unlike previous methods in the literature, is not limited to thin plates but extends to cylindrical shells and more complex geometries. Moreover it is capable of predicting the total r.m.s. displacement response, which is scarce in the literature. The developed method can be utilized to investigate structures with discontinuities in material and thickness under different boundary conditions of structure and fluid.

A few case studies were presented to illustrate the applicability of the proposed random method. Calculations were undertaken for a thin plate under different boundary conditions of structure and flow, excited by a turbulent boundary layer in subsonic flow.

The results appear to be reasonable however the absence of experimental data precludes comparison. To the author's knowledge there is no reference in the literature for the total r.m.s. displacement of a plate or an open curved structure subjected to this type of random pressure. Therefore the validity of the proposed method was established through analysis of a thin cylindrical shell subjected to an internal fully-developed turbulent subsonic flow. The total r.m.s. radial displacement of the cylinder was predicted using our method and compared favorably with an analytical solution available in the literature obtained by Lakis and Païdoussis. Although different expressions for correlations were adapted in the proposed method and in Lakis' work, good agreement was found. Lakis validated his results by comparison with Clinch's experimental measurements; this indicates that our method is sound and practicable.

For lightly damped structures ($\zeta_r << 1$) the cross-product terms in Eq. 3.14 contribute very little to the random response and are therefore ignored in this analysis. However, structures with appreciable damping ratios can be analyzed using this method, if the cross terms are taken into account. In this study damping ratio has been assumed equal for all mode shapes, however better results will be obtained if damping ratios are measured for all chosen mode shapes. It should be emphasized that the wall-pressure correlation functions employed in this analysis are applicable for flow velocities corresponding to subsonic flow with Mach number below 0.3.

5.3 Future studies

The method developed in the first part of this thesis can be applied to model parallel plates or channels subjected to potential flow. Also, it can be extended to study the dynamic behavior of thin curved shells such as turbine blades subjected to flowing fluid. Apart from the inertial effect of the stationary fluid, additional effects associated with flow velocity can be considered as centrifugal and Coriolis-type forces and respectively accounted as stiffness and damping of the fluid.

In a further study, we plan to extend our approach to investigate the vibration of a hydraulic turbine submerged in a quiescent fluid or subjected to turbulent flow. An extension of this work to investigate parallel plates and channels subjected to a fully-developed turbulent boundary layer is in progress.

As for other future development, the proposed method in the second phase of this thesis can be readily extended to predict the response of three-dimensional thin curved structures such as hydraulic turbine blades to turbulent boundary layer random pressure fields using flat shell elements with five degrees of freedom per node. The same statistical properties, i.e. wall-pressure power spectral density and cross correlation functions are applicable.

It should be pointed out that in the present study, solely the inertial effect of the flow has been taken into account. Therefore, another extension to this work would be to consider the effects of all of the components (i.e. centrifugal and Coriolis forces)

arising from the presence of flowing fluid on the natural frequencies of the system and the total r.m.s. displacement response.

REFERENCES

[1] J. W. S. Rayleigh, *Theory of Sound*. New York: Dover Publication, 1945.

[2] H. Lamb, *Hydrodynamics*, 6th ed. New York: Dover Publications, 1945.

[3] M. P. Païdoussis, "Flow-induced instabilities of cylindrical structures," presented at Proceedings of the U.S. National Congress of Applied Mechanics, Austin, TX, USA, 1986.

[4] M. P. Païdoussis, *Fluid-Structure Interactions: Slender Structures and Axial Flow, Vol. I*. London: Academic Press, 1998.

[5] M. P. Païdoussis, *Fluid-Structure Interactions: Slender Structures and Axial Flow, Vol. II*. London: Elsevier Academic Press, 2004.

[6] F. Axisa and J. Antunes, *Modelling of Mechanical Systems: Fluid-Structure Interaction, Vol. 3*. Amsterdam: Elsevier, 2006.

[7] H. J. P. Morand and R. Ohayon, *Fluid-Structure Interaction: Applied Numerical Methods*. New York: Wiley and Sons, 1995.

[8] M. S. Marcus, "Finite-element method applied to the vibration of submerged plates," *Journal of Ship Research*, vol. 22, no. 2, pp. 94-99, 1978.

[9] O. C. Zienkiewicz and P. Bettess, "Fluid-structure dynamic interaction and wave forces. An introduction to numerical treatment," *International Journal for Numerical Methods in Engineering*, vol. 13, no. 1, pp. 1-16, 1978.

[10] M. K. Kwak, "Hydroelastic vibration of rectangular plates," *Transactions of the ASME. Journal of Applied Mechanics*, vol. 63, no. 1, pp. 110-15, 1996.

[11] K. Nagaya and J. Takeuchi, "Vibration of a plate with arbitrary shape in contact with a fluid," *Journal of the Acoustical Society of America*, vol. 75, no. 5, pp. 1511-1518, 1984.

[12] S. M. Soedel and W. Soedel, "On the free and forced vibration of a plate supporting a freely sloshing surface liquid," *Journal of Sound and Vibration*, vol. 171, no. 2, pp. 159-171, 1994.

[13] Y.-W. Kim and Y.-S. Lee, "Coupled vibration analysis of liquid-filled rigid cylindrical storage tank with an annular plate cover," *Journal of Sound and Vibration*, vol. 279, no. 1-2, pp. 217-235, 2005.

[14] J. R. Cho, H. W. Lee, and S. Y. Ha, "Finite element analysis of resonant sloshing response in 2-D baffled tank," *Journal of Sound and Vibration*, vol. 288, no. 4-5, pp. 829-845, 2005.

[15] H. M. Koh, J. K. Kim, and J.-H. Park, "Fluid-structure interaction analysis of 3-D rectangular tanks by a variationally coupled BEM-FEM and comparison with test results," *Earthquake Engineering & Structural Dynamics*, vol. 27, no. 2, pp. 109-124, 1998.

[16] A. A. Lakis and S. Neagu, "Free surface effects on the dynamics of cylindrical shells partially filled with liquid," *Journal of Sound and Vibration*, vol. 207, no. 2, pp. 175-205, 1997.

[17] A. A. Lakis, G. Brusuc, and M. Toorani, "Fluid free surface effect on the vibration analysis of cylindrical shells," presented at Société Française

d'Énergie Nucléaire - International Congress on Advances in Nuclear Power Plants - ICAPP 2007, "The Nuclear Renaissance at Work", Nice, France, 2008.

[18] E. Hernandez, "Approximation of the vibration modes of a plate and shells coupled with a fluid," *Journal of Applied Mechanics, Transactions ASME*, vol. 73, no. 6, pp. 1005-1010, 2006.

[19] K.-H. Jeong and K.-J. Kim, "Free vibration of a circular cylindrical shell filled with bounded compressible fluid," *Journal of Sound and Vibration*, vol. 217, no. 2, pp. 197-221, 1998.

[20] P. B. Gonçalves and R. C. Batista, "Frequency response of cylindrical shells partially submerged or filled with liquid," *Journal of Sound and Vibration*, vol. 113, no. 1, pp. 59-70, 1987.

[21] A. A. Lakis and M. P. Païdoussis, "Free vibration of cylindrical shells partially filled with liquid," *Journal of Sound and Vibration*, vol. 19, no. 1, pp. 1-15, 1971.

[22] A. A. Lakis and M. P. Païdoussis, "Dynamic analysis of axially non-uniform thin cylindrical shells," *Journal of Mechanical Engineering Science*, vol. 14, no. 1, pp. 49-71, 1972.

[23] A. A. Lakis and R. Dore, "General method for analyzing contact stresses on cylindrical vessels," *International Journal of Solids and Structures*, vol. 14, no. 6, pp. 499-516, 1978.

[24] A. A. Lakis, P. V. Dyke, and H. Ouriche, "Dynamic analysis of anisotropic fluid-filled conical shells," *Journal of Fluids and Structures*, vol. 6, no. 2, pp. 135-162, 1992.

[25] A. A. Lakis, N. Q. Tuy, and A. Selmane, "Analysis of axially non-uniform thin spherical shells," presented at Proceedings of the International Symposium on Structural Analysis and Optimization, Paris, France, 1989.

[26] A. Selmane and A. A. Lakis, "Dynamic analysis of anisotropic open cylindrical shells," *Computers and Structures*, vol. 62, no. 1, pp. 1-12, 1997.

[27] U. S. Lindholm, D. D. Kana, and H. N. Abramson, "Breathing vibrations of circular cylindrical shell with internal liquid," *Journal of the Aero/Space Sciences*, vol. 29, no. 9, pp. 1052-1059, 1962.

[28] R. P. S. Han and J. D. Liu, "Free vibration analysis of a fluid-loaded variable thickness cylindrical tank," *Journal of Sound and Vibration*, vol. 176, no. 2, pp. 235-253, 1994.

[29] R. K. Jain, "Vibration of fluid-filled, orthotropic cylindrical shells," *Journal of Sound and Vibration*, vol. 37, no. 3, pp. 379-388, 1974.

[30] M. Amabili and G. Dalpiaz, "Breathing vibrations of a horizontal circular cylindrical tank shell, partially filled with liquid," *Journal of Vibration and Acoustics, Transactions of the ASME*, vol. 117, no. 2, pp. 187-191, 1995.

[31] J. Mistry and J. C. Menezes, "Vibration of cylinders partially-filled with liquids," *Journal of Vibration and Acoustics, Transactions of the ASME*, vol. 117, no. 1, pp. 87-93, 1995.

[32] K. H. Jeong and S. C. Lee, "Fourier series expansion method for free vibration analysis of either a partially liquid-filled or a partially liquid-surrounded circular cylindrical shell," *Computers and Structures*, vol. 58, no. 5, pp. 937-946, 1996.

[33] U. S. Lindholm, D. D. Kana, W. H. Chu, and H. N. Abramson, "Elastic vibration characteristics of cantilever plates in water," *Journal of Ship Research*, vol. 9, no. 1, pp. 11-22, 1965.

[34] Y. Fu and W. G. Price, "Interaction between a partially or totally immersed vibrating cantilever plate and the surrounding fluid," *Journal of Sound and vibration*, vol. 118, no. 3, pp. 495-513, 1987.

[35] M. R. Haddara and S. Cao, "A study of the dynamic response of submerged rectangular flat plates," *Marine Structures*, vol. 9, no. 10, pp. 913-933, 1996.

[36] A. Ergin and B. Ugurlu, "Linear vibration analysis of cantilever plates partially submerged in fluid," *Journal of Fluids and Structures*, vol. 17, no. 7, pp. 927-939, 2003.

[37] J. K. Kim, H. M. Koh, and I. J. Kwahk, "Dynamic response of rectangular flexible fluid containers," *Journal of Engineering Mechanics*, vol. 122, no. 9, pp. 807-817, 1996.

[38] M. C. Kim and S. S. Lee, "Hydroelastic analysis of a rectangular tank," presented at MSC Aerospace User's Conference, Newport Beach, California, 1997.

[39] H. F. Bauer, "Hydroelastic vibrations in a rectangular container," *International Journal of Solids and Structures*, vol. 17, no. 7, pp. 639-52, 1981.

[40] Y. K. Cheung and D. Zhou, "Coupled vibratory characteristics of a rectangular container bottom plate," *Journal of Fluids and Structures*, vol. 14, no. 3, pp. 339-357, 2000.

[41] H. F. Bauer and W. Eidel, "Hydroelastic vibrations in a two-dimensional rectangular container filled with frictionless liquid and a partly elastically covered free surface," *Journal of Fluids and Structures*, vol. 19, no. 2, pp. 209-220, 2004.

[42] I. Dyer, "Response of plates to a decaying and convecting random pressure field," *The Journal of the Acoustical Society of America*, vol. 31, no. 7, pp. 922-928, 1959.

[43] A. C. Eringen, "Response of beams and plates to random loads," *American Society of Mechanical Engineers -- Transactions -- Journal of Applied Mechanics*, vol. 24, no. 1, pp. 46-52, 1957.

[44] C. A. Mercer, "Response of multi-supported beam to random pressure field," *Journal of Sound and Vibration*, vol. 2, no. 3, pp. 293-306, 1965.

[45] H. Wagner and B. Rama Bhat, "Linear response of an elastic plate to actual random load," *Archive of Applied Mechanics (Ingenieur Archiv)*, vol. 39, no. 3, pp. 149-158, 1970.

[46] M. M. Stanisic, "Response of plates to random load," *Journal of Acoustical Society of America*, vol. 43, no. 6, pp. 1351-1357, 1968.

[47] G. M. Lindberg and M. D. Olson, "Vibration modes and random response of a multi-bay panel system using finite elements," National Research Council of Canada Report No. LR-492, 1967.

[48] M. D. Olson, "A consistent finite element method for random response problems," *Computers and Structures*, vol. 2, no. 1-2, pp. 163-180, 1972.

[49] A. Powell, "On the fatigue failure of structures due to vibrations excited by random pressure fields," *The Journal of the Acoustical Society of America*, vol. 30, no. 12, pp. 1130-1135, 1958.

[50] I. Elishakoff and L. Zhu, "Random vibration of structures by the finite element method," *Computer Methods in Applied Mechanics and Engineering*, vol. 105, no. 3, pp. 359-373, 1993.

[51] M. G. Cottis and J. G. Jasonides, "The response of a finite thin cylindrical shell to random pressure fields," presented at Acoustical fatigue in Aerospace structures; Proceeding of the second international conference, Dayton, Ohio, USA, April 29-May 1 1964.

[52] M. G. Cottis, "On the dynamic response of an orthotropic finite cylindrical shell to an arbitrary pressure field," *Journal of Sound and Vibration*, vol. 7, no. 1, pp. 31-38, 1968.

[53] S. Nemat-Nasser, "On response of shallow thin shells to random excitations," *American Institute of Aeronautics and Astronautics Journal*, vol. 6, no. 7, pp. 1327-1331, 1968.

[54] I. Elishakoff, "On the role of cross-correlations in the random vibrations of shells," *Journal of Sound and Vibration*, vol. 50, no. 2, pp. 239-252, 1977.

[55] T. Y. Yang and R. K. Kapania, "Finite element random response analysis of cooling tower," *Journal of Engineering Mechanics*, vol. 110, no. 4, pp. 589-609, 1984.

[56] G. M. Corcos, "Resolution of pressure in turbulence," *Journal of the Acoustical Society of America*, vol. 35, no. 2, pp. 192-199, 1963.

[57] G. M. Corcos, "The resolution of turbulent pressures at the wall of a boundary layer," *Journal of Sound and Vibration* vol. 6, no. 1, pp. 59-70, 1967.

[58] L. Maestrello, "Design criterion of panel structure excited by turbulent boundary layer," *Journal of Aircraft*, vol. 5, no. 4, pp. 321-328, 1968.

[59] T. M. Farabee, "Spectral features of wall pressure fluctuations beneath turbulent boundary layers," *Physics of Fluids A (Fluid Dynamics)*, vol. 3, no. 10, pp. 2410-2420, 1991.

[60] J. E. Ffowcs Williams, "Boundary-layer pressures and the Corcos model: A development to incorporate low-wavenumber constraints," *Journal of Fluid Mechanics*, vol. 125, pp. 9-25, 1982.

[61] T. M. Farabee and F. E. Geib, "Measurements of boundary layer pressure fields with an array of pressure transducers in a subsonic flow," NSRDC Report No. 76-0031, 1976.

[62] H. P. Bakewell, G. F. Carey, J. J. Libuka, H. H. Schloemer, and W. A. Von Winkle, "Wall pressure correlations in turbulent pipe flow," U. S. Navy Underwater Sound Laboratory, New London, CT. Report No. 559, 1962.

[63] G. M. Corcos, "Structure of turbulent pressure field in boundary-layer flows," *Journal of Fluid Mechanics*, vol. 18, no. 3, pp. 353-378, 1964.

[64] W. W. Willmarth and C. E. Wooldridge, "Measurements of fluctuating pressure at wall beneath thick turbulent boundary layer," *Journal of Fluid Mechanics*, vol. 14, no. 2, pp. 187-210, 1962.

[65] M. K. Bull, "Wall-pressure fluctuations associated with subsonic turbulent boundary layer flow," *Journal of Fluid Mechanics*, vol. 28, no. 4, pp. 719-764, 1967.

[66] D. J. J. Leclercq and X. Bohineust, "Investigation and modelling of the wall pressure field beneath a turbulent boundary layer at low and medium frequencies," *Journal of Sound and Vibration*, vol. 257, no. 3, pp. 477-501, 2002.

[67] Y.-T. Lee, W. K. Blake, and T. M. Farabee, "Modeling of wall pressure fluctuations based on time mean flow field," *Journal of Fluids Engineering, Transactions of the ASME*, vol. 127, no. 2, pp. 233-240, 2005.

[68] W. K. Blake, *Mechanics of Flow-Induced Sound and Vibration, Vol. II: Complex Flow-Structure Interaction*. London: Academic Press Inc., 1986.

[69] P. Leehey, "Structural excitation by a turbulent boundary layer: An overview," *Journal of vibration, acoustics, stress, and reliability in design*, vol. 110, no. 2, pp. 220-225, 1988.

[70] M. G. Cottis and J. G. Jasonides, "Excitation of finite cylindrical shells by boundary-layer pressure fluctuations (A)," *Journal of Acoustical Society of America*, vol. 36, no. 5, pp. 1046, 1964.

[71] J. M. Clinch, "Prediction and measurement of the vibrations induced in thin-walled pipes by the passage of internal turbulent water flow," *Journal of Sound and Vibration*, vol. 12, no. 4, pp. 429-451, 1970.

[72] A. A. Lakis and M. P. Païdoussis, "Prediction of the response of a cylindrical shell to arbitrary or boundary-layer-induced random pressure fields," *Journal of Sound and Vibration*, vol. 25, no. 1, pp. 1-27, 1972.

[73] W. A. Strawderman and R. S. Brand, "Turbulent-flow-excited vibration of a simply supported, rectangular flat plate," *The Journal of the Acoustical Society of America*, vol. 45, no. 1, pp. 177-192, 1969.

[74] F. Han, R. J. Bernhard, and L. G. Mongeau, "Prediction of flow induced structural vibration and sound radiation using energy flow analysis," *Journal of Sound and Vibration*, vol. 227, no. 4, pp. 685-709, 1999.

[75] F. Birgersson, N. S. Ferguson, and S. Finnveden, "Application of the spectral finite element method to turbulent boundary layer induced vibration of plates," *Journal of Sound and Vibration*, vol. 259, no. 4, pp. 873-891, 2003.

[76] P. Vitiello, S. De Rosa, and F. Franco, "Convected field analysis of flat panels response to turbulent boundary layer induced excitation," *Aerospace Science and Technology*, vol. 12, no. 1, pp. 91-104, 2008.

[77] S. De Rosa and F. Franco, "Exact and numerical responses of a plate under a turbulent boundary layer excitation," *Journal of Fluids and Structures*, vol. 24, no. 2, pp. 212-230, 2008.

[78] S. Finnveden, F. Birgersson, U. Ross, and T. Kremer, "A model of wall pressure correlation for prediction of turbulence-induced vibration," *Journal of Fluids and Structures*, vol. 20, no. 8, pp. 1127-1143, 2005.

[79] D. Mazzoni, "An efficient approximation for the vibro-acoustic response of a turbulent boundary layer excited panel," *Journal of Sound and Vibration*, vol. 264, no. 4, pp. 951-971, 2003.

[80] F. Birgersson, S. Finnveden, and G. Robert, "Modelling turbulence-induced vibration of pipes with a spectral finite element method," *Journal of Sound and Vibration*, vol. 278, no. 4-5, pp. 749-772, 2004.

[81] S. A. Hambric, Y. F. Hwang, and W. K. Bonness, "Vibrations of plates with clamped and free edges excited by low-speed turbulent boundary layer flow," *Journal of Fluids and Structures*, vol. 19, no. 1, pp. 93-110, 2004.

[82] C. Maury, P. Gardonio, and S. J. Elliott, "A wavenumber approach to modelling the response of a randomly excited panel, part I: General theory," *Journal of Sound and Vibration*, vol. 252, no. 1, pp. 83-113, 2002.

[83] D. R. Thomas and P. A. Nelson, "Feedback control of sound radiation from a plate excited by a turbulent boundary layer," *Journal of the Acoustical Society of America*, vol. 98, no. 5 pt 1, pp. 2651-2662, 1995.

[84] Y. Kerboua, A. A. Lakis, M. Thomas, and L. Marcouiller, "Hybrid method for vibration analysis of rectangular plates," *Nuclear Engineering and Design*, vol. 237, no. 8, pp. 791-801, 2007.

[85] Y. Kerboua, A. A. Lakis, M. Thomas, and L. Marcouiller, "Vibration analysis of rectangular plates coupled with fluid," *Applied Mathematical Modelling*, vol. 32, no. 12, pp. 2570-2586, 2008.

[86] M. K. Au-Yang, *Flow-Induced Vibration of Power and Process Plant Components*. New York: ASME Press, 2001.